NTNU – Trondheim
Norwegian University of
Science and Technology

Investigation of how Silica Nanoparticle Adsorption Affects Wettability in Water-Wet Berea Sandstone

An Experimental Study

Anne Tinnen Kaasa

Petroleum Geoscience and Engineering
Submission date: June 2013
Supervisor: Ole Torsæter, IPT
Co-supervisor: Jon Kleppe, IPT

Norwegian University of Science and Technology
Department of Petroleum Engineering and Applied Geophysics

"To know that you know,

and to know that you don't know

- that is real wisdom."

- Confucious

Abstract

Retention, or nanoparticle deposition, on the walls of porous media has been shown to cause alterations in rock properties, such as porosity and permeability. This thesis investigated the possible alterations in wetting preferences of Berea sandstone as an effect of silica nanoparticle (SNP) adsorption on the pore surfaces. Reservoir wettability governs the behaviour of several physical properties in the pore spaces, making it an important parameter in multiphase fluid flow and more importantly; in petroleum recovery.

Through experimental studies, both hydrophilic and hydrophobic SNPs with an average particle size of 7 nm have been tested as wettability changers. Nanofluids with particle concentrations of 0,01 wt. %, 0,1 wt. % and 0,5 wt. % were mixed for each particle type. Hydrophilic SNPs were suspended in 3 wt. % brine and hydrophobic in absolute ethanol. Tests were conducted on pairs of Berea core plugs with compatible porous and permeable properties. The Amott-Harvey method was employed to determine the wetting preferences of the rock, both before and after injection of silica nanofluids. Contact angle measurements by the imaging method were conducted to see how SNPs affect fluid interfaces at a solid surface.

Porosity testing showed evidence of particle retention while permeability impairment was only seen for the highest nanoparticle concentrations. This indicated that adsorption was the functioning retention mechanism. None of the nanofluids, regardless of concentration, had any apparent effect on the resulting Amott-Harvey wettability index (WI). However, hydrophobic SNPs affected the rate of spontaneous imbibition. Contact angles between oil, brine and glass was changed due to the presence of SNPs demonstrating that the hydrophilic and hydrophobic groups have the ability to alter the interfacial tensions (IFT) in the system.

Sammendrag

Det er påvist at en viss andel solide partikler holdes igjen i det porøse mediet ved injeksjon av nanofluider. Dette kan føre til forringelse av viktige egenskaper i bergarten, slik som porøsitet og permeabilitet. Denne hovedoppgaven er rettet mot å undersøke hvordan tilbakeholdte silikat-nanopartikler (SNP) påvirker fuktegenskapene til opprinnelig vann-fuktende Berea sandstein. Fuktegenskapene til et reservoar styrer i stor grad viktige fysiske egenskaper i porerommene utgjør dermed en betydningsfull parameter i flerfase-strømning, og ikke minst; i petroleumsutvinning.

Gjennom eksperimentelle forsøk har både hydrofile og hydrofobe SNP, med en gjennomsnittlig partikkelstørrelse på 7 nm, blitt testet som potensielle fukt-endrere. Nanofluider av ulik konsentrasjon, 0,01 vekt- %, 0,1 vekt- % og 0,5 vekt- %, ble blandet for begge partikkeltypene. Hydrofile partikler ble suspendert i en 3 vekt- % saltløsning og de hydrofobe i absolutt etanol. Kjerneprøver av Berea sandstein med like porøse og permeable egenskaper har blitt testet i par. Amott-Harvey metoden ble benyttet for å bestemme de fuktende preferansene til kjernene både før og etter injeksjon av nanofluider. Kontaktvinkler mellom fluider og glass har blitt målt ved bilde-metoden, for å understreke effekten av nanopartiklene.

Testing av porøsitet påviste at en andel partikler ble holdt igjen i porene. Reduksjon i permeabilitet ble kun observert for de høyeste partikkelkonsentrasjonene. Dette indikerte at adsorpsjon var gjeldene retensjonsmekanisme. Ingen av de testede nanofluidene viste tegn til å endre Amott-Harvey fukt-indeksen, men hydrofobe partikler påvirket den spontane imbiberingsraten. Kontaktvinklene mellom olje, saltløsning og glass ble endret ved tilførsel av SNP. Dette demonstrerer at partiklene deres funksjonelle grupper har egenskaper som påvirker systemets grenseflatespenning.

Acknowledgements

This master thesis was carried out at the Norwegian University of Science and Technology (NTNU), in the Department of Petroleum Engineering and Applied Geophysics.

I would like to express my gratitude to all of those who have educated, inspired, guided, influenced and not least supported me during my years of studies.

Special thanks to my advisor, Professor Ole Torsæter, a wonderful teacher and my calm and reassuring supporter in times were the light in the end of the tunnel was barely visible. Ph.D. candidate Shidong Li deserves a lot of credit for helping me formulate my problem description and for guiding me through it, despite our disagreements. Thanks to Ph.D. candidate Luky Hendraningrat and lab supervisor Roger Overå for excellent training and assistance in the lab.

Yet, the most important motivators this year must be my loyal friends and partners in crime. You know who you are and I hope I've managed to show that I appreciate you all. Particular gratitude to Marthe Å. Birkeland; lab just wouldn't be the same without you!

All parts of this master thesis has been written independently and in accordance with rules set down by the Examination Regulations made by the Norwegian University of Science and Technology. I hereby declare that, apart from properly referenced quotations, this master thesis is my own work and contains no plagiarism.

Anne Tinnen Kaasa

Trondheim, 10.06.2013

Table of Contents

List of Tables

List of Figures

List of Figures

1 Introduction

1.1 Motivation

Nanotechnology is making its entry in all thinkable areas of research. The oil and gas industry is picking up on the trend and are investing vast amounts of money into new technology to enhance production from existing fields. Possible applications of engineered Silica Nanoparticles (SNP) in Enhanced Oil Recovery (EOR) have been investigated (Kaasa 2012) and the literature show that the unique characteristics of SNPs make them interesting in terms of altering reservoir properties and enhancing current EOR agents. However, research on nanoparticles is still in an initial phase and much work is required before pilot-testing and employment of SNPs is realistic in field-scale projects.

Before new technology is applied to a reservoir it is desirable to know as much as possible about the potential effects and to obtain accurate predictions of the outcome. Therefore it is crucial to establish both qualitative and quantitative information about SNPs and their behaviour in porous media through thorough laboratory work.

Recent flooding tests of silica nanofluids in water-wet Berea sandstone showed that SNPs are retained on the porous surfaces by adsorption (Hendraningrat and Shidong 2012, Engeset 2012). It is assumed that the adsorbed SNPs will create either a hydrophilic or hydrophobic monolayer in the pore spaces and it is desirable to investigate whether this adsorption can lead to favourable alteration of the reservoir wettability index (WI). Wettability is a key reservoir property that control fluid saturation, distribution and flow through the porous media. If SNP's can offer a way to alter reservoir wettability in turns of increased recovery it can open up for prolonged operational time of existing fields and provide large economic benefits.

1.2 Goal

The main aim of this thesis is to obtain fundamental information on how pure engineered silica nanoparticles affect the wetting preferences of initially water-wet Berea sandstone. Another goal for this thesis is to build on the groundwork of research conducted to promote application of SNPs in the petroleum industry. Due to the limited time available and the scope of this research, tests will only be conducted on initially water-wet Berea Sandstone. Hopefully, this work can create a platform for additional testing and provide useful data for future continuation on the topic.

1.3 Approach and Organisation

This thesis is an experimental study with extra emphasis on reservoir properties and a literature review on silica nanoparticles. Some of the theoretical content is transferred from my project thesis and adjusted to be in accordance with the current problem. It will be organized as follows:

- Chapter 2 gives an overview of the main reservoir and fluid properties that govern the internal processes of a hydrocarbon reservoir, including wettability.
- Chapter 3 introduce silica nanoparticles, their properties and characteristics as well as risks and hazards related to these particles.
- Chapter 4 describes the experimental equipment and procedures employed in laboratory testing for this thesis.
- Chapter 5 presents the results from the experiments and a numerical evaluation.
- In chapter 6 the results are discussed, analysed and limitations are examined. Relevant literature and similar research by other authors are reviewed.
- Chapter 7 rounds up this thesis by drawing conclusions on the findings and presenting further recommendations.

2 Reservoir and Fluid Properties

An adequate comprehension of reservoir and fluid properties is important to understand how recovery of petroleum functions. When calculating and analysing these properties at the exploratory stage of a field, even small deviations can cause major problems and disadvantages later, during production.

2.1 Reservoir Properties

Hydrocarbon reservoirs are highly complex systems with large heterogeneities and varying conditions. It is common to divide different reservoir models by their size scale (Figure 2.1). The parameters which control fluid flow and determine the possible recovery of petroleum are found at the microscopic scale. These values are normally averaged and represented in larger reservoir- and field scales to simplify calculations and modelling. Therefore, a great understanding of microstructures and their physical properties are required to accurately determine the macroscopic properties of the reservoir media.

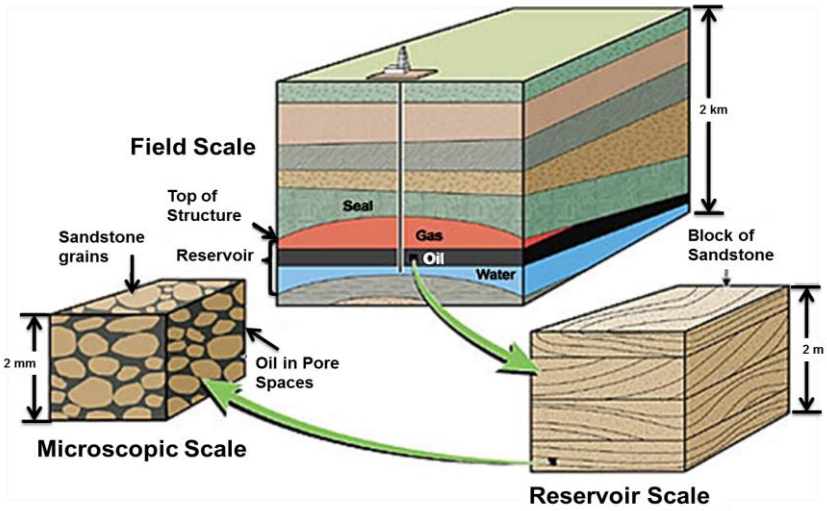

Figure 2.1: Complexity of hydrocarbon reservoir representation (Zitha et al. 2011)

2.1.1 Porosity

Porosity, φ, is defined as the storage capacity of the rock and is considered one of the most important properties of a reservoir. Pores are free spaces or channels in the solid material and porosity denotes the ratio of pore volume, V_p, over the total bulk volume, V_b. Pore volume can be expressed by subtracting grain volume, V_g, from the bulk volume. Porosity can be determined by core analysis and well logging and is expressed in percentage or as a fraction.

Porosity:
$$\varphi = \frac{V_p}{V_b} = \frac{V_b - V_g}{V_b} \tag{2.1}$$

Primary porosity forms during deposition of sediments, while secondary porosity is caused by geological processes like ground stresses, water movement or geological activities that take place subsequent to the formation of the sediment.

Absolute or total porosity takes into account closed pore spaces and is therefore not as interesting as the effective porosity. Effective porosity corresponds to interconnected pores that allow fluid flow through the formation and is a measure of the producible fluids in the reservoir (Torsæter and Abtahi 2003).

Porosity depends on grain- structure, size, sorting and packing (Figure 2.2). It is further affected by compaction, consolidation and cementation. Rocks are compressible under pressure and porosity decreases as compaction pressure increases with depth (Bear 1988).

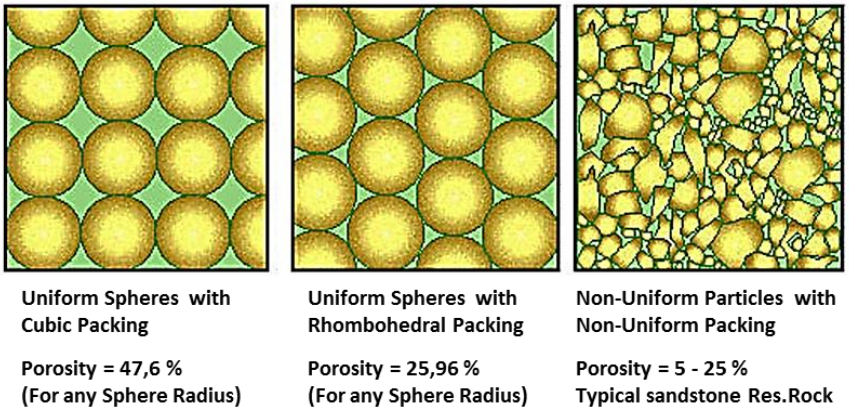

Figure 2.2: Porosity is dependent on grain distribution (www.petroleumonline.com 2012)

2.1.2 Saturation

Saturation, S, is defined as the ratio of a specific phase volume over the total fluid volume in the pores. To estimate a satisfactory approximation of the hydrocarbon volumes in a reservoir, saturations at every point of the reservoir should be known (Torsæter and Abtahi 2003). For the following; w, o and g denotes water, oil and gas respectively.

Phase saturations:

Water: $$S_w = \frac{V_w}{V_p}, \quad (2.2)$$

Oil: $$S_o = \frac{V_o}{V_p}, \quad (2.3)$$

Gas: $$S_g = \frac{V_g}{V_p} \quad (2.4)$$

Summation of saturations: $$S_w + S_o + S_g = 1 \quad (2.5)$$

2.1.3 Surface- and Interfacial Tension

Surface tension, σ, is defined as the contractile tendency of a liquid surface exposed to a gas. The liquid will work to expose a minimum free surface towards the gas, often taking the form of a sphere or droplet. Similarly the interfacial tension (IFT) is defined as the contractile tendency of two or more immiscible liquids in contact and can also be considered a measure of the immiscibility between the fluids. Tensions occur due to molecular properties at the surface or interface which cause an increase of the internal pressure of the fluid. IFT is often denoted for both surface and interfacial tension.

Figure 2.3 illustrates a spherical cap subjected to IFT around the base of the cap and two normal pressures P_1 and P_2 at every point on the surface of the cap. Interfacial tensions cause the sphere to contract, in order to reduce its free surface. If the pressure difference is sufficient the cap will burst or collapse (Torsæter and Abtahi 2003).

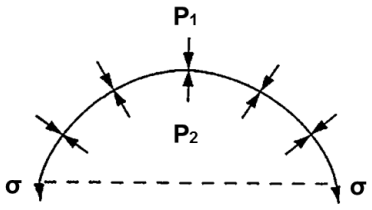

Figure 2.3:Capillary equilibrium of a spherical cap (Torsæter and Abtahi 2003)

2.1.4 Capillary Pressure

Capillary pressure, P_c, is defined as the pressure difference existing between two immiscible fluid phases across the interface that separates them, under capillary equilibrium (Heinemann 2005). The greater pressure will always occur in the non-wetting phase (Terry 2000). The capillary pressure is proportional to the IFT and the wetting angle, and inversely proportional to the effective radius, r, of the interface.

Capillary pressure: $$P_c = P_{non-wetting} - P_{wetting} = \frac{2 \cdot \sigma \cdot \cos\theta}{r} \quad (2.6)$$

The capillary pressure in a porous media is dependent on the chemical composition of the hydrocarbons and solid phase, the fluid saturation and the pore size distribution. Capillary pressure is also a function of saturation history (Torsæter and Abtahi 2003). A typical capillary pressure curve is shown in Figure 2.4.

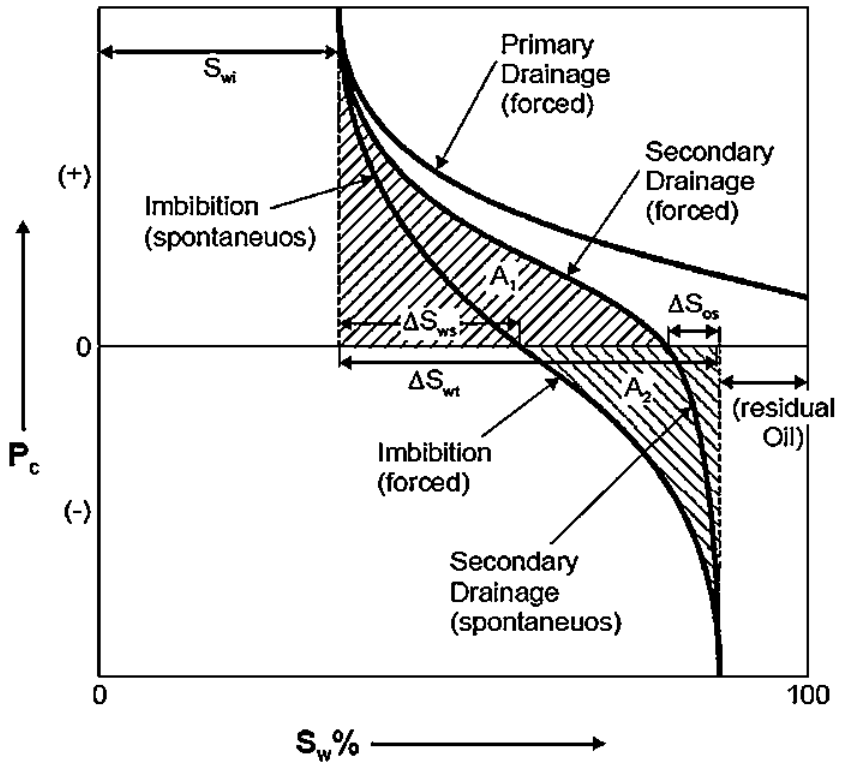

Figure 2.4: Capillary Pressure Curve (Torsæter and Abtahi 2003)

2.1.5 Wettability

Wettability is defined as the ability of a fluid to spread or adhere on a rock surface in presence of another fluid. It is a result of the molecular attractions and repulsions exerted between each fluid and the solid present. Wettability is a measure of what fluid the solid prefer. This is a key parameter in the production of hydrocarbons as it determines the initial fluid distributions in the porous media and plays a major role in flow processes (Heinemann 2005).

The degree of wetting in a matrix-fluid system is dependent on the IFT, σ, between the fluid and the solid surface. It can be measured by the contact angle, θ, which occurs at the fluid-fluid interface on the solid. For θ < 90° the fluid is defined as wetting phase and for θ > 90° the fluid is non-wetting, as illustrated in Figure 2.5. Angles equal to 90° indicates neutral or intermediate wetting and for θ ~ 180° the phase is totally wetting.

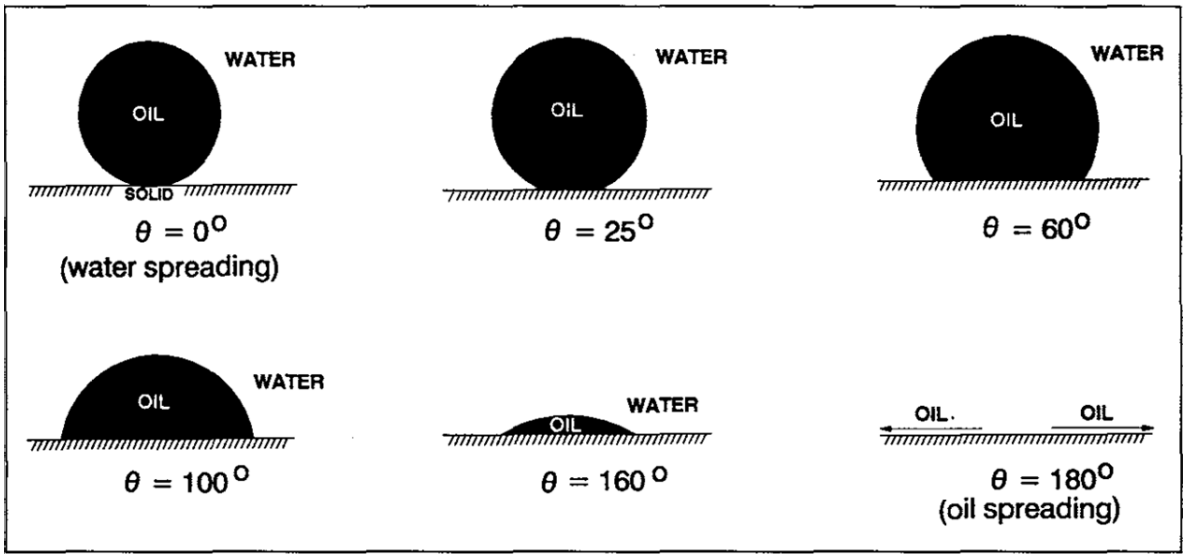

Figure 2.5: Wettability illustrated by examples of contact angles and spreading (Morrow 1990)

Young's equation allows for calculations of the wetting angle when the interfacial tensions are known at a state of equilibrium. l, g and s denote liquid, gas and solid respectively.

Young's Equation: $$\sigma_{lg} \cdot \cos\theta = \sigma_{sg} - \sigma_{sl} \quad (2.7)$$

The wettability of a reservoir will determine how the fluids are positioned in the pore spaces and it governs fluid flow. Figure 2.6 shows three cases with similar saturation conditions. In the water-wet case the water clings to the grains as a film, trapping oil in the center of the pores. The opposite can be seen in the oil-wet case. For mixed-wet situations some surfaces attracts water while some attracts oil. Further, wettability influences the physical behaviour of the reservoir. Capillary pressure, fluid saturation, waterflood behaviour, relative permeability and multiphase flow are strongly related to the wettability (Anderson 1986).

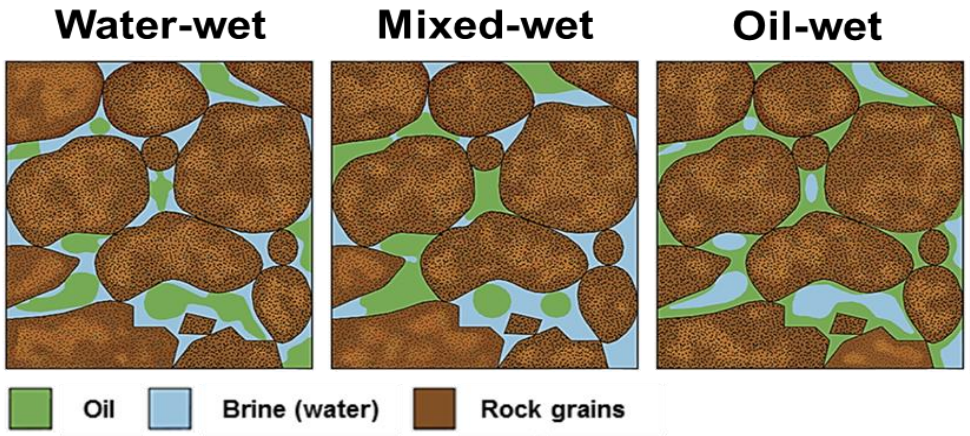

Figure 2.6: Fluid distribution at pore-level for different wettability (Abdallah et al. 1986)

Drainage and imbibition are important concepts in wettability. Drainage describes the process that occurs when the wetting phase is decreasing in saturation, while imbibition is the opposite process where the wetting phase saturation is increasing. If the saturating fluid in the reservoir is non-wetting it will be spontaneously displaced by the surrounding fluid. If not, it will only be displaced if the excess pressure applied to the surrounding fluid is equal to or higher than the capillary pressure for the largest pores (Cossé 1993).

Wettability is dependent on factors such as the mineralogy of the reservoir rock, pore geometry, geological mechanisms, the chemical compositions of the present fluids, pressure and temperature as well as changes in saturation, pressure and compositions during production (Heinemann 2005). The degree of wetting is strongly affected by the adsorption or desorption of polar constituents in the oil phase and the film deposition and spreading capability of the oleic phase (Agbalaka et al. 2008).

Bennett et al. (2004) suggest that surface active components in crude oil, such as phenols, can adsorb on water-wet mineral surfaces in the pore spaces as seen in Figure 2.7. Phenols have low molecular weight and are water-soluble surfactants that allow for heavier hydrophobic petroleum components to access the mineral surfaces over time. This means that, with aging, a water-wet reservoir can be rendered intermediate or oil-wet.

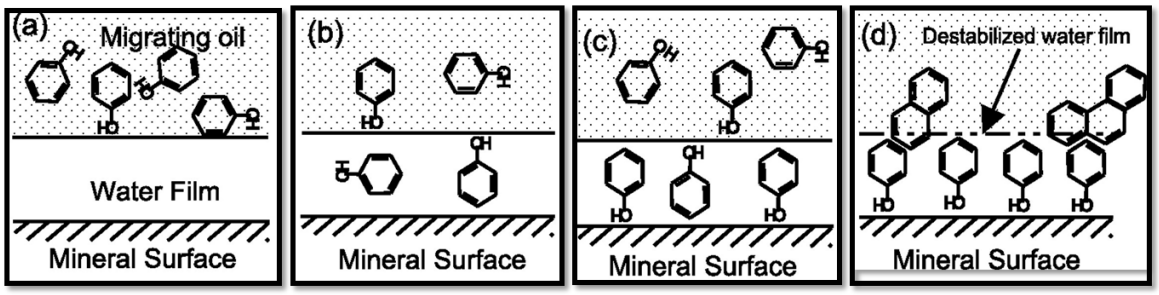

Figure 2.7: Illustration of Wettability alteration on mineral surfaces (Bennett et al. 2004)

a) Phenols in crude oil migrates and contact water film
b) Oil-water partitioning of phenols
c) Oil-water partitioning and adsorption on surface
d) Phenols cause water film disruption and subsequent sorption of higher molecular weight hydrocarbon components

It is much debated what wetting phase is the optimal for recovery of hydrocarbons (Gupta and Mohanty 2011, Morrow 1990) and this divergence in observed results is caused by several modifying factors (Agbalaka et al. 2008);

- Difficulties or constraints in reproducing the original wetting state of the rock
- Lack of unified procedures for collecting, handling and storing cores
- The adopted method for determining the wetting state of the rock

2.1.6 Permeability

Permeability, k, is defined as the ability of a porous media to transmit fluid through interconnected pores (Figure 2.8). This is a tensorial property, which means it is a function of position and pressure. While pressure dependence often is neglected, the variance in position can cause spatially changes in permeability by three or more factors of 10 in a typical formation (Lake 1989).

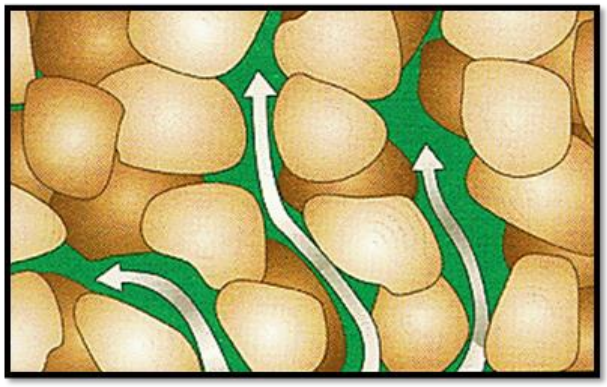

Figure 2.8: Fluid flow through interconnected pores (MPG Petroleum 2003)

Darcy's law describes laminar, one phase, steady-state fluid flow with a volumetric flow rate, Q, through a cross section, A. u is the superficial or apparent velocity of the flow. For a given dynamic fluid viscosity, μ, and a pressure drop, dP, over the length, dx, permeability can be determined (Cossé 1993).

Darcy's Law:

$$\frac{Q}{A} = u = -\frac{k}{\mu} \cdot \frac{dP}{dx} \tag{2.8}$$

The measured permeability, in the considered direction, is the specific or absolute permeability which refers to 100 % saturation of a one-phase fluid. This is rarely the case in reservoir formations and it is therefore necessary to generalise Darcy's law to describe simultaneous flow of more than one fluid.

Effective permeability, k_{phase}, is the transmission of one phase that inhabits less than 100% saturation of the pore space. Relative permeability, $k_{r,phase}$, is the ratio of effective permeability of a phase, in presence of other phases, to the absolute permeability.

Relative permeability: $$k_{r,phase} = \frac{k_{phase}}{k} \tag{2.9}$$

Relative permeability makes it possible to extend Darcy's law to immiscible three-phase, water-oil-gas systems. For a system were water is linearly displacing oil in a thin tube of porous media, where ρ is the phase density, g is the gravitational constant and α the inclination angle, Darcy's law can be expressed by the volumetric flux, q, for each phase;

Volumetric flux, oil: $$q_o = A \cdot \frac{k \cdot k_{ro}}{\mu_o} \cdot \left(\frac{\partial P_o}{\partial x} + \rho_o g \sin\alpha\right) \tag{2.10}$$

Volumetric flux, water: $$q_w = A \cdot \frac{k \cdot k_{rw}}{\mu_w} \cdot \left(\frac{\partial P_w}{\partial x} + \rho_w g \sin\alpha\right) \tag{2.11}$$

The dependence of saturation and saturation history on relative permeability is illustrated by relative permeability curves (Figure 2.9), showing end-point saturations, end-point permeabilities and the drainage and imbibition processes (Torsæter and Abtahi 2003).

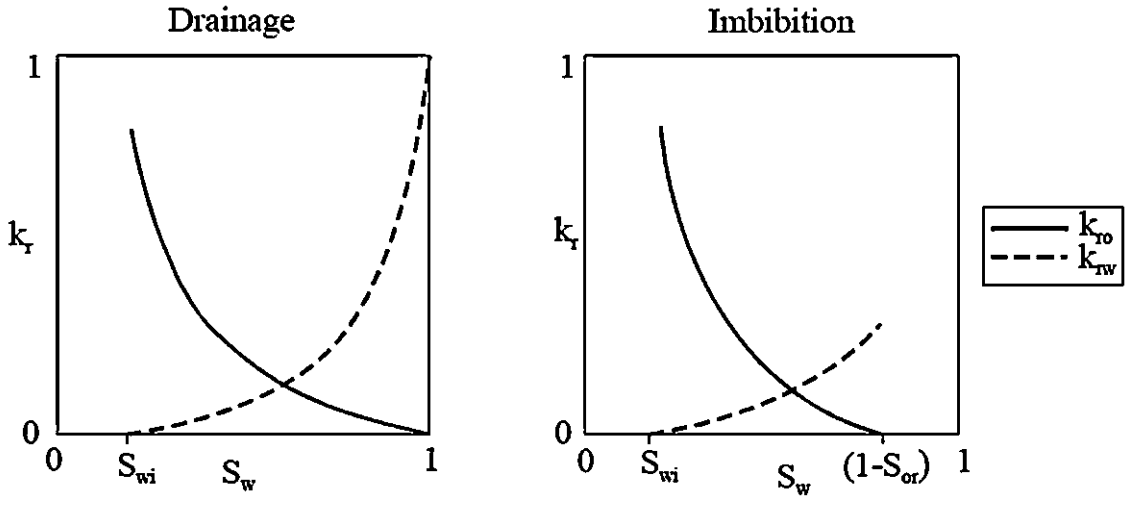

Figure 2.9: Relative Permeability Curves for a typical water-wet system (Torsæter and Abtahi 2003)

2.2 Fluid Properties

Petroleum fluids are highly complex mixtures made up of large amounts of molecules and each mixture behaves differently in various situations due to intermolecular reactions. Nevertheless, it is highly important to understand the phase behaviour of pure components to better understand mixtures. Phase behaviour describes the conditions of temperature and pressure for which different phases of a fluid can exist (McCain 1990) and in reservoir engineering, Pressure-Volume-Temperature (PVT) properties of hydrocarbon fluids are of special interest.

Phase diagrams, as shown in Figure 2.10, are figurative representations of phase changes due to variations in pressure and temperature. Most petroleum reservoir fluids are defined as either "oil" or "gas" and can be described by a two-component phase envelope. The phase envelope is bound on one side by the bubble-point line and the dew-point line on the other. The two lines are joined at the critical point where all the properties of the liquid and gas becomes identical. Determined by the location on the phase diagram, according to temperature and pressure a reservoir fluid can be classified as dry gas, wet gas, gas condensate or oil (Whitson and Brulé 2000).

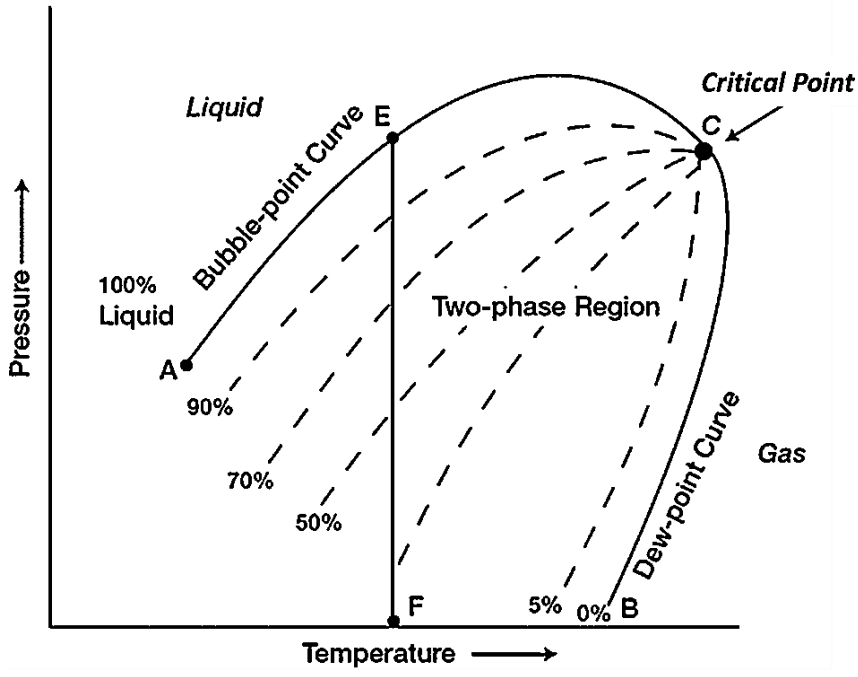

Figure 2.10: Generalized Black Oil Phase Diagram (Ahmed 2006)

2.2.1 Density

Density, ρ, is defined as mass, m, of fluid per unit volume, V. This is a fluid property that generally varies significantly with pressure, P, and temperature, T. It is therefore important to report density together with explicitly stated pressure and temperature. Standard international reference temperature and pressure is 273 K and 1 atm (approx. 0,1 MPa) (Bear 1988).

Density:
$$\rho = \frac{m}{V} \tag{2.12}$$

Specific gravity, γ, is defined as the ratio of the density of a liquid to that of pure water, or the density of a gas over that of air, at a stated temperature.

Specific gravity:
$$\gamma = \frac{\rho_{liquid}}{\rho_{water}} \quad \text{or} \quad \frac{\rho_{gas}}{\rho_{air}} \tag{2.13}$$

The American Petroleum Institute (API) has adopted a hydrometer with a different scale for oils lighter than water, referred to as the API scale.

API scale:
$$°\text{API} = \frac{141{,}5}{\gamma} - 131{,}5 \tag{2.14}$$

2.2.2 Viscosity

Viscosity is defined as a fluid's resistance to yield to shear stress, τ, when the fluid is in motion, or put in other words; the internal resistance of a fluid to flow. The resistance is caused by intermolecular friction exerted when layers of fluids attempt to slide by one another (Torsæter and Abtahi 2003). $\frac{\partial u}{\partial y}$ is the shear rate.

Shear stress:
$$\tau_{yz} = \mu \cdot \frac{\partial u}{\partial y} \tag{2.15}$$

The dynamic viscosity, μ, is the resistance a fluid encounters when it is forced into motion by a moving upper plate at constant velocity, as shown in Figure 2.11. For Newtonian fluids, such as all gases and most simple fluids, this result in a linear fluid velocity profile in the x-direction. The velocity is dependent on the distance from the static lower plate. In these cases the shear stress is proportional to the shear rate.

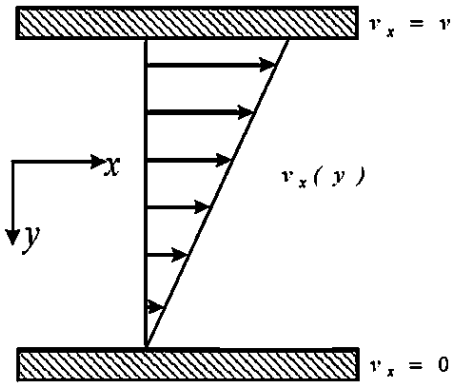

Figure 2.11: Steady-state velocity profile of fluid between two non-slip surfaces **(Torsæter and Abtahi 2003)**

The kinematic viscosity, ν, is defined as the ratio of dynamic viscosity over fluid density.

Kinematic viscosity: $$\nu = \frac{\mu}{\rho} \tag{2.16}$$

Liquid viscosity is generally highly dependent on temperature and varies with pressure only when high pressures are attained. Variations in the viscosity of gases at constant temperature are small until pressures in the order of critical pressure are obtained. For most liquids, except water, viscosity increases with pressure at constant temperature. In most cases though, the effect of pressure on viscosity is neglected.

Temperature causes opposite effects on the viscosity of liquids compares to gases; when the temperature is decreasing the viscosity of gases at low pressure will decrease, while the viscosity of a liquid will increase. This is due to the basic mechanisms of molecular momentum exchange in the fluid (Bear 1988).

2.2.3 Compressibility

Compressibility, β, is defined as the relative change in volume when a constant mass of fluid is subjected to changes in normal pressure or tension.

Compressibility:
$$\beta = -\frac{1}{V} \cdot \frac{dV}{dP} = \frac{1}{\rho} \cdot \frac{d\rho}{dP} \tag{2.17}$$

The negative sign indicates that volume is decreasing as pressure increases. Further, it can be seen that fluid density increases as pressure increases. Fluid compressibility is also a function of temperature and will increase with increasing temperature under constant pressure (Bear 1988). As shown in Figure 2.12 the free movement and spacious arrangement of molecules in a gas makes it highly compressible compared to a liquid, where the molecules are already packed close together (Ebbing and Gammon 2009). The complex composition of petroleum fluids affect compressibility (Dorinson and Ludema 1985). Further, particular molecular structures, such as cyclization, will decrease the rotational freedom characteristics in hydrocarbons and thereby drastically decrease compressibility.

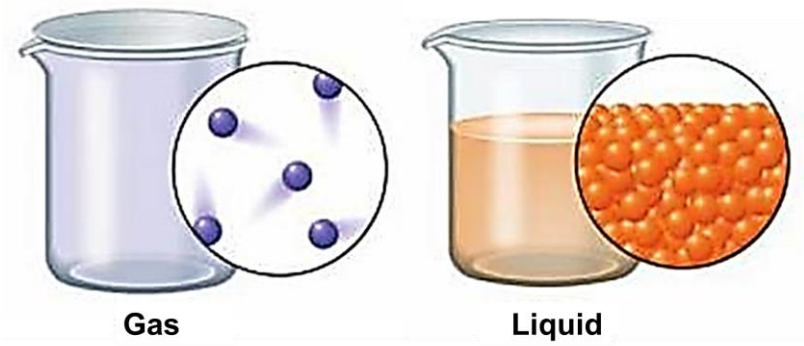

Figure 2.12: Molecular representation of a gas and a liquid (Ebbing and Gammon 2009)

Determination of hydrocarbon compressibility is of great importance for predicting the expected pressure behaviour in the reservoir as well as for calculating the total reservoir volume (Mullins et al. 2002)

.

3 Silica Nanoparticles

"Nano" is the prefix for a billionth, meaning that a nanometer (nm) equals $1 \cdot 10^{-9}$ meter. Nanotechnology is defined as the fabrication, manipulation and application of objects in the size range of 1 to 100 nm (Edwards 2008). What distinguish nanotechnology from other technologies are the unique properties that nanostructures obtain due to their nanoscale proportions. The trend of miniaturization of materials began in the early 60's when utilization and development of the unique structural, optical, mechanical, chemical and thermal properties of nanomaterials became feasible (Choi 1998). Since then, advances in nanotechnology have put on speed and nanostructures and materials are now implemented in several industries, such as medicine, electronics, aviation and the energy sector.

Nanoparticles, or ultrafine particles, have a diameter ranging from 1 to 100 nm and they are invisible to the naked eye. A significant characteristic of nanoparticles is their high surface area to volume ratio, as this scale with the inverse of the particle radius. Due to this quality, nanoparticles exhibit many interesting and sometimes unexpected properties. Nanoparticles are passive nanostructures that represent almost the only part of nanotechnology with current commercial significance (Ramsden 2009).

Silica is the common name for inorganic ceramic materials composed of silicon dioxide (SiO_2) and it is the most abundant mineral in the crust of the earth. Silica atoms are non-metal oxides and consist of four oxygen atoms surrounding one silicon atom in a tetrahedral formation. Material density for silica range between 2,17 - 2,65 g/cm^3 (Lines 2012). The strong, directional covalent bonding within the atom results in very hard materials. However, the structural arrangement of silica atoms varies considerably due to the flexibility of bridging between the atoms (Zumdahl and DeCoste 2012). Silica can be found naturally or produced synthetically and occurs in a wide range of structures, from totally amorphous forms to highly crystalline forms, such as quartz. Silica can be porous or non-porous, anhydrous or hydroxylated (Napierska et al. 2010).

3.1 Production

The wide range of desirable shapes, sizes, structures and functionalities of SNPs opens up for production by a large number of methods, both mechanically and synthetically. What approach to adopt is dependent on which can produce the desired properties, and then on cost (Ramsden 2009). There are two main categories for fabrication of nanostructured systems (Figure 3.1); "top down" and "bottom up" manufacturing (Edwards 2008).

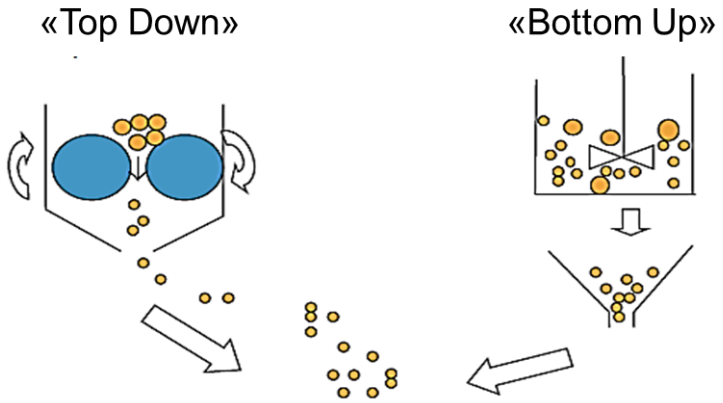

Figure 3.1: "Top Down" and "Bottom Up" production of SNP (Rahman and Padavettan 2012)

3.1.1 "Top down" Production

The "top down" approach utilizes physical methods and suggests that nanostructures can be formed by etching or ultra-miniaturization of larger structures. Machining, lithographic processes and milling are ways to fragment or divide a bulk material, producing a new structure with desired and suitable properties at a nanoscale. Milling is the mechanical alloying or attrition that can be operated in a large scale. Machining and lithographic processes consist of either the use of X-rays, UV-light or electrons and ions to project a given pattern onto a photo-resisting surface. (Brydson and Hammond 2005). Natural mineral silica, such as quartz, tridymite and cristobalite are found in crystalline forms. However, due to the occurrence of metal impurities and other contaminates in natural silica resources, it is not favourable to fabricate SNPs for use in scientific or industrial applications by the "top down" approach (Rahman and Padavettan 2012).

3.1.2 "Bottom up" Production

This approach was suggested by Richard Feynman in 1960. The vision was to fabricate materials at the atomic or molecular scale, using methods of self-organization and self-assembly of the individual building block. Chemical synthesis and a highly controlled deposition and growth of materials under high temperatures can cause an atomic diffusion process that forms a reaction product. Synthesis can be carried out in both solid, liquid or vapour phase. Grain growth inhibitors are necessary to prevent too large grain sizes (Kelsall et al. 2005). Most synthetic silica, such as colloidal silica, silica gels, pyrogenic silica and precipitated silica are highly pure and most often produced as amorphous powder. Reversed microemulsion, flame hydrolysis and sol-gel processes are common methods for chemical synthesising of SNPs (Rahman and Padavettan 2012).

Microemulsions are thermodynamically stable dispersions of two immiscible fluids, such as oil and water. Reversed microemulsion is a method that make use of surfactant molecules dissolved in organic solvents to form spherical micelles. Figure 3.2 illustrates that in the presence of water, the polar head groups organize themselves by self-assembly to form micro-cavities containing water, called reversed micelles (Eastoe, Hollamby, and Hudson 2006).

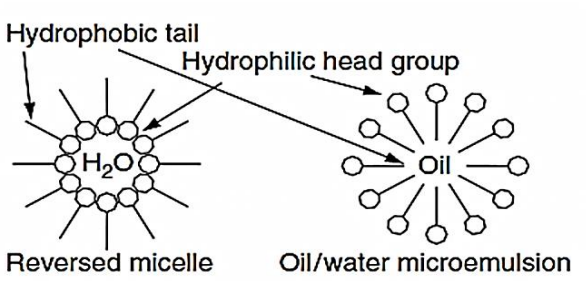

Figure 3.2: Schematic diagram of reversed micelle (Brydson and Hammond 2005) and micro-emulsion of SNPs

SNPs can be grown inside these micro-cavities by carefully controlling the addition of silicon alkoxides and catalyst into the medium containing the reversed micelles. Eastoe, Hollamby, and Hudson (2006) found that particle growth is strongly dependent on intermicellar exchange rates. The particle size appears to be determined by concentrations, the employed type of solvent and surfactants, ionic additives and the

molar ratio. Although this method is associated with high costs and difficulties removing the surfactants from the final product, it provides a way of synthesising monodisperse nanoparticles in a controlled matter.

Flame hydrolysis, also known as Chemical Vapour Deposition (CVD) is the prominent method for commercial production of SNPs in powder form (Rahman and Padavettan 2012). The approach consists of high temperature flame decomposition of metal-organic precursors. In synthesis of SNPs, a reaction between silicon tetrachloride ($SiCl_4$), hydrogen and oxygen is created over a high temperature burner. Nanosized particles form by coagulation and/or surface reactions of the vaporized solids (Pratsinis 1998). The final product is known as fumed silica, a very versatile material with stable behaviour and hydrophilic properties (Amiri, Øye, and Sjöblom 2009). Disadvantages related to flame hydrolysis are difficulties in controlling particle size, morphology and phase composition.

Sol-gel processes involve hydrolysis and condensation of metal alkoxides or organic salts in the presence of a mineral acid or a base as catalyst. Production of pure and homogenous silica particles under kind conditions makes this approach widely employed. These processes hold the ability to control particle size, size distribution and morphology through systematic monitoring of reaction parameters. Dependent on the reaction conditions the resulting particles will be formed as either spherical or gel networks (See Figure 3.3) (Rahman and Padavettan 2012).

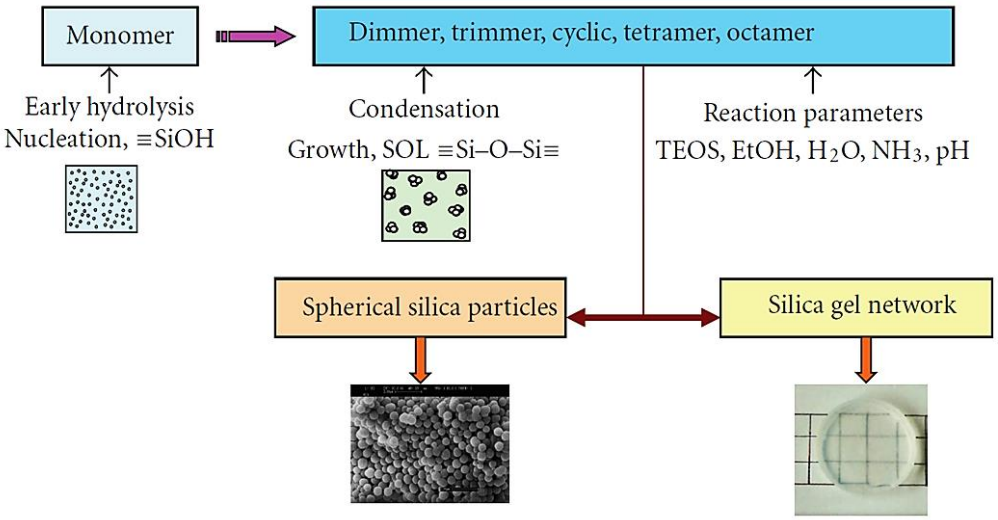

Figure 3.3: Schematic illustration of sol-gel silica formation (Rahman and Padavettan 2012)

3.2 Characteristics and Properties

Silica nanoparticles are water-soluble, non-toxic, odourless particles that can easily be fabricated and modified at low cost (Metin, Bonnecaze, and Nguyen 2012). They are characterized by their very low bulk density, about 0,04 – 0,1 g/cm^3, and a high specific surface area, typically 200 – 300 m^2/g (Napierska et al. 2010). SNPs have a pH in the range of 3-5 (Elkem Silicon Materials 2010).

Material properties are determined by observing the combined effects of a large number of similar particles in a 3D-system. Many material properties are continuously modified as a function of system size. Totally new phenomena occur at the nanoscale and new research is required to predict changes in nanomaterial properties (Kelsall et al. 2005).

3.2.1 Structural Properties

When the particle size is decreased the interatomic spacing is changed as the percentage of available atoms at the surface of the particle is reduced. The lattice structure at the surface of the particle may vary from that of the bulk material (Christian et al. 2008). As a result of the small radius of curvature in a nanoparticle the internal pressure will rise and induce a higher compressive strain that compel the interatomic spacing to increase (Brydson and Hammond 2005). Scanning Electron Microscopes (SEM) can be used to photograph SNPs. Figure 3.4 shows that the morphology can range from amorphous spheres to perfect crystals. Costa, Leite, and Galembeck (2003) observed that morphology and aggregation characteristics of SNPs are strongly related to particle size.

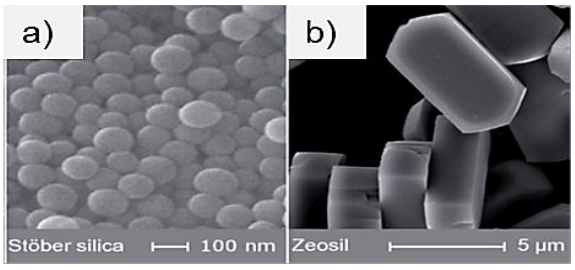

Figure 3.4: SEM - Different morphologies of silica nanoparticles. (Napierska et al. 2010) a) Spherical Stöber silica. b) Crystalline Zeosil

3.2.2 Mechanical Properties

Silica is inherently a brittle material. However, the high surface area to volume ratio of SNPs seems to enhance interface-driven processes such as plasticity, ductility and strain to failure. These mechanical properties are related to the atomic structural arrangement in the material at the nanoscale (Garcia 2010). Toughness is highly dependent on the ease of formation or the presence of defects in the material. When the particle size in a material is decreased so is the ability to support such defects (Brydson and Hammond 2005). Carroll (2009) showed that material strength increases when the grain size is reduced. This phenomenon is explained by considering that fewer dislocations are occurring within a material consisting of a smaller particle size, thus a greater applied stress is needed to break the material.

3.2.3 Chemical Properties

The physical-chemical properties of SNPs are reasonably well known and Paparazzo et al. (1992) found that they have a core structure of SiO_2 but a surface chemistry that is more comparable to a formula of $Si(O)_{(2-x)}(OH)_{(2x)}$. Costa, Leite, and Galembeck (2003) argue that the chemical composition of SNPs is changing with particle size after observing differences in swelling coefficients that strongly depend on the chemical nature of the involved phases. Rate, selectivity, efficiency and control of chemical reactions of particles can be highly improved at the nanoscale (Kelsall et al. 2005).

One of the main advantages of silica nanoparticles is their capacity of chemical functionalization or modification of the surface. Active sites, surface coating or terminal groups can be attached to the SNPs to obtain desired properties. Functionalization of SNPs is commonly used to create very hydrophilic or very hydrophobic particles. They are rendered hydrophilic by covalent grafting of neutral, hydrophilic silane with a hydroxyl group on one end, and hydrophobic by forming Si-O-Si bridges with a sulfonic acid group (Miranda, Lara, and Tonetto 2012).

3.2.4 Thermal Properties

Nanoparticles have increased surface energy compared to bulk material, making them thermodynamically unstable, or metastable (Cao 2004). The pronounced curvature of the particle surface, due to the large ratio of surface area to mass, has an effect on the melting temperature. Figure 3.5 represent how the melting temperature of silicon particles change with changes in particle radius (Carroll 2009).

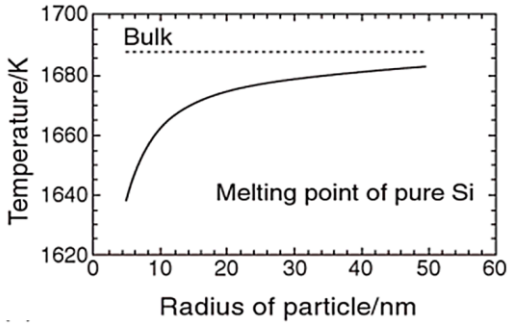

Figure 3.5: Melting point is a function of particle radius (Carroll 2009)

3.2.5 Optical Properties

Particle size plays an important role in changes in optical properties. Figure 3.6 illustrates how suspended SNPs of different sizes and concentrations will reflect light at distinct wavelengths (Zhao et al. 2012). The large surface area to volume ratio affects absorption and scattering of incident light and quantum size effects have been observed experimentally for many nanocrystalline semiconductors. Defects within a nanoparticle can result in nonlinear optic effects (Trindade, O'Brien, and Pickett 2001).

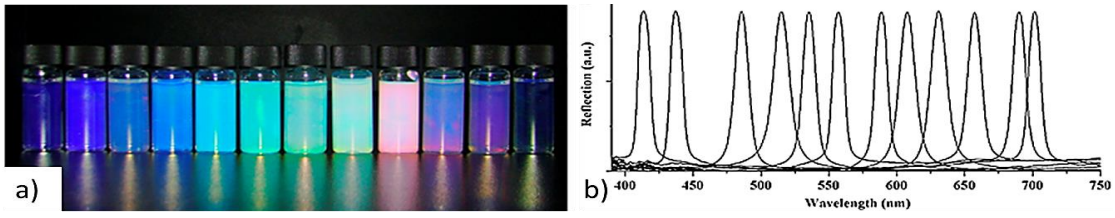

Figure 3.6: a) Optical images and b) characteristic reflection peaks for suspended SNPs of varying particle sizes and concentrations (Zhao et al. 2012)

3.3 Risks, Safety and Environmental Considerations

The effects and impacts of employing nanosilica in existing fields of research is not adequately understood and there is a lack of appropriate risk management framework for this type of research (Yokel and MacPhail 2011). The commercialisation of nanotechnology has pushed the rate at which new materials and products are developed. However, research on how they impact on human health, safety and the environment has not seen the same advance.

3.3.1 Nanotoxicity

Nanotoxicology refers to the study of how nanostructures interact with biological systems. It emphasise to illustrate the way physical and chemical properties of nanostructures relates to the induction of toxic biological responses (Fischer and Chan 2007). The fine size of a silica nanoparticle makes it small enough to penetrate almost any substance. Toxicity-studies in rats demonstrate that exposure to SNPs produce enhanced toxicity responses when compared with larger-sized particles of similar composition. Particularly, inhalation of nanoparticles cause lung toxicity (Figure 3.7), as depositions in the alveolar regions of the lung results in inflammations (Warheit 2008). However, according to the World Health Organization and the US Department of Agriculture, amorphous SNPs are considered safe for humans (Barik, Sahu, and Swain 2008).

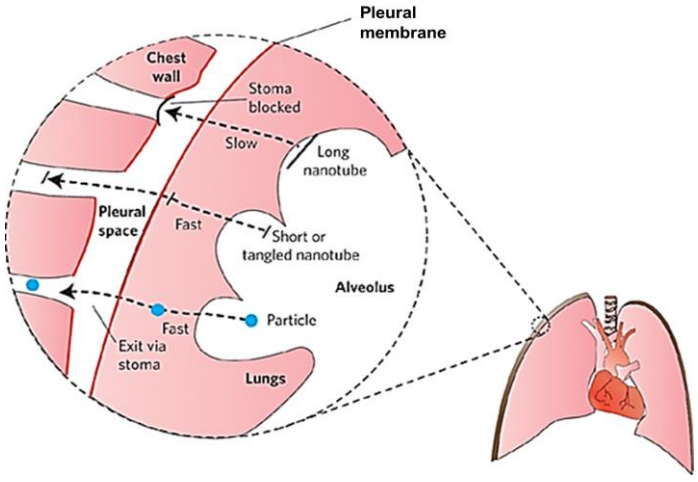

Figure 3.7: Movement of nano-materials through the lung (Donaldson and Poland 2009)

3.3.2 Occupational Health and Safety

Laboratory environments that work with preparation of nanoscale systems require a high degree of environmental control. As a result of the small size of nanomaterial systems, they are vulnerable to even the smallest levels of contamination. Due to the fact that nanoparticles are capable of penetrating through biological matter, precautions must be taken at workplaces that utilize nanomaterials. Great care should be taken when handling or breathing in environments that involve manufacturing of and work with nanoparticles. Special care must also be taken when storing and transporting nanomaterials due to higher chemical reactivity (Brydson and Hammond 2005).

Given the potential health concerns and the uncertainties related to silica nanomaterials, all workplaces in contact with such materials should implement health surveillance and medical monitoring. Controlling of exposure and protection of workers through appropriate protective equipment and procedures must be a priority (Schulte et al. 2008). Gloves, protective glasses and a filtered mask should be worn during direct handling of silica nanoparticles.

3.3.3 Environmental Concerns

Silica nanoparticles are naturally occurring in the environment and exist stably in nearly all components of the Earth. Nature is costumed to these particles and they play important roles in natural chemical characteristics and processes. Nevertheless, the introduction of manufactured SNPs can disrupt or alter these processes and cause destructive outcomes (Wigginton, Haus, and Hochella Jr 2007). Adams, Lyon, and Alvarez (2006) found in their study that nanosized silica in high concentrations show antibacterial activity in the presence of light. The high surface area to volume ratio of SNPs can make them very reactive or catalytic and thereby make them environmentally harmful (Christian et al. 2008). Wigginton, Haus, and Hochella Jr (2007) argue that an important way to understand the consequences of dispersing synthetic silica nanoparticles in the environment is to closely monitor the behaviour of naturally occurring nanoparticles.

4 Experimental Procedures and Apparatus

This chapter will cover the laboratory setup that was needed to carry out this thesis. Experiments were conducted at the Institute of Petroleum Technology, NTNU. All tests were conducted in room temperature with equipment available in the student laboratory.

4.1 Rock, Nanoparticles and Fluids

4.1.1 Rock

The cores used in these experiments were Berea Sandstone from a quarry in the US. All cores were drilled from the same slab and should exhibit similar properties (Figure 4.1). Berea sandstone is a sedimentary rock known for its good porosity and permeability, making it well-suited as a reservoir rock. It is a relatively homogenous rock with well-sorted and well-rounded predominately quartz grains. Minor amounts of feldspar, dolomite and clays also occur (Øren and Bakke 2003). Clean sandstones are commonly water-wet due to stronger molecular forces between quartz grains and water than between quartz and oils.

Figure 4.1: 16 numbered Berea sandstone core plugs

4.1.2 Nanoparticles

AEROSIL® 300 from Evonik Industries is > 99,8 wt.% pure, strongly hydrophilic, monodispersed, spherical fumed silica (SiO_2) nanoparticles. The specific surface area is 300 ± 30 m^2/g and the average particle diameter is 7nm.

AEROSIL® R106 from Evonik Industries is manufactured on the basis of AEROSIL® 300 and is rendered strongly hydrophobic by a silane; Octamethylcyclotetrasiloxane (D4). A deacidification process is further used to receive a product with very low residual chloride content. This is a monodispersed, spherical fumed silica with a specific surface area of 250 ± 30 m^2/g. The average particle diameter is 7nm (Evonik 2012).

4.1.3 Oil

Refined oil, n-Decane ($C_{10}H_{22}$) was used in these experiments due to its accessibility in higher volumes. This is a colourless, alkane hydrocarbon that is nonpolar and does not dissolve in polar liquids, such as water. A red colouring agent was added for identification during testing. n-Decane will from here on out generally be referred to as the oil.

4.1.4 Solvents

A synthetic 3,0 wt. % brine solution was prepared by mixing distilled and deionized water with sodium chloride (NaCl) and stirred thoroughly with a magnetic stirrer.

Absolute alcohol or ethanol (C_2H_8O) with low water content is a volatile, flammable and colourless liquid. It is commonly used as a solvent for laboratory and industrial applications where water will be immiscible or react with other chemicals.

4.1.4 Nanofluids

A nanofluid (NF) is a stable and diluted suspension of nanoparticles in a solvent (Figure 4.2). As seen in Table 4.1, six NFs were prepared with three different concentrations for each type of SNPs. All solutions are mixed by weight percentage (wt. %)

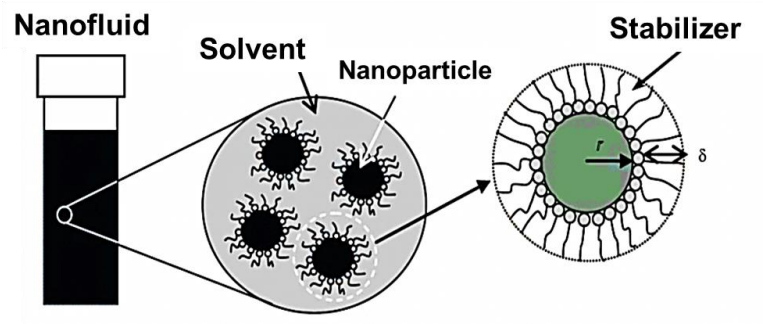

Figure 4.2: Schematic representation of a nanofluid (Bucak 2011)

Table 4.1: Prepared nanofluids

Nanoparticle	Nanofluid concentration
Hydrophilic	0,01 wt.%
	0,1 wt.%
	0,5 wt.%
Hydrophobic	0,01 wt.%
	0,1 wt.%
	0,5 wt.%

Hydrophilic SNPs were suspended in 3 wt. % brine and these solutions will be referred to as hydrophilic NFs. Hydrophobic SNPs were suspended in absolute ethanol and these solutions will be referred to as hydrophobic NFs. Each solution was mixed well with a magnetic stirrer for several minutes before applying an ultrasonic processor for up to ten minutes to assure complete suspension. To avoid possible settling and agglomeration of particles the nanofluids were prepared within the same week of usage.

4.1.5 Density, Viscosity and pH

Densities of brine, oil and nanofluids were measured using a pycnometer. This accurately made flask can be filled with a precisely known volume of liquid. The difference in weight of the empty flask and the weight of the filled flask is divided by the volume to determine the density.

Pycnometer density:

$$\rho_{fluid} = \frac{m_{filled\ pycnometer} - m_{empty\ pycnometer}}{V_{Pycnometer}} \quad (4.1)$$

Viscosities were measured with a capillary viscometer, also known as an Ubbelohde viscometer. This U-shaped glass tube consists of a narrow bore (the capillary) on one side with a container bulb above and two measuring bulbs with known volume on the other. Fluid flows from the container bulb down through the capillary tube and up the other side due to gravitational forces. The time it takes for a fluid to pass between marks above and below the measuring bulbs are multiplied with a conversion factor, K, exceptional for each bulb. The obtained value is the kinematic viscosity, ν, of the fluid in Stokes.

Average kinematic viscosity:

$$\bar{\vartheta}_{fluid} = \frac{K_1 \cdot (t_1 - corr.) + K_2 \cdot (t_2 - corr.)}{2} \quad (4.2)$$

The average kinematic viscosity from the two bulbs is multiplied with fluid density to attain the dynamic viscosity, μ, in centipoise. Three different viscometers with different conversion factors and capillary sizes were utilized for measuring fluid viscosity.

Dynamic viscosity:

$$\mu_{fluid} = \bar{\vartheta}_{fluid} \cdot \rho_{fluid} \quad (4.3)$$

pH of the aqueous liquids were measured by a Metromh 827 pH-meter which gives an exact measurement of 0,001 pH. Fluid temperatures are also measured accurately at the same time.

4.2 Cleaning and Preparing Core Samples

Considering that the cores were not drilled from an actual reservoir they should initially be relatively clean and without residual hydrocarbon fluids. However, cleaning and drying of some core plugs were done to become familiarized with the equipment. Cleaning of cores are done to remove any fluids or particles present, in order to correctly measure porosity and permeability. Another reason for core cleaning is to restore the initial wettability of the core after contamination during drilling and handling (Gant and Anderson 1988). Several methods can be used to clean core plugs, such as solvent injection/extraction, Dean Stark and Vacuum distillation. For this case it is not necessary to measure any initial saturation so the Soxhlet Extraction method was used.

Soxhlet Extraction

The Soxhlet apparatus is the most commonly used method for cleaning cores in the laboratory and provides a simple and gentle distillation of the fluids and salts within the core plug. The process can be slow, ranging from several days to several weeks, depending on the properties of the pore fluids and the rock permeability (Torsæter and Abtahi 2003). Other disadvantages are the fact that solvent may not contact all pores in the core due to small pore throats and occasionally the solvent can cause alterations in wettability (Gant and Anderson 1988). Different types of solvents are used according to the fluids being removed and it is important that the solvent employed is not reacting with the minerals in the core. For cleaning out oils it is common to use toluene as solvent. In this case the core plugs were initially oil-free and methanol was used to remove any salt or interstitial water.

Figure 4.3 illustrates the Soxhlet apparatus used. Four Berea sandstone plugs were placed in the thimble. Methanol was heated in the Pyrex flask and kept at a boiling temperature of 64,7°C (Sigma-Aldrich 2013). The vapour rose up through the sidearm of the apparatus before continuing up into the condenser. Warm methanol started to drip down onto the cores, soaking them. Methanol, dissolved salts and some interstitial water were collected in the siphon which periodically self-emptied into the Pyrex flask due to gravitational forces. The methanol was then be reheated and the cleaning circle continued.

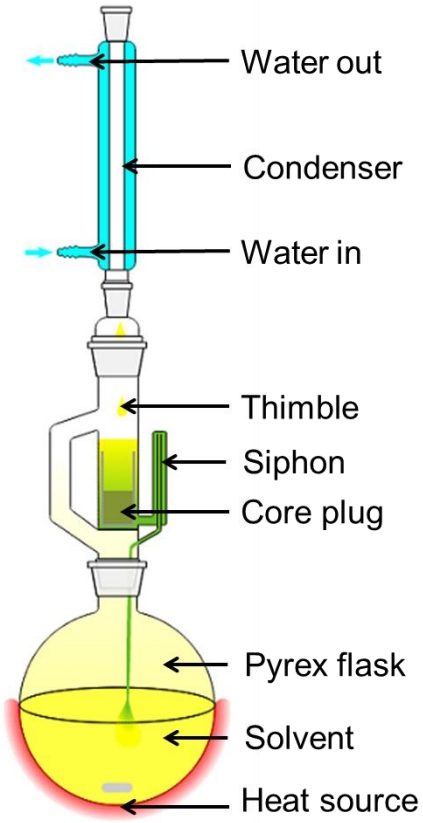

Figure 4.3: Soxhlet apparatus (Harwood and Moody 1989)

After cleaning, the cores were dried in an oven with controlled humidity to prevent damage due to boiling or desiccation of clays. Removal of any residual solvent or interstitial water must be done without altering the minerals in the core, such as clay. The drying temperature was set to 60 °C and the cores dried for approximately 4 days.

4.3 Porosity Measurements

Core analysis provides simple determination of porosity as no assumptions are needed about elements such as mineral composition or borehole effects. By measuring two out of three quantities, bulk volume, pore volume or grain volume, porosity can easily be determined by equation (2.1). A drawback is that a core plug represents a smaller rock volume than what can be reached by a logging tool. Therefore the porosity values gathered from well testing are usually more accurate than from core analysis in heterogeneous reservoirs (Torsæter and Abtahi 2003).

4.3.1 Dry Weight and Bulk Volume Measurements

The dry weight of the core plug is an important parameter as it allows for porosity calculations as well as further density and saturation determinations. A scale with the precision of 0,01g was used to weigh all 16 core plugs.

For core plugs of non-geometric shapes, bulk volume is normally determined by observing the displaced volume of a fluid with known density with a plug immersed in the fluid. The fluid must be prevented from entering the pore spaces of the rock, either by coating the plug, fully saturate the it with the same fluid in advance or by using mercury. In volumetric procedures the displaced volume of fluid is used directly to calculate the bulk volume. In gravimetric determination the loss in weight of the plug immersed in a fluid or the change in weight of a pycnometer with and without the plug is observed.

Due to the uniform cylindrical shape of the given core plugs, bulk volume were computed by measuring the diameter, d, and height, h, of each core (See Figure 4.4). The bulk volume of a cylinder is given by;

Bulk volume of cylinder:

$$V_b = \pi \cdot \left(\frac{d}{2}\right)^2 \cdot h \qquad (4.4)$$

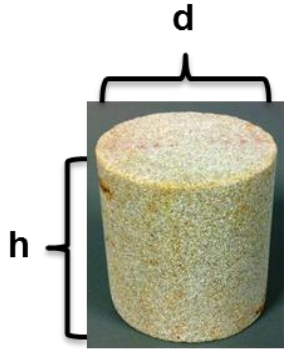

Figure 4.4: Bulk volume

4.3.2 Helium Porosimeter

Pore and grain volume can be determined by using the principle of helium expansion and employing Boyle's law (4.5) on a closed system under isothermal conditions. This method yields the effective porosity of the matrix. Helium is preferred due to its small molecules that quickly penetrate even small pores and the high diffusivity allows for porosity measurements of low permeability rocks. Further, helium is an inert gas and does not adsorb on the rock surface. Under normal pressures and temperatures for testing it can be considered an ideal gas, simplifying calculations (Torsæter and Abtahi 2003).

Boyle's Law:
$$P_1 \cdot V_1 + P_2 \cdot V_2 = P \cdot (V_1 + V_2) \tag{4.5}$$

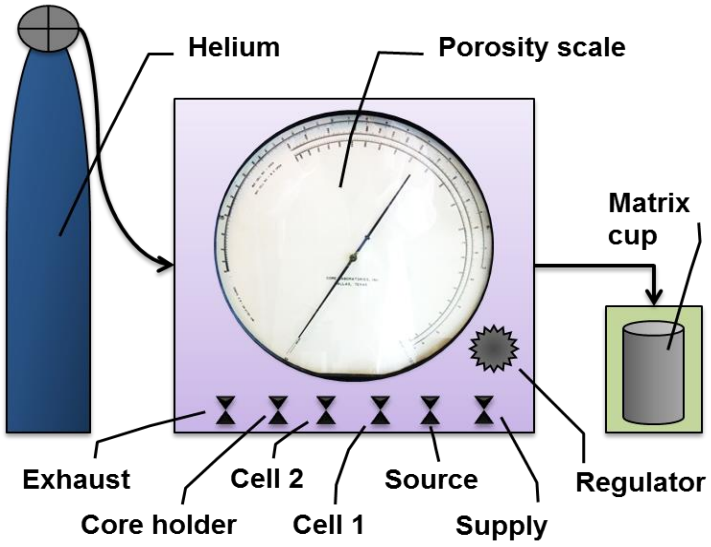

Figure 4.5: Schematic of Helium Porosimeter

A schematic of the helium porosimeter is shown in Figure 4.5. The grain volume, V_g, of each core plug is determined by the difference in volume of an empty matrix cup, V_1, and the matrix cup filled with the core plug, V_2. Helium supply at a predetermined pressure, P, was used and the volumes can be read directly from the scale. Porosity was then calculated by the following equation;

Effective Porosity:
$$\varphi = \frac{V_p}{V_b} = \frac{V_b - V_g}{V_b} = \frac{V_b - (V_1 - V_2)}{V_b} \tag{4.6}$$

4.4 Permeability Measurements

Permeability can be determined by passing a fluid of known viscosity through a core plug of known dimensions. For laminar flow, with a measured flow rate is and recorded pressure drop, Darcy's law (2.8) can be used. Various methods are used depending on core size, shape and consolidation, type of fluids used, available pressure and the permeability range (Torsæter and Abtahi 2003).

Constant Head Air Permeameter

This is one of the most common methods for permeability testing on clean and dry core plugs in the laboratory. Air is used as flowing fluid as it reaches steady state rapidly, it will not alter the minerals in the rock and it is easy to obtain 100 % fluid saturation.

Figure 4.6 illustrates the air permeameter setup. Air is run through the system and regulated by two reduction valves on each side of the Hassler cell, where the core plug is placed. Manometers show the pressures P_1 and P_2 before and after the cell and the air flow rate, Q, can be read from the flow meter.

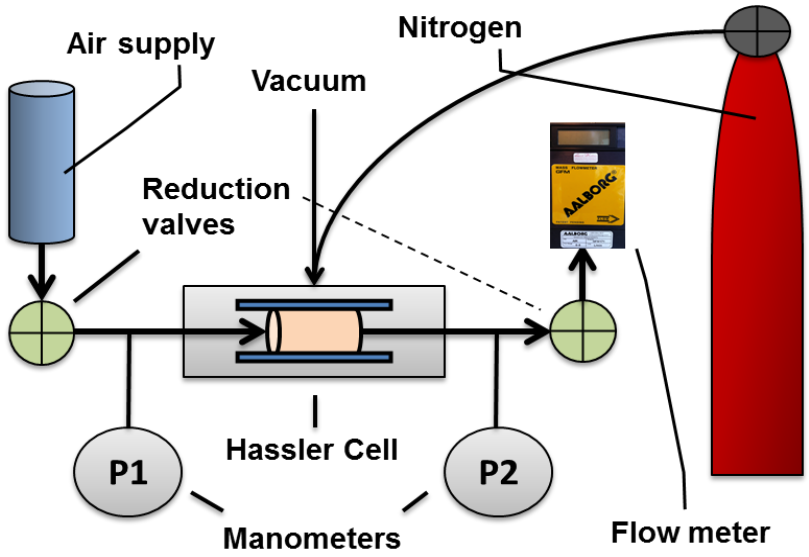

Figure 4.6: Schematic of Constant Head Air Permeameter

The Hassler cell (Figure 4.7) is a core holder fitted with a flexible rubber tube and an external pressure inlet connected to a nitrogen tank. These features give the cell excellent tightness, options for higher ΔP across the cell and the possibility of measuring cores of different sizes (Torsæter and Abtahi 2003).

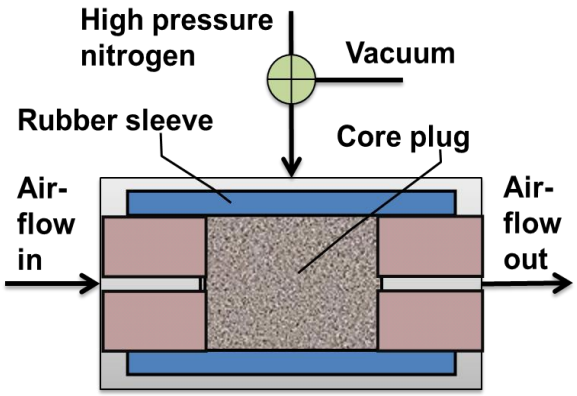

Figure 4.7: Schematic of Hassler cell

Each core plug were placed in the Hassler cell and surrounded by a sleeve pressure of approximately 15 bar. In that way it was made sure that the air flow through the core only happened in the longitudinal direction. The upstream and downstream reduction valves were adjusted to maintain a constant pressure drop, ΔP = 0,4 bar, and to provide laminar flow through the length, L, of the core. Four measurements were taken for each core and the air permeability, k_{air}, was calculated using equation (4.7)

Air Permeability:
$$k_{air} = \frac{2 \cdot Q_{atm} \cdot \mu_{air} \cdot L \cdot P_{atm}}{A \cdot (P_1^2 - P_2^2)} \quad (4.7)$$

Where μ_{air} = 0,0179cp and P_{atm} = 1,01bar at room temperature.

A plot of the air permeability vs. the mean pressure, P_m, is used to find the Klinkenberg constant and the absolute permeability for each core.

Mean Pressure:
$$P_m = \frac{P_1 + P_2}{2} \quad (4.8)$$

4.5 Saturating / Flooding of Cores

12 core plugs were chosen for the main experiment and they were paired up as seen in Table 4.2 according to similarities in porosity and permeability. The remaining four core plugs were taken out for initial wettability testing.

Table 4.2: Flooding setup

Core type	SNP type	Pair	Core nr	Nanofluid concentration
Water wet Berea sandstone	Hydrophilic SNP	Pair 1	# 1	0,01 %
			# 7	0,01 %
		Pair 2	# 3	0,1 %
			# 12	0,1 %
		Pair 3	# 4	0,5 %
			# 8	0,5 %
	Hydrophobic SNP	Pair 4	# 5	0,01 %
			# 14	0,01 %
		Pair 5	# 11	0,1 %
			# 13	0,1 %
		Pair 6	# 15	0,5 %
			# 16	0,5 %

First the cores were saturated with their assigned nanofluid by use of a vacuum pump (Figure 4.9) and further they were soaked in the nanofluid in beakers for a week. The beakers were placed in an oven at 80°C for a short while to enhance retention. The solvents, especially ethanol, started to evaporate and the nanoparticles clogged together in the highest concentrations, so they were placed back in room temperature.

A flooding pump (Figure 4.8) was used to force nanofluids through the cores in order to obtain fully saturated cores and to secure a dispersed adsorption of particles. The two cores in each pair were placed in the Hassler cell in series with a sleeve pressure of about 15 bar. Paraffin was pumped into a piston cylinder filled with a nanofluid in the other end. All the air in the system was pumped out before the Hassler cell was connected to the system. A steady rate of 2 ml/min was applied for about half an hour while manually monitoring the pump pressure. After flooding, all cores were put in the oven at 60°C to dry for 2 days.

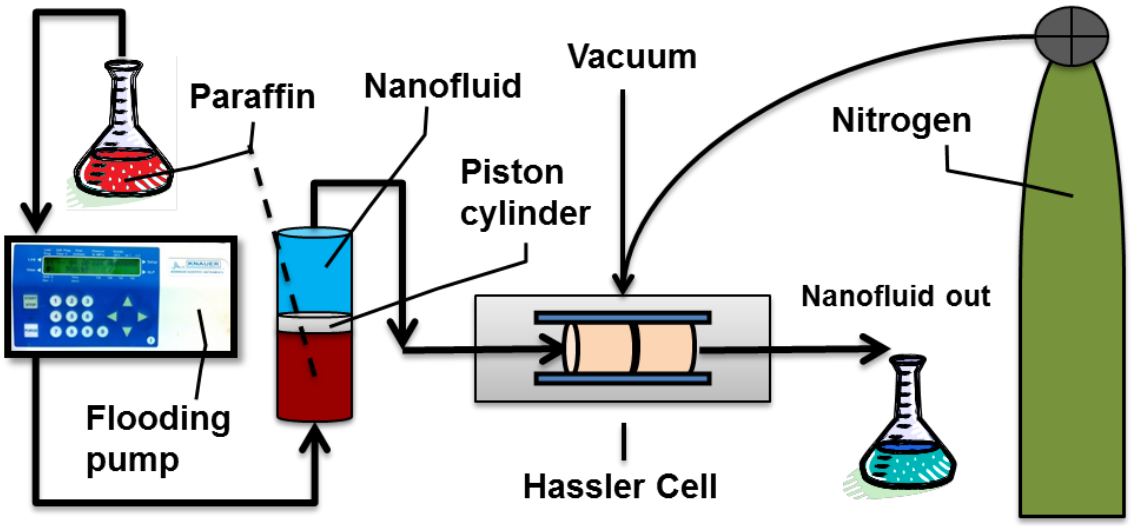

Figure 4.8: Schematic of flooding pump apparatus

4.6 Wettability Measurements

Wettability is difficult to measure in situ but it can be determined by several methods in the laboratory. To obtain representative information on reservoir wettability by experimental procedures some conditions have to be fulfilled (Torsæter and Abtahi 2003);

- Surface properties of the rock should not be damaged.
- The entire wetting range, from very water wet to very oil wet, should be differentiated.
- Results should include the effects of micro-heterogeneities of the rock
- Results should not be dependent on parameters such as rock permeability and fluid viscosity unless these parameters can be isolated
- Results should be reproducible both with respect to a given core sample and also between different cores having the same rock properties.

The Amott-Harvey method with centrifuging was picked to measure wettability in this thesis; although a wide range of procedures are available. Petrographic microscopes or Scanning Electron Microscopes (SEM) fitted with environmental stages can be used to measure wetting angles on small rock samples by direct observation. It can be quite hard to get good data from this type of measurement and the accuracy is low (Glover 2011). Nuclear Magnetic Resonance (NMR) can be used to see changes in longitudinal relaxation time and it allows for measurements of the rate of imbibition (Freedman et al. 2003, Perez Carrillo et al. 2010).

The US Bureau of Mines (USBM) has developed a centrifuge test where the core plugs spins at stepwise increasing speeds. The displaced fluid volume is recorded as a function of the force required to overcome the capillary forces in the pore spaces (Abdallah et al. 1986). This is a rapid method that employs native fluids without being dependent of the oil viscosity. The USBM centrifuge test is a better physically and mathematically grounded test than the Amott-Harvey method but it were not chosen for these experiments due to limited availability and operational difficulties.

Amott-Harvey Method

The Amott-Harvey method utilizes imbibition and drainage in a two-fluid system to measure wettability. Four core plugs plus one extra were chosen for initial wettability testing and the rest of the cores were tested after nanofluid flooding and drying. The clean and dry core plugs were first saturated with oil in a vacuum pump setup (See Figure 4.9). The cores were placed in a beaker inside the vacuum chamber and the valve at the fluid holder was closed. The vacuum pump creates an under-pressure of approx. 100 mbar to extract all fluids from the system. The valve connected to the pump was closed before gently opening the fluid valve. When the core plugs were completely soaked in oil all valves were closed and the cores were left to saturate for 30-60 minutes.

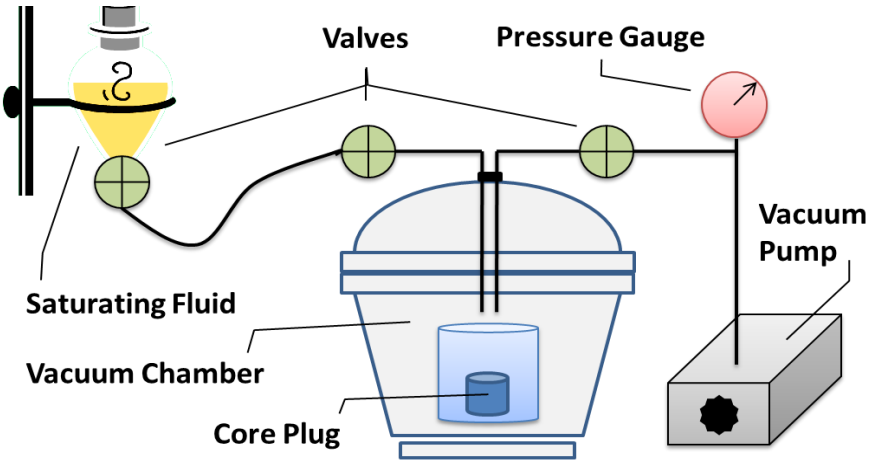

Figure 4.9: Vacuum pump setup

When the cores were properly saturated they were placed in imbibition cells surrounded by brine, as seen in Figure 4.10 a). Brine imbibed into the core plug and oil started to seep out, ascending to the graded cylinder at the top of the cell. The displaced volume was regularly noted to keep track of the rate of imbibition. After approximately 4-5 days, when equilibrium was reached, the total volume of oil was recorded. Then the cores were taken out of the cells, quickly dried off and weighed. Each core was placed in a centrifuge holder, surrounded by brine. Three holders could be centrifuged at one time and each holder were carefully weighed and replenished with brine to get the exact same weight. The centrifuge allows for a weight difference of < 0,03g between the three holders in order to be balanced and able to spin straight.

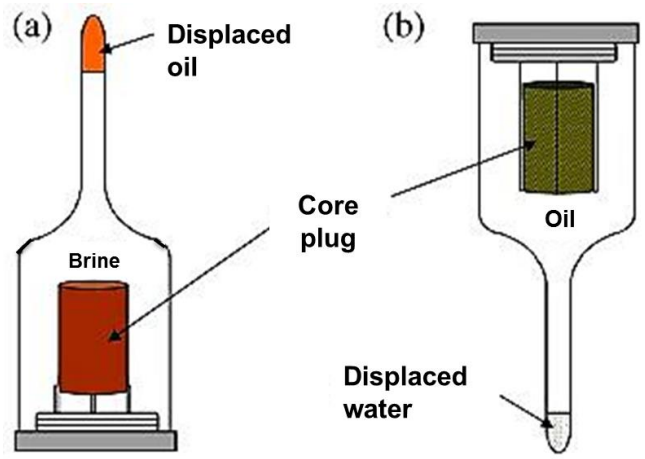

Figure 4.10: Amott cells; (Afrapoli et al. 2009)
a) Imbibition of water. b) Drainage of water

The centrifuge was set to 3000 rounds per minute (RPM) for approximately one hour to force the remaining oil down to residual saturation. Then the cores were taken out, quickly dried off and weighed again. The difference in weight before and after the centrifuge was divided by the density difference between brine and oil to find the displaced volume of oil for each core. At this point all cores were saturated with brine at residual oil saturation. They were placed in drainage cells, as seen in Figure 4.10 b), and surrounded by oil for 6-7 days to allow for spontaneously drainage. Forced drainage by centrifuge was not applied as no brine was drained from the cores in the drainage cells.

The Amott-Harvey wettability index (WI) was calculated using equation (4.9), where V_{o1} and V_{o2} represent spontaneous and forced imbibition volumes. V_{w1} and V_{w2} represent spontaneous and forced drainage volumes. r_w stands for the ratio of oil displaced by brine and r_o stands for the ratio of brine displaced by oil.

Amott-Harvey Wettability Index:

$$WI = \frac{V_{O1}}{V_{O1}+V_{O2}} - \frac{V_{W1}}{V_{W1}+V_{W2}} = r_W - r_O \qquad (4.9)$$

The Amott-Harvey WI will be a number between -1,0 and 1.0 where;

- WI = 0,3 - 1,0 → Completely water-wet
- WI = 0,0 → Neutral-wet
- WI = -1,0 - -0,3 → Completely oil wet

4.7 Contact Angles

Another conventional way to measure rock wettability is by determining the contact angle, θ, at the interface between the surface and fluids involved. The adhesion tension, A_T, which is a function of the IFT determines the wetting preferences of the solid.

Adhesion tension: $$A_T = \sigma_{so} - \sigma_{sw} = \sigma_{wo} \cdot \cos\theta \quad (4.10)$$

Where so, sw and wo denotes solid-oil, solid-water and water-oil tensions respectively.

Imaging Method

Contact angles, θ, can be measured by a variety of methods, such as by tilting plate method, capillary rise method and Wilhelmy gravitational method. However, the imaging method is commonly used as it measures the contact angle directly for a drop of liquid on a solid plate surrounded by an immiscible fluid of lower density.

By definition the contact angle is measured through the denser liquid, which in this case would be the brine solutions. However, since most of the oil used in the previous experiments was coloured red and would be reused for testing of contact angles most tests are carried out with drops of the less dense fluid in the denser. However, difficulties in obtaining stable and trustworthy results led to the decision of measuring hydrophilic SNPs through both the oil and the brine. This way the obtained results could be compared to see whether they correspond with each other. Owing to the fact that absolute ethanol is miscible in both water and oil, hydrophobic SNPs were suspended in oil to see how they influence the contact angle of the oil in contact with brine. Three different concentrations were prepared; 0,01 wt. %, 0,1 wt. % and 0,5 wt. %. This oil was also red and tests were only conducted on drops of oil in water. The full overview of conducted imaging tests is given in Table 4.3.

Table 4.3: Contact angle measurements by imaging method

Nr	Drop	Surrounding fluid
1	Oil	Brine
2	Oil	0,01 wt. % hydrophilic NF
3	Oil	0,1 wt. % hydrophilic NF
4	Oil	0,5 wt. % hydrophilic NF
5	Brine	Oil
6	0,01 wt. % hydrophilic NF	Oil
7	0,1 wt. % hydrophilic NF	Oil
8	0,5 wt. % hydrophilic NF	Oil
9	0,01 wt. % hydrophobic NF	brine
10	0,1 wt. % hydrophobic NF	brine
11	0,5 wt. % hydrophobic NF	brine

The imaging method setup is illustrated in Figure 4.11 showing a glass cell container located between a light source and a magnifying camera. A glass plate, representing sandstone, were placed on poles in the cell and surrounded by one of the liquids. A small drop of the liquid to be measured through was placed either underneath or on top of the glass plate, depending on the densities of the two liquids, using a syringe. The camera magnified the drop and presented an image on the connected computer. Adjustments and calibrations were out manually to get a clear and focused image of the drop and surface before recording 60 frames over 1 hour. The software Attension Theta measured the dimensions of the drop and employed the found values in contact angle calculations. A mean value between the contact angles on the left and right side of each image were calculated. Then an overall mean contact angle was calculated for the entire experiment.

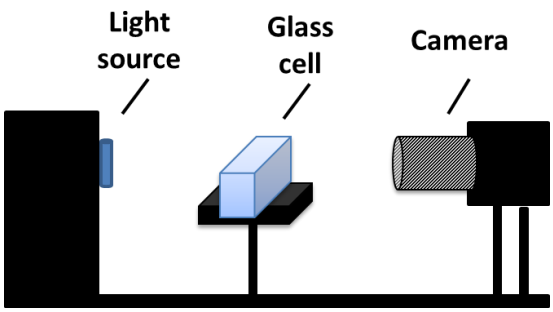

Figure 4.11: Imaging method setup

For each picture the baseline between the solid surface and the drop must be defined by manual adjustments in the software. This enables the software to recognise the drop and to find the best matching contact angles on both sides of the drop. The contact angles are drawn up on the drop images as illustrated in Figure 4.12. Table 4.4 show the wetting definitions according to contact angles, depending on the fluid it is measured through.

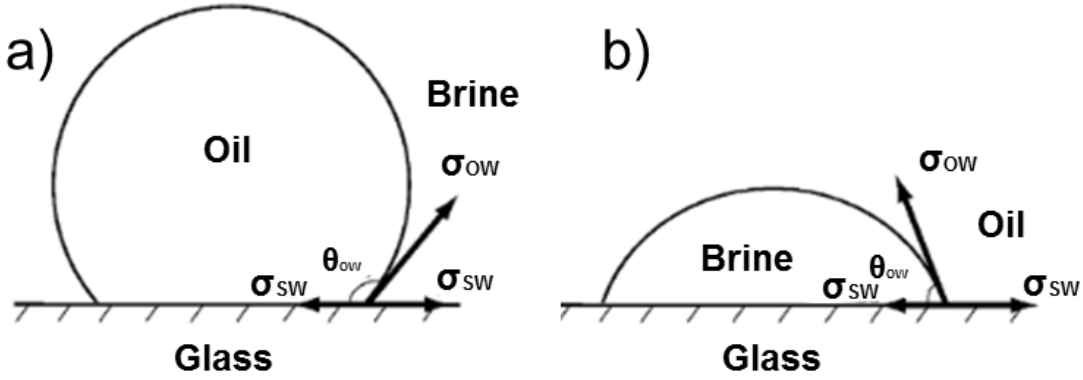

Figure 4.12: Schematic of contact angles in a water-wet glass-oil-brine system. a) Oil-drop in brine and b) brine-drop in oil

Table 4.4: Wetting definitions according to contact angle

Contact angle θ	a) Oil-drop in brine	b) Brine-drop in oil
< 62°	Oil-wet	Water-wet
62° - 133°	Intermediate wet	Intermediate wet
> 133°	Water-wet	Oil-wet

5 Results and Evaluation

In this chapter all of the relevant calculated values and the final results from the experimental procedures are presented. All data is given in Appendix A and the numerical results are evaluated here in correlation to their significance and possible sources of error.

5.1 Initial Porosity and Permeability

In Figure 5.1 the initial porosity (dark grey) and permeability (light grey) for all 16 cores are presented graphically. Porosity data, core dimensions and weights are given in Appendix A-1 while permeability data and Klinkenberg plots are given in Appendix A-2.

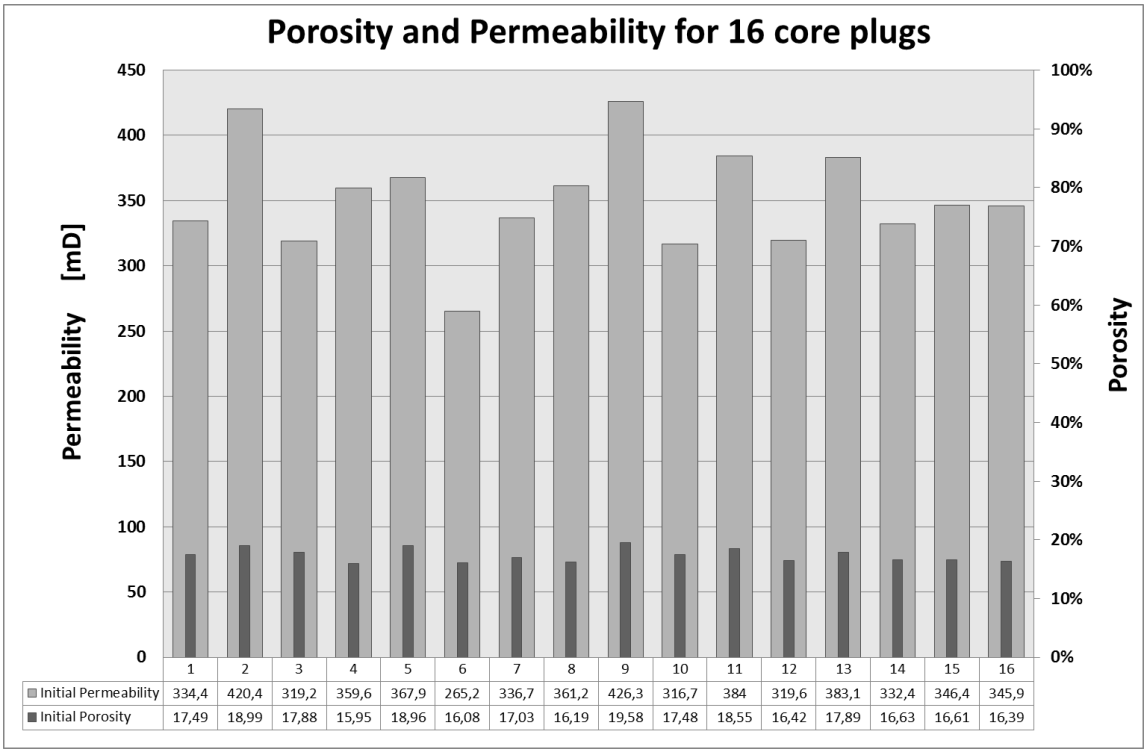

	1	2	3	4	5	6	7	8	9	10	11	12	13	14	15	16
Initial Permeability	334,4	420,4	319,2	359,6	367,9	265,2	336,7	361,2	426,3	316,7	384	319,6	383,1	332,4	346,4	345,9
Initial Porosity	17,49	18,99	17,88	15,95	18,96	16,08	17,03	16,19	19,58	17,48	18,55	16,42	17,89	16,63	16,61	16,39

Figure 5.1: Graphical presentation of initial porosity and permeability of core plugs

The core plugs show variations in porosity ranging from 16 % to 19,6 % which is within the expected range for this type of rock. Berea sandstone is in general quite homogenous and the plugs are all drilled from the same slab. Therefore the deviations are most likely a result of inaccurate dimension-measurements and/or inexact readings from the porosimeter scale. Small inequalities in the plugs can occur due to uneven pore- and grain size distribution. Core plugs with a large number of closed pores will not show a high effective porosity, while cracks or fractures can affect the porosity the opposite way.

The initial permeability of the cores ranges from about 265 mD to 425 mD. Again, the results are most probably caused by errors in measuring core dimensions. Further, when air permeability is measured, even small adjustments in the differential pressure across the core result in noticeable differences in the absolute permeability. It is assumed that all the plugs are drilled in the same longitudinal direction but if this is not the case this might cause significant disparities between the permeability of different cores. Plugs with finer grains or a greater content of mixed grains, laminations and fewer interconnected pores will show a lower permeability. Small cracks or fractures on the other hand may cause increased permeability.

Overall, the 16 core plugs seems to hold similar porous and permeable properties, making them well suited for the experiments in this thesis.

5.2 Initial Wettability Index

Due to limited time and under the assumption that all the core plugs exhibited similar initial wettability it was decided to only the four core plugs that showed the largest deviations in porosity and permeability. An extra core drilled from the same sandstone slab was also chosen, for centrifuge purposes. Owing to a limited number of Amott-cells the testing was divided into two sets. Core # 9 and # 10 was measured before the rest of the experiments; whilst # 2, # 6 and the extra core were measured after all other wettability tests were finished.

Results from initial wettability testing are presented in Table 5.1. In addition, a graph of spontaneous imbibition rates for the first four hours is shown in Appendix A-3. Forced drainage by centrifuge was refrained from for all cores as no brine was drained out of the core plugs after two weeks in the spontaneous drainage cells.

Table 5.1: Initial wettability testing on five core plugs

Core plug	Spontaneous imbibition Vo1 [ml]	Forced imbibition Vo2 [ml]	Spontaneous drainage Vw1 [ml]	Forced drainage Vw2 [ml]	Wettability Index WI
# 2	4,35	0,21	0	-	**0,9548**
# 6	3,60	0,17	0	-	**0,9545**
# 9	4,90	1,25	0	-	**0,7963**
# 10	3,75	0,91	0	-	**0,8041**
# Extra	4,00	0,27	0	-	**0,9357**

Cores # 9 and # 10 indicate an initial wettability index of approximately 0,8 while core # 2, # 6 and Extra show approximately 0,95. All cores are by definition very water-wet and the difference of 0,15 only represent a deviation of 0,075 % on the WI scale. Errors may have occurred as a result of dissimilar factors when conducting the initial wettability tests in two sets. The time allowed in the imbibition cells before centrifuging is also an important factor that affect the end-result. The large differences in forced imbibition volumes also indicate that weighing of wet core plugs before and after the centrifuge involves a great deal of inaccuracy.

5.3 New Porosity and Permeability

New tests of porosity and permeability were conducted after all 6 pairs of cores were flooded, soaked in different nanofluids and then dried in the oven. The results are given in Table 5.2 and compared with the old values to see any alterations. All new porosity data are given in Appendix A-4 and all new permeability data can be found in Appendix A-5.

Table 5.2: Changes in porosity and permeability after flooding of nanofluids

Pair	Core plug	Old porosity	New porosity	Deviation	Old permeability [mD]	New permeability [mD]	Deviation [mD]
1	# 1	17,49 %	**15,34 %**	-2,14 %	334,4	**354,6**	20,2
	# 7	17,03 %	**14,68 %**	-2,36 %	336,7	**334,4**	-2,3
2	# 3	17,88 %	**15,44 %**	-2,45 %	319,2	**335,3**	16,1
	# 12	16,42 %	**15,13 %**	-1,29 %	319,6	**333,8**	14,2
3	# 4	15,95 %	**14,67 %**	-1,28 %	359,6	**275,4**	-84,2
	# 8	16,19 %	**15,12 %**	-1,07 %	361,2	**141,1**	-220,1
4	# 5	18,96 %	**16,61 %**	-2,35 %	367,9	**373,0**	5,1
	# 14	16,63 %	**14,70 %**	-1,93 %	332,4	**328,1**	-4,3
5	# 11	18,55 %	**16,41 %**	-2,14 %	384,0	**348,9**	-35,1
	# 13	17,89 %	**15,96 %**	-1,93 %	383,1	**378,4**	-4,7
6	# 15	16,61 %	**15,33 %**	-1,28 %	346,4	**230,0**	-116,4
	# 16	16,39 %	**15,33 %**	-1,06 %	345,9	**171,0**	-174,9

All core plugs showed a small reduction in porosity, ranging from 1 % to 2,5 %. This is a strong indication that a portion of the injected particles are retained in the pore volume during flooding. Even if some reduction may be a result of nonconformities of the porosimeter, incorrect readings from the scale or other sources of error, the deviations are too compatible to be caused by such contingencies alone.

The changes in permeability differ strongly for the different pairs and cores flooded with the highest nanofluid concentration have the largest impairment. This seems natural as there are more particles to be passed through the cores. The slight increase in permeability in some of the cores that were flooded with lower concentrations is most probably a consequence of inexact air permeability measurements and human error margins. Additionally, the rubber sleeve in the Hassler cell was replaced in between the two rounds of testing.

5.4 New Wettability Index

The results from wettability tests on the 12 core plugs after flooding of nanoparticles are shown in Table 5.3. Curves showing spontaneous imbibition rates for the first four hours of testing can be found in Appendix A-6.

Table 5.3: Wettability index after nanofluid flooding

Pair	Core plug	Spontaneous imbibition Vo1 [ml]	Forced imbibition Vo2 [ml]	Spontaneous drainage Vw1 [ml]	Forced drainage Vw2 [ml]	Wettability Index WI
1	# 1	4,25	0,12	0	-	**0,9717**
	# 7	3,90	0,66	0	-	**0,8547**
2	# 3	3,95	0,50	0	-	**0,8873**
	# 12	3,60	0,61	0	-	**0,8555**
3	# 4	3,75	0,46	0	-	**0,8914**
	# 8	2,80	0,39	0	-	**0,8792**
4	# 5	4,20	0,78	0	-	**0,8440**
	# 14	3,30	0,88	0	-	**0,7902**
5	# 11	3,80	0,64	0	-	**0,8554**
	# 13	3,80	0,75	0	-	**0,8347**
6	# 15	3,10	0,52	0	-	**0,8575**
	# 16	3,10	0,47	0	-	**0,8674**

Only one core, # 1, show a somewhat elevated wettability index compared to the initial values, that ranged between 0,8 and 0,95. Core # 14 shows the lowest value, while all the other cores are represented within the initial range. All cores are, by definition, still considered very water-wet

These results suggest that neither hydrophilic SNPs in brine, nor hydrophobic SNPs in ethanol affect the wetting preferences of the sandstone cores. However, hydrophobic nanoparticles in ethanol affect the rate of spontaneous imbibition as can be seen in the graphs in Appendix A-6.

5.5 Fluid Properties

For contact angle purposes, densities and viscosities of all relevant liquids were measured and the results are given for hydrophilic SNPs in Table 5.4 and for hydrophobic SNPs in Table 5.5. pH were measured for the aqueous solutions. Additional data from pycnometer density measurements are found in Appendix A-7 and Ubbelohde viscometer measurements in Appendix A-8.

Table 5.4: Properties of brine and hydrophilic AEROSIL® 300 in brine at 21,5°C

	Brine 3 wt.%	0,01 wt.%	0,1 wt.%	0,5 wt. %
Density [g/cm^3]	1,020	1,019	1,020	1,022
Viscosity [cp]	1,007	0,983	1,137	1,453
pH	6,37	5,69	5,13	4,46

For hydrophilic nanoparticles suspended in brine, a slight increase in density is seen for the highest concentration. The viscosity is increasing with increasing concentration. Difficulties in cleaning the viscometers to satisfaction have most likely affected the resulting viscosity to some degree. Further, particles may have partially blocked the capillary tube and reduced the ability for the fluids to flow. pH is steadily decreasing with increased concentration.

Table 5.5: Properties of oil and hydrophobic AEROSIL® R106 in oil at 21,5°C

	Oil	0,01 wt. %	0,1 wt. %	0,5 wt. %
Density [g/cm^3]	0,729	0,724	0,723	0,726
Viscosity [cp]	0,900	0,894	0,894	0,903

For hydrophobic nanoparticles suspended in oil, there are small changes in density and viscosity, although no clear trends can be seen. The equipment used for both density and viscosity is very sensitive to poor cleaning routines and small traces of contaminants can affect the results. The accuracy of the scale used when weighing the pycnometer is a very important factor.

5.6 Contact Angles

Contact angles were measured on a glass plate by the imaging method, taking one picture every minute for one hour. For drops of fluids with lower density than the surrounding fluid, the drop was placed underneath the plate. Otherwise the drop was resting on top of the plate. The mean contact angle from all images in each experiment was calculated by the software Attension Theta and the results are presented in Table 5.6. Curves showing the changes in mean contact angle over time together with pictures of all drops at the beginning and end of each experiment can be found in Appendix A-9.

Table 5.6: Contact angles between different fluids in contact with a glass plate

Drop	Surrounding fluid	Mean θ [deg]	Standard deviation [deg]	Mean Volume [microl]	Standard deviation [microl]
n-Decane	Brine	150,09	0,16	13,63	0,01
n-Decane	0,01 wt % hydrophilic NF	160,41	0,71	14,51	0,02
n-Decane	0,1 wt % hydrophilic NF	151,50	0,95	9,41	0,02
n-Decane	0,5 wt % hydrophilic NF	149,13	1,17	9,04	0,04
Brine	n-Decane	21,04	0,05	5,23	0,28
0,01 wt % hydrophilic NF	n-Decane	21,49	0,43	2,24	0,02
0,1 wt % hydrophilic NF	n-Decane	10,73	0,12	1,48	0,08
0,5 wt % hydrophilic NF	n-Decane	9,44	0,07	1,51	0,06
0,01 wt % hydrophobic NF	brine	135,03	6,66	7,12	0,11
0,1 wt % hydrophobic NF	brine	144,90	4,28	7,90	0,11
0,5 wt % hydrophobic NF	brine	128,58	6,88	6,67	0,16

For hydrophilic nanofluids, measurements were conducted for both a drop of oil in the NF and also a drop of NF in the oil. Although there are some deviations in the found values the results show hydrophilic SNPs are rendering the system more water-wet. For hydrophobic SNPs in oil the measurements got very unstable and the end results show large deviations. The contact angles are decreased compared to pure oil in brine, indicating that also this system becomes more water wetting. It is uncertain what effects are causing the observed results, but there are a lot of sources of error involved.

Impure equipment, too short equilibrium time, varying drop sizes, moving drops, errors in manually adjusting the image baseline and deviations in the mixed fluids are just some of the possible causes of inaccurate imaging method results.

6 Discussion

This chapter discuss in detail the results found in this thesis and compare them to similar and relevant research and literature. As the author had minimal previous laboratory experience the limitations of this study are emphasized.

6.1 Retention of Silica Nanoparticles

It was obvious, by testing of porosity after injecting nanofluids through the core plugs that a small portion of the particles were retained in the pore spaces. The same indications was also seen for Engeset (2012) during his flooding experiments. Nunes et al. (2010) illustrates in Figure 6.1 how injection of suspended particles cause formation damage. The particles are "filtered out" as the fluid move through the porous media, gradually decreasing the particle concentration as a function of the distance from the injection point.

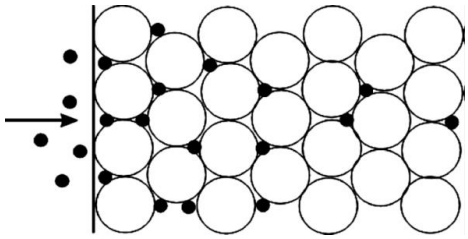

Figure 6.1: Retention of particles in porous media (Nunes et al. 2010)

Four different physical mechanisms commonly cause particles to retain in the pores (Figure 6.2). Log-jamming occurs when smaller particles clog together and block pore-throats. Accumulation of particles are governed by the injection flow rate, pore size distribution and particle concentration and size (Skauge, Spildo, and Skauge 2010). Mechanical entrapment (straining) can happen when particles of greater size than the pore throats are injected. Mechanical retention increases with increasing particle size, increasing fineness of the pores and decreasing flow velocity (Svoboda 2004).

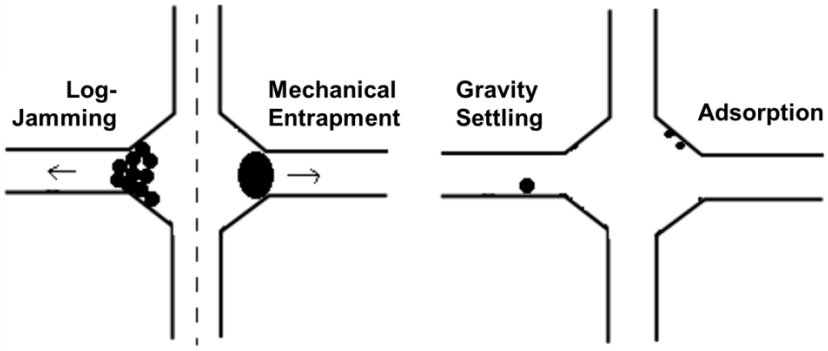

Figure 6.2: Four different entrapment mechanisms (Engeset 2012)

Gravity settling or sedimentation occurs when the injected particles have a higher density than the carrying fluid. The density difference, flow rate and flow pattern, particle concentration and particle size plays important roles on the rate at which the particles settle and eventually block the pore spaces (Maxey and Corrsin 1986).

Due to the low specific gravity and small particle size of the utilized nanoparticles, only 7 nm, it is most probable that the retention mechanism that occurred during flooding was adsorption. Gao (2007) describes adsorption as a retention mechanism that causes the particles to cling to the rock surfaces due to Brownian motion and the electrostatic interaction between the migrating particles and the solid surface. The high surface area of the nanoparticles plays an important role in the adsorption process as it increases the surface energy of the particle. It is claimed by Ju et al. (2002) that is leads to an increased tendency of silica nanoparticles to adsorb on the walls of porous media. In addition, (Yu et al. 2012) argue that the presence of clay in sandstone enhance SNP adsorption.

Gao (2007) found that for small particles the surface adsorption will normally increase proportionally with particle concentration. Contending results have been found in this thesis. It seems like the lowest nanoparticle concentrations are affecting the porosity the most. This might be due to the fact that these particles are transported steadily through the cores and are retained evenly. Whereas for higher concentrations the flooding of core-pairs in series lead to the first core acting as a filter where the particles eventually clogged together and caused log-jamming at the fluid inlet of the Hassler cell (See Figure 6.3). This might have prevented major portions of the particles to travel through the cores.

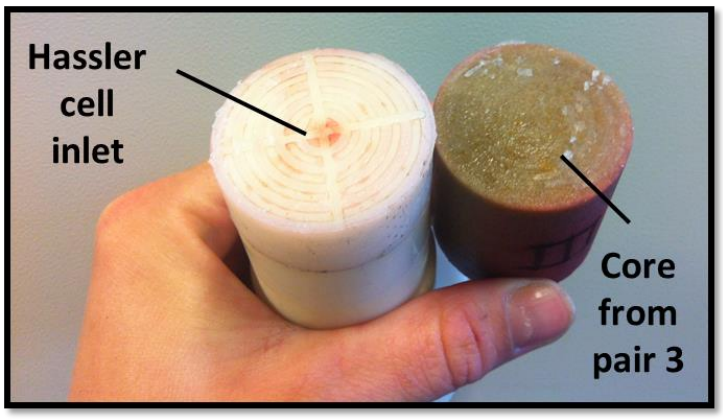

Figure 6.3: Core with visible layer of nanoparticles at the inlet after flooding

Similar to what Engeset (2012) found in his studies there were major permeability impairments in cores flooded with the highest nanofluid concentration. Further, the core in each pair that was placed next to the flooding inlet had a considerably higher reduction in permeability than the other. As these results don't correspond to a greater reduction in porosity, the assumption of a filtering effect at the flooding inlet, caused by log-jamming of the particles is strengthened.

Concentration analysis of the collected effluent fluids after flooding should have been conducted to determine the loss of particles in the flooding process. SEM imaging can be used for such purposes and could confirm that particles were retained in the core plugs (Alaskar et al. 2012). Further, the flooding pump pressure should have been recorded to register when the permeability started to decrease and the cores should have been flooded separately to secure comparable conditions for wettability testing.

6.2 Alteration of Wettability

Clean Berea sandstone is commonly very water-wet so it was expectable that the five core plugs tested for initial wettability showed strongly water-wetting tendencies. The highest and lowest values showed a 0,075 % deviation in the Amott-Harvey WI. These differences in values seem appropriate as the testing was divided into two rounds with somewhat different conditions.

Cores # 9 and # 10 where tested before the others due to a limited number of Amott cells available and because the time set aside for experiments were scarce. The core plugs were saturated with oil only a couple of hours before they were placed in the Amott cells. Core # 2, # 6 and the extra core (chosen for centrifuge balance purposes) were tested when all other wettability tests were finished. These cores were soaked in oil for several days before they were placed in the Amott cells. The dissimilarities may also be the reason for the distinctions in the imbibition rate curves seen in Appendix A-3. It was assumed that all of the other core plugs in the experiment exhibited similar initial wetting properties. With more time available, all plugs should obviously have been more extensively tested, although the assumption should be fair for this small amount of plugs from a supposedly homogenous slab of sandstone.

The wettability index for the rest of the cores was tested after flooding of nanofluids. In theory the flooding of nanofluids and succeeding adsorption of SNPs in the core plugs should form a layer of particles on the pore walls. This would further imply that the already water-wet rock could be rendered even more water-wet by employing strongly hydrophilic particles, or intermediate to oil-wet by employing strongly hydrophobic particles. None of the presumed adsorption effects after nanofluid flooding was registered by the Amott-Harvey method, indicating that neither hydrophilic nor hydrophobic SNPs alter the Amott-Harvey WI of initially very water-wet Berea sandstone.

The rates of imbibition were also recorded for all the cores during the first four hours of each experiment, as it is suggested by Morrow (1990) that these results supplement the indices found by the Amott-Harvey method. Curves of imbibed volumes vs. time are shown in Appendix A-3 and Appendix A-6. Cores flooded with hydrophilic SNPs show quite similar trends to the ones seen during initial wettability testing, while the hydrophobic SNPs seem to slow down the process to some extent. These trends provide information on the dynamic IFT and wetting phenomena in the cores that are not reflected by the Amott method (Rabiei et al. 2013).

Application of the Amott-Harvey method to measure wettability was a decision based on the available equipment in the laboratory as well as the apprehension that this method is commonly used in the oil industry (Glover 2011). It is not always possible to reproduce reservoir wetting conditions at room temperature. However, this procedure is relatively simple and provides a good indication of the average wetting preferences of the rock. Although this method is accepted it has no validity as an absolute measurement as it is not based on any mathematical foundation, only on the analytical fact that the wetting fluid generally will imbibe a core spontaneously and displace the non-wetting fluid (Morrow 1990).

Anderson (1986) discuss the topic of the recommended time period a core plug should spend in the Amott cells to obtain credible values. Amott suggested an arbitrary time period of 20 hours for spontaneous imbibition and drainage. Anderson recommends that the cores are allowed a time limit of 1-2 weeks or until imbibition is complete. This can take several months, depending on parameters such as permeability and fluid viscosities. It was decided to end spontaneous imbibition after 4-5 days when it seemed like equilibrium was reached due to the limited time. This may have resulted in a lower imbibed volume than the actual equilibrium value, causing an underestimation of the wettability index. However, the relatively good permeability of the cores should make these errors small. It is more likely that any inaccuracies are a consequence of the manually recorded fluid volumes from the graded cylinder on the Amott cells. Further, some amounts of liquids might have been lost during the assembling of the cells, before the volume-recording started.

All wettability tests in this thesis were performed in room temperature and under atmospheric pressure. Pressure and temperature will influence the wetting preferences of the rock and so will variables such as fluid salinities, ionic strengths, pH and rheological properties (Amiri, Øye, and Sjöblom 2009). The ratio of spontaneous imbibition to forced imbibition is used to reduce the influence of other factors, such as relative permeability, viscosity and the initial saturation of the rock (Anderson 1986).

Ju et al. (2002) conducted an extensive study involving laboratory testing, computer simulations and field testing to see how nanosized hydrophobic polysilicon effect the wettability of sandstone. Wettability was measured by finding the contact angle of a drop of water on a furbished sandstone plate smeared with a mix of diesel and hydrophobic SNPs. Compared to a clean plate of sandstone the results showed a great change in the rock wettability. Further they conducted water displacement experiments to verify the alterations in wettability by enhancing the effect of the flooding. Their simulation model and field testing also indicates that hydrophobic SNPs positively alter sandstone wettability in favour of increased recovery.Onyekonwu and Ogolo (2010) claimed that hydrophilic and neutral SNPs dispersed in ethanol had the ability to change the rock wettability, seen by improving oil recovery during nanofluid flooding. The study, however, displayed no direct way of measuring the changes in wettability.

6.3 Contact angles

Contact angles are a universal measure of the wetting preferences of a surface. It was therefore determined to use the imaging method to find contact angles between fluids and the surface to back up the results seen from the Amott-Harvey method. New nanofluids were mixed and it was decided to test through both the denser and less dense fluid for hydrophilic fluids and only through the less dense fluid for hydrophobic fluids. This was mainly due to the fact that the oil used for mixing nanofluids had been coloured red and would be impossible to see through. Clear n-Decane was used when measuring hydrophilic drops resting on the glass plate.

The imaging drop method is simple in concept but proved to be quite challenging in practice. This method put stringent demands to the cleaning procedures, as any contamination or residue of cleaning agents will affect the results (Torsæter and Abtahi 2003). Proper adjustment of camera settings, to get both the drop and the glass plate in focus, even though they are located at different distances from the lens, turned out to be complicated and might have ended up compromising both to some degree.

Similar experiments were conducted by Metin, Baran Jr, and Nguyen (2012) were the presence of different types of SNPs showed slight changes in contact angle. In this thesis, for hydrophilic particles the trend show that the water-wetting tendencies of the glass surface increase with increasing particle concentration. Torsater, Li, and Hendraningrat (2013) observed the same results in their study. For hydrophobic drops, measurements were very unstable and the results are therefore not trustworthy. However, the contact angle seems to decrease when particles are added to the oil, indicating that the system becomes more oil-wetting. No certain trend could be seen and this may be explained by looking at the start and end pictures of these drops, shown in Appendix A-9 where many of the drops clearly continued to subside or move during the experiments.

Ideally, in the case of hydrophilic NF, if the measured angles are correct, the pairs of experiments with corresponding fluids should have a total mean contact angle equal to 180°. This is only the case for 0,01 wt. % hydrophilic NF and oil, where the sum of the two measured mean contact angles results in 181,49°. However, the accompanying graphs of mean contact angle vs. time (Appendix A-9) show that most of the drops require more time to reach a state of equilibrium. Therefore the found results are doubtful.

Additional problems could be identified from the pictures of the drops from each experiment. For the highest concentration of hydrophilic NF it was hard to adjust the camera light settings correctly to see the drop of oil, as the NF solution was unclear. Difficulties in placing stable drops onto and especially underneath the glass plate became an issue. Small angles of tilt in the glass plate caused some of the drops to constantly move and eventually roll off the edge of the plate. The time available for contact angle determination made full optimization of these measurements impossible. Nevertheless, the results are important to get an indication of how SNPs affect contact angles.

Yoon and Garrell (2008) found that the advancing contact angle obtained by tilting the surface is generally somewhat larger than the static contact angle (See Figure 6.4). However, the imaging method software calculates a mean contact angle between the receding and advancing angles of each drop and it is assumed that the attained resulting values are within an acceptable range of deviation.

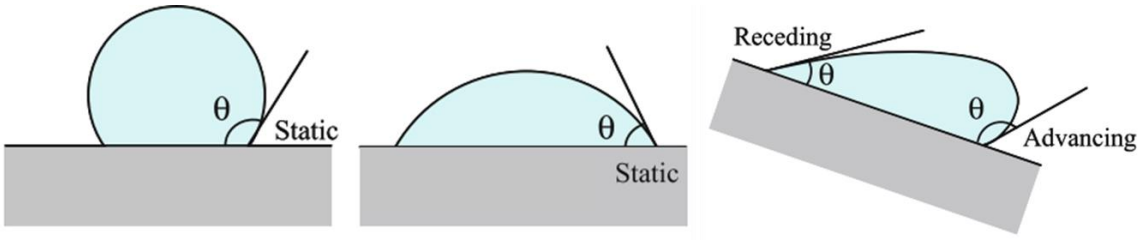

Figure 6.4: Static vs. receding/ advancing contact angles (Yoon and Garrell 2008)

For the hydrophobic SNPs suspended in oil it was even harder to obtain oil drops that were stable and still underneath the glass plate, especially for the highest nanoparticle concentration. This caused large deviations in the calculated mean contact angles. The contact angles are measured based on the IFTs at the interface between the solid state and the two fluids involved. Wasan, Nikolov, and Kondiparty (2011) claim that the complex nature of the interactions between the particles in the NF and the solid surface greatly alters the spreading dynamics due to a structural disjoining pressure gradient at the interface (See Figure 6.5). The creation of a wedge film of nanoparticles at the base of the drop disrupts the smooth surface of the drop. This affects the IFT between the fluids involved and thereby also the contact angle.

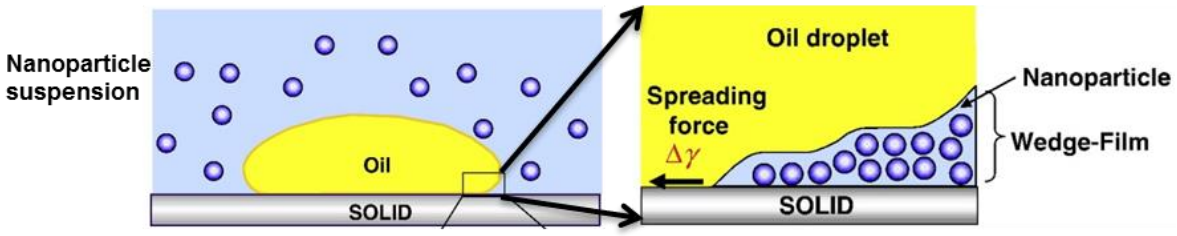

Figure 6.5: Illustration of wedge-film at the base of the drop due to disjoining pressure (Wasan, Nikolov, and Kondiparty 2011)

Apart from previously mentioned errors of margin, the measured contact angle are not directly comparable with the Amott-Harvey wetting results. The tests were conducted on a glass plate and not on the surface of Berea sandstone or a plate of quartz. However, Anderson (1986) argue contact angle measurements do not take into account the roughness, heterogeneity or complexity of the reservoir rock. In addition it was hard to get hold of polished thin sections of the rock and therefore it was decided to simplify the experiments by using easily available glass plates instead. Further, it is easier to clean a glass plate properly in between experiments. Considering that the glass plate is made up of quartz, the dominating mineral in sandstone, it is nevertheless fair to assume some coherence between the two measuring methods. Other sources of error include possible variances in the concentrations of mixed fluids utilized in the two methods, manual operating of the glass plate baseline in the software and very unstable drops that failed to reach equilibrium during testing.

The observed results from contact angle measurements are strong indicators that the wetting properties of a system can be altered by employing silica nanoparticles. However, the Amott-Harvey wettability index seems incapable of detecting the same phenomena that cause these changes. It might be the dynamic IFTs that are changed, rather than the wetting properties of the reservoir rock. This should be studied closer.

6.4 Limitations and Complications

Experimental studies are time-consuming and they require a well-planned setup from the beginning. In the case of mistakes, misunderstandings or damages there are little room for fresh starts and it is not always possible to reproduce identical conditions or to obtain the same desired effects. The minimal laboratory experience possessed, combined with little knowledge of the apparatus to use and the procedures to follow at the start-up of this thesis, has definitely been a limitation.

Small deviations and errors in observations, calculations and results conducted early on in the study may have caused large ripple-effects in the further work. As several of the laboratory methods used, such as the porosimeter scale and the Amott cells, require manual reading of values it is expected that the error margins in the final results are high. However, all measurements are conducted as precisely as possible to eliminate any large deviations and it is believed that the final results are to be trusted.

The short time available and the scope of this study led to some hasted decisions and some experiments had to be cut short to reach the goals. In hindsight it is easy to point out some things that should have been done differently; the core plugs should not have been flooded in series as this gave the two plugs in each pair unequal properties; the pump pressure required during flooding and the particle concentration of the collected effluents should have been recorded; cores should have been allowed more time in the Amott cells; and more time should definitely have been put aside for contact angle measurements. To obtain more definite results, more core plugs should have been tested and a more extensive study including flooding experiments, IFT measurements and sensitivity analysis should have been carried out.

Lack of existing studies and published literature on the topic of SNPs related to wettability has led to critical review of available articles and other sources of information. Laboratory work has been an eye-opener to how experimental results are obtained. It is easy to see how desired effects can be produced by applying different methods, changing parameters or simply referring to a selected number of previous studies.

7 Conclusion

This study was focused on testing how pure, engineered silica nanoparticles affect the Amott-Harvey wettability index of initially water-wet Berea sandstone. Contact angles were measured by the imaging method to point out occurring phenomena at the intersection between glass and fluids in the presence of SNPs. Drawn upon observations and calculated results the following can be said;

7.1 Findings

- Porosity reduction without major permeability impairment after nanofluid flooding indicates that adsorption is the governing mechanism for retention of particles.
- Pure hydrophilic and hydrophobic SNPs show few signs of altering the Amott-Harvey wettability index of initially water-wet Berea sandstone, regardless of concentration.
- Hydrophobic SNPs seems to affect the rate of spontaneous imbibition in water-wet Berea sandstone.
- Contact angles are somewhat affected by the presence of silica nanoparticles. Water-wetting tendencies increase with higher concentrations of hydrophilic SNPs. Hydrophobic SNPs suspended in oil seems to render the system more oil-wet.
- Increased oil-recovery observed during flooding of silica nanofluids may be causing changes in the interfacial tensions between the fluids in the pore spaces rather than alterations in the wettability of the rock, which the Amott-Harvey WI is unable to detect.

However, it is not confident to draw robust conclusions on the given results with the limited studies conducted in this thesis.

7.2 Further Recommendations

First of all, it is recommended to carry out close investigation of how SNPs affect the interfacial tension between fluids. Further, this should be compared to studies on wettability alterations of surfaces due to adsorption of SNPs. This will help determine the usefulness of SNPs as surfactants or wettability-changers in EOR.

Secondly, future studies should look into new and improved methods for measuring wettability. NMR, amongst other methods, seems to hold a promising outlook and can possibly offer credible determination of wettability, saturation and fluid viscosities at in-situ conditions (Freedman et al. 2003). In addition, transport of nanoparticles in porous media needs to be examined more closely to predict how SNPs behave during flooding and to understand which forces prevail at the nanoscale.

Last, but not least it is evident that the effect of SNPs on sandstone wettability lacks sufficient research. More extensive testing on rocks with different wetting preferences, such as neutral or oil-wet rock would present a broader spectre of results. To allow the cores to age in nanofluids for a longer period of time could possibly result in a different outcome. Sensitivity analyses should be conducted to see the combined effect of SNPs and variables such as salinity, pH, pressure and temperature.

References

Abdallah, Wael, Jill S Buckley, Andrew Carnegie, John Edwards, Bernd Herold, Edmund Fordham, Arne Graue, Tarek Habashy, Nikita Seleznev, and Claude Signer. 1986. "Fundamentals of wettability." *Technology* no. 38:1125-1144.

Adams, Laura K, Delina Y Lyon, and Pedro JJ Alvarez. 2006. "Comparative eco-toxicity of nanoscale TiO_2, SiO_2, and ZnO water suspensions." *Water research* no. 40 (19).

Afrapoli, M. Shabani, C. Crescente, S. Alipour, and O. Torsaeter. 2009. "The effect of bacterial solution on the wettability index and residual oil saturation in sandstone." *Journal of Petroleum Science and Engineering* no. 69 (3–4):255-260.

Agbalaka, Chinedu, Abhijit Dandekar, Shirish Patil, Santanu Khataniar, and James Hemsath. 2008. The effect of wettability on oil recovery: a review. Paper read at SPE Asia Pacific Oil and Gas Conference and Exhibition.

Ahmed, T. 2006. *Reservoir engineering handbook*: Gulf Professional Publishing.

Alaskar, Mohammed, Morgan Ames, Steve Connor, Chong Liu, Yi Cui, Kewen Li, and Roland Horne. 2012. "Nanoparticle and Microparticle Flow in Porous and Fractured Media--An Experimental Study." *SPE Journal* no. 17 (4):1160-1171.

Amiri, A., G. Øye, and J. Sjöblom. 2009. "Influence of pH, high salinity and particle concentration on stability and rheological properties of aqueous suspensions of fumed silica." *Colloids and Surfaces A: Physicochemical and Engineering Aspects* no. 349 (1):43-54.

Anderson, William. 1986. "Wettability literature survey-part 1: rock/oil/brine interactions and the effects of core handling on wettability." *Journal of Petroleum Technology* no. 38 (10):1125-1144.

Barik, TK, B Sahu, and V Swain. 2008. "Nanosilica—from medicine to pest control." *Parasitology research* no. 103 (2):253-258.

Bear, Jacob. 1988. *Dynamics of Fluids in Porous Media*. New York: Dover Publications, Inc.

Bennett, B, JO Buckman, BFJ Bowler, and SR Larter. 2004. "Wettability alteration in petroleum systems: the role of polar non-hydrocarbons." *Petroleum Geoscience* no. 10 (3):271-277.

Brydson, R.M., and C. Hammond. 2005. "Generic methodologies for nanotechnology: classification and fabrication." *Nanoscale Science and Technology*:1-55.

Bucak, S. 2011. "Importance of Defining when Applying." *J Chem Eng Process Technol* no. 2:e101.

Cao, G. 2004. *Nanostructures & nanomaterials: synthesis, properties & applications*: World Scientific Publishing Company.

Carroll, J.J. 2009. *Natural gas hydrates: a guide for engineers*: Gulf Professional Publishing.

Choi, S.U.S. 1998. Nanofluid technology: Current status and future research. Argonne National Lab., IL (US).

Christian, P., F. Von der Kammer, M. Baalousha, and T. Hofmann. 2008. "Nanoparticles: structure, properties, preparation and behaviour in environmental media." *Ecotoxicology* no. 17 (5):326-343.

Cossé, R. 1993. *Basics of Reservoir Engineering - Oil and Gas Field Development Techniques*. Paris: Éditions Technip.

Costa, Carlos AR, Carlos AP Leite, and Fernando Galembeck. 2003. "Size dependence of Stöber silica nanoparticle microchemistry." *The Journal of Physical Chemistry B* no. 107 (20):4747-4755.

Donaldson, Ken, and Craig A. Poland. 2009. "Nanotoxicology: New insights into nanotubes." *Nat Nano* no. 4 (11):708-710.

Dorinson, A, and Kenneth C Ludema. 1985. *Mechanics and chemistry in lubrication*. Vol. 9: Elsevier Science Limited.

Eastoe, Julian, Martin J Hollamby, and Laura Hudson. 2006. "Recent advances in nanoparticle synthesis with reversed micelles." *Advances in colloid and interface science* no. 128:5-15.

Ebbing, D.D., and S.D. Gammon. 2009. *General chemistry*: Cengage Learning.

Edwards, S.A. 2008. *The Nanotech pioneers*. Germany: Wiley-Vch.

Elkem Silicon Materials. 2010. Elkem Nanosilica 999.

Engeset, Bjørnar. 2012. *The Potential of Hydrophilic Silica Nanoparticles for EOR Purposes*, Petroleum Engineering and Applied Geophysics, NTNU, Trondheim.

Evonik. *AEROSIL products* 2012. Available from http://corporate.evonik.com/en/products/search-products/pages/search.aspx.

Fischer, Hans C., and Warren C. W. Chan. 2007. "Nanotoxicity: the growing need for in vivo study." *Current Opinion in Biotechnology* no. 18 (6):565-571. doi: http://dx.doi.org/10.1016/j.copbio.2007.11.008.

Freedman, R, N Heaton, M Flaum, GJ Hirasaki, C Flaum, and M H? rlimann. 2003. "Wettability, saturation, and viscosity from NMR measurements." *SPE Journal* no. 8 (4):317-327.

Gant, Preston, and William Anderson. 1988. "Core cleaning for restoration of native wettability." *SPE formation evaluation* no. 3 (1):131-138.

Gao, C. 2007. "Factors Affecting Particle Retention in Porous Media." *Emirates Journal for Engineering Research* no. 12 (3):7.

Garcia, Andre P. 2010. Hierarchical and size dependent mechanical properties of silica and silicon nanostructures inspired by diatom algae. DTIC Document.

Glover, Paul. 2011. Wettability. Lecture Notes - Formation Evaluation MSc Course.

Gupta, R, and KK Mohanty. 2011. "Wettability alteration mechanism for oil recovery from fractured carbonate rocks." *Transport in porous media* no. 87 (2):635-652.

Harwood, L.M., and C.J. Moody. 1989. *Experimental Organic Chemistry: Principles and Practice*: John Wiley & Sons, Limited.

Heinemann, Zoltán E. 2005. *Fluid Flow in Porous Media*. Edited by DI Barbara Schatz. Vol. 1. Loeben: University of Leoben.

Hendraningrat, L., and L. Shidong. 2012. A Glass Micromodel Experimental Study of Hydrophilic Nanoparticles Retention for EOR Project. Paper read at SPE Russian Oil and Gas Exploration and Production Technical Conference and Exhibition.

Ju, Binshan, Shugao Dai, Zhian Luan, Tiangao Zhu, Xiantao Su, and Xiaofeng Qiu. 2002. A study of wettability and permeability change caused by adsorption of nanometer structured polysilicon on the surface of porous media. Paper read at SPE Asia Pacific Oil and Gas Conference and Exhibition.

Kaasa, Anne Tinnen. 2012. *Application of Engineered Silica Nanoparticles in Enhanced Oil Recovery*. Project, Petroleum Engineering and Applied Geophysics, NTNU, Trondheim.

Kelsall, R.W., I.W. Hamley, M. Geoghegan, and J. Wiley. 2005. *Nanoscale science and technology*: Wiley Online Library.

Lake, Larry W. 1989. *Enhanced Oil Recovery*. New Jersey: Prentice-Hall, Inc.

Lines, Murray. *Silica - Silicon Dioxide (SiO2)* 2012. Available from http://www.azom.com/article.aspx?ArticleID=1114.

Maxey, MR, and S Corrsin. 1986. "Gravitational settling of aerosol particles in randomly oriented cellular flow fields." *Journal of Atmospheric Sciences* no. 43:1112-1134.

McCain, William D. 1990. *The properties of petroleum fluids*. 2 ed. Tulsa, Oklahoma: PennWell Publishing Company.

Metin, C., R. Bonnecaze, and Q. Nguyen. 2012. The Viscosity of Silica Nanoparticle Dispersions in Permeable Media. Paper read at SPE International Oilfield Nanotechnology Conference.

Metin, Cigdem O, Jimmie R Baran Jr, and Quoc P Nguyen. 2012. "Adsorption of surface functionalized silica nanoparticles onto mineral surfaces and decane/water interface." *Journal of Nanoparticle Research* no. 14 (11):1-16.

Miranda, C., L. Lara, and B. Tonetto. 2012. Stability and Mobility of Functionalized Silica Nanoparticles for Enhanced Oil Recovery Applications. Paper read at SPE International Oilfield Nanotechnology Conference.

Morrow, Norman. 1990. "Wettability and its effect on oil recovery." *Journal of Petroleum Technology* no. 42 (12):1476-1484.

MPG Petroleum. *Oil & Gas Fundamentals* 2003. Available from http://mpgpetroleum.com/fundamentals.html.

Mullins, Oliver C, Andrew Kurkjian, Robin McGowan, Thomas Distefano, and Ian Traboulay. 2002. Methods and apparatus for optically measuring fluid compressibility downhole. Google Patents.

Napierska, D., LC Thomassen, D. Lison, J.A. Martens, and P.H. Hoet. 2010. "The nanosilica hazard: another variable entity." *Part Fibre Toxicol* no. 7 (1):39.

Nunes, M, Pavel Bedrikovetski, B Newbery, R Paiva, C Furtado, and ALS de Souza. 2010. "Theoretical definition of formation damage zone with applications to well stimulation."

Onyekonwu, M., and N. Ogolo. 2010. Investigating the Use of Nanoparticles in Enhancing Oil Recovery. Paper read at Nigeria Annual International Conference and Exhibition.

Paparazzo, E., M. Fanfoni, E. Severini, and S. Priori. 1992. "Evidence of Si–OH species at the surface of aged silica." *Journal of Vacuum Science & Technology A: Vacuum, Surfaces, and Films* no. 10 (4):2892-2896.

Perez Carrillo, Edgar Rricardo, Jose Zapata Arango, Mauricio Gonzalez Ortiz, and Maria Herrera V. 2010. Improvements in Routine Core Analysis on Whole Core. Paper read at SPE Latin American and Caribbean Petroleum Engineering Conference.

Pratsinis, Sotiris E. 1998. "Flame aerosol synthesis of ceramic powders." *Progress in Energy and Combustion Science* no. 24 (3):197-219.

Rabiei, Arash, Milad Sharifinik, Ali Niazi, Abdolnabi Hashemi, and Shahab Ayatollahi. 2013. "Core flooding tests to investigate the effects of IFT reduction and wettability alteration on oil recovery during MEOR process in an Iranian oil reservoir." *Applied microbiology and biotechnology*:1-13.

Rahman, Ismail Ab, and Vejayakumaran Padavettan. 2012. "Synthesis of silica nanoparticles by sol-gel: size-dependent properties, surface modification, and applications in silica-polymer nanocomposites—a review." *Journal of Nanomaterials* no. 2012:8.

Ramsden, Jeremy. 2009. "Essentials of Nanotechnology." In. http://bookboon.com: Ventus Publishing ApS.

Schulte, P., C. Geraci, R. Zumwalde, M. Hoover, and E. Kuempel. 2008. "Occupational risk management of engineered nanoparticles." *Journal of occupational and environmental hygiene* no. 5 (4):239-249.

Sigma-Aldrich. *Methanol* 2013. Available from http://www.sigmaaldrich.com/chemistry/solvents/methanol-center.html.

Skauge, T., K. Spildo, and A. Skauge. 2010. Nano-sized particles for EOR. Paper read at SPE Improved Oil Recovery Symposium.

Svoboda, Jan. 2004. *Magnetic techniques for the treatment of materials*: Kluwer Academic Pub.

Terry, R.E. 2000. Enhanced oil recovery. Encyclopedia of Physical Science and Technology. Academic Press.

Torsater, Ole, Shidong Li, and Luky Hendraningrat. 2013. A Coreflood Investigation of Nanofluid Enhanced Oil Recovery in Low-Medium Permeability Berea Sandstone. Paper read at 2013 SPE International Symposium on Oilfield Chemistry.

Torsæter, Ole, and Manoochehr Abtahi. 2003. Experimental Reservoir Engineering Laboratory Workbook. edited by Department of Petroleum engineering and Applied Geophysics NTNU.

Trindade, T., P. O'Brien, and N.L. Pickett. 2001. "Nanocrystalline semiconductors: synthesis, properties, and perspectives." *Chemistry of Materials* no. 13 (11):3843-3858.

Warheit, David B. 2008. "How Meaningful are the Results of Nanotoxicity Studies in the Absence of Adequate Material Characterization?" *Toxicological Sciences* no. 101 (2):183-185. doi: 10.1093/toxsci/kfm279.

Wasan, Darsh, Alex Nikolov, and Kirti Kondiparty. 2011. "The wetting and spreading of nanofluids on solids: Role of the structural disjoining pressure." *Current Opinion in Colloid & Interface Science* no. 16 (4):344-349. doi: http://dx.doi.org/10.1016/j.cocis.2011.02.001.

Whitson, Curtis H., and Michael R. Brulé. 2000. *Phase Behavior*. Vol. 20. Texas: Society of Petroleum Engineers.

Wigginton, N.S., K.L. Haus, and M.F. Hochella Jr. 2007. "Aquatic environmental nanoparticles." *J. Environ. Monit.* no. 9 (12):1306-1316.

www.petroleumonline.com. *Online Module: Porosity* 2012. Available from http://www.petroleumonline.com/modules/m005/hl_005_009.asp.

Yokel, R.A., and R.C. MacPhail. 2011. "Engineered nanomaterials: exposures, hazards, and risk prevention." *J Occup Med Toxicol* no. 6 (7).

Yoon, Jeong-Yeol, and Robin L Garrell. 2008. "Biomolecular Adsorption in Microfluidics." In *Encyclopedia of Microfluidics and Nanofluidics*, 68-76. Springer.

Yu, Jianjia, Cheng An, Di Mo, Ning Liu, and Robert Lee. 2012. Study of adsorption and transportation behavior of nanoparticles in three different porous media. Paper read at SPE Improved Oil Recovery Symposium.

Zhao, Yuanjin, Zhuoying Xie, Hongcheng Gu, Lu Jin, Xiangwei Zhao, Baoping Wang, and Zhongze Gu. 2012. "Multifunctional photonic crystal barcodes from microfluidics." *NPG Asia Mater* no. 4.

Zitha, P., R. Felder, D. Zornes, K. Brown, and K. Mohanty. *Increasing Hydrocarbon Recovery Factors*. SPE Technology Updates 2011. Available from http://www.spe.org/tech/.

Zumdahl, Steven S, and Donald J DeCoste. 2012. *Chemical principles*: Brooks/Cole Publishing Company.

Øren, Pål-Eric, and Stig Bakke. 2003. "Reconstruction of Berea sandstone and pore-scale modelling of wettability effects." *Journal of Petroleum Science and Engineering* no. 39 (3):177-199.

Nomenclature

A = Area, $[m^2]$

A_T = Adhesion tension, $[N/m]$

d = Diameter, [m]

dP = Differential pressure

dx = Length interval

$\frac{du}{dy}$ = Shear rate

g = Gravitational const, ~9,81 $[m/s^2]$

h = height, [m]

k = Permeability, [mD]

k_{air} =Air permeability, [mD]

k_{phase} = Effective permeability, [mD]

$k_{r,phase}$ = Relative permeability, [mD]

L = Length, [m]

m = Mass, [kg]

P = Pressure, [Pa]

P_{atm} = Atmospheric pressure, [Pa]

P_C = Capillary pressure, [Pa]

q = Volumetric flux, [m/s]

Q = Volumetric flow rate, $[m^3/s]$

r = Radius, [m]

S = Saturation

T = Temperature, [K]

u = Superficial velocity, [m/s]

V = Volume, $[m^3]$

V_b = Bulk Volume, $[m^3]$

V_g = Grain Volume, $[m^3]$

V_p = Pore Volume, $[m^3]$

α = Inclination angle, [deg]

β = Fluid compressibility, [1/Pa]

φ = Porosity, [%]

σ = Interfacial tension, [N/m]

θ = Contact angle, [deg]

ρ = Density, $[kg/m^3]$

γ = Specific gravity

τ = Shear stress, [Pa]

μ = Dynamic viscosity, [cP]

ϑ = Kinematic viscosity, [stokes]

π = Constant PI, ~3,14

Abbreviations

CVD = Chemical Vapour Deposition

EOR = Enhanced Oil Recovery

IFT = Interfacial Tension

NF = Nanofluid

nm = Nanometer

NMR = Nuclear Magnetic Resonance

PVT = Pressure-Volume-Temperature

RPM = Rounds Per Minute

SEM = Scanning Electron Microscope

SNP = Silica NanoParticle

USBM = US Bureau of Mines

WI = Wettability Index

wt. % = Weight percentage

Subscripts

o = Oil

w = Water

g = Gas

l = Liquid

s = Solid

Appendix A - Calculation Data and Results

A-1 Core Dimensions and Porosity

Table A-1: Core dimensions and Porosity

Core nr	Diameter [cm]	Height [cm]	Bulk Volume [cm^3]	Dry weight [g]	V1 [cm^3]	V2 [cm^3]	Grain Volume [cm^3]	Pore Volume [cm^3]	Porosity
# 1	3,83	4,05	46,66	**102,32**	57,00	18,50	38,50	8,16	**17,49 %**
# 2	3,83	4,05	46,66	**100,41**	57,00	19,20	37,80	8,86	**18,99 %**
# 3	3,83	4,08	47,01	**102,91**	57,00	18,40	38,60	8,41	**17,88 %**
# 4	3,82	4,08	46,76	**103,27**	57,50	18,20	39,30	7,46	**15,95 %**
# 5	3,83	4,07	46,89	**101,33**	57,00	19,00	38,00	8,89	**18,96 %**
# 6	3,83	4,07	46,89	**103,29**	57,50	18,15	39,35	7,54	**16,08 %**
# 7	3,82	4,07	46,65	**103,01**	57,00	18,30	38,70	7,95	**17,03 %**
# 8	3,83	4,07	46,89	**103,15**	57,50	18,20	39,30	7,59	**16,19 %**
# 9	3,83	4,08	47,01	**100,58**	57,00	19,20	37,80	9,21	**19,58 %**
# 10	3,83	4,06	46,77	**102,72**	57,00	18,40	38,60	8,17	**17,48 %**
# 11	3,83	4,06	46,77	**101,47**	57,00	18,90	38,10	8,67	**18,55 %**
# 12	3,83	4,05	46,66	**102,83**	57,50	18,50	39,00	7,66	**16,42 %**
# 13	3,82	4,07	46,65	**101,97**	57,00	18,70	38,30	8,35	**17,89 %**
# 14	3,83	4,05	46,66	**103,66**	57,00	18,10	38,90	7,76	**16,63 %**
# 15	3,83	4,08	47,01	**103,22**	57,50	18,30	39,20	7,81	**16,61 %**
# 16	3,83	4,08	47,01	**103,46**	57,50	18,20	39,30	7,71	**16,39 %**

A-2 Permeability and Klinkenberg Plots

Table A-2: Air permeability measurements for core #1 - #8

Core nr	Area [cm^2]	Length [cm]	P1 [bar]	P2 [bar]	Pm [bar}	Qatm [L/min]	Qatm [cm^3/s]	1/Pm [1/bar]	kair [D]	Klinkenberg constant, b	Permeability [mD]
# 1	11,521	4,05	1,40	1,00	1,20	2,60	43,33	0,833	0,57	0,288	**334,4**
			1,60	1,20	1,40	2,84	47,33	0,714	0,54		
			1,80	1,40	1,60	3,15	52,50	0,625	0,52		
			2,00	1,60	1,80	3,33	55,50	0,556	0,49		
# 2	11,521	4,05	1,40	1,00	1,20	3,22	53,67	0,833	0,71	0,355	**420,4**
			1,60	1,20	1,40	3,60	60,00	0,714	0,68		
			1,80	1,40	1,60	3,91	65,17	0,625	0,65		
			2,00	1,60	1,80	4,15	69,17	0,556	0,61		
# 3	11,521	4,08	1,40	1,00	1,20	2,00	33,33	0,833	0,44	0,155	**319,2**
			1,60	1,20	1,40	2,28	38,00	0,714	0,43		
			1,80	1,40	1,60	2,52	42,00	0,625	0,42		
			2,00	1,60	1,80	2,70	45,00	0,556	0,40		
# 4	11,461	4,08	1,40	1,00	1,20	1,90	31,67	0,833	0,42	0,082	**359,6**
			1,60	1,20	1,40	2,20	36,67	0,714	0,42		
			1,80	1,40	1,60	2,47	41,17	0,625	0,41		
			2,00	1,60	1,80	2,69	44,83	0,556	0,40		
# 5	11,521	4,07	1,40	1,00	1,20	2,99	49,83	0,833	0,66	0,359	**367,9**
			1,60	1,20	1,40	3,30	55,00	0,714	0,63		
			1,80	1,40	1,60	3,62	60,33	0,625	0,60		
			2,00	1,60	1,80	3,78	63,00	0,556	0,56		
# 6	11,521	4,07	1,40	1,00	1,20	1,56	26,00	0,833	0,35	0,095	**265,2**
			1,60	1,20	1,40	1,74	29,00	0,714	0,33		
			1,80	1,40	1,60	1,95	32,50	0,625	0,32		
			2,00	1,60	1,80	2,16	36,00	0,556	0,32		
# 7	11,461	4,07	1,40	1,00	1,20	2,53	42,17	0,833	0,56	0,274	**336,7**
			1,60	1,20	1,40	2,80	46,67	0,714	0,54		
			1,80	1,40	1,60	3,03	50,50	0,625	0,51		
			2,00	1,60	1,80	3,29	54,83	0,556	0,49		
# 8	11,521	4,07	1,40	1,00	1,20	2,00	33,33	0,833	0,44	0,103	**361,2**
			1,60	1,20	1,40	2,30	38,33	0,714	0,44		
			1,80	1,40	1,60	2,61	43,50	0,625	0,43		
			2,00	1,60	1,80	2,78	46,33	0,556	0,41		

Table A-3: Air permeability measurements for core #9 - #16

Core nr	Area [cm^2]	Length [cm]	P1 [bar]	P2 [bar]	Pm [bar}	Qatm [L/min]	Qatm [cm^3/s]	1/Pm [1/bar]	kair [D]	Klinkenberg constant, b	Permeability [mD]
# 9	11,521	4,07	1,40	1,00	1,20	3,75	62,50	0,833	0,83	0,496	**426,3**
			1,60	1,20	1,40	4,14	69,00	0,714	0,79		
			1,80	1,40	1,60	4,44	74,00	0,625	0,74		
			2,00	1,60	1,80	4,69	78,17	0,556	0,69		
# 10	11,521	4,08	1,40	1,00	1,20	2,19	36,50	0,833	0,49	0,205	**316,7**
			1,60	1,20	1,40	2,46	41,00	0,714	0,47		
			1,80	1,40	1,60	2,72	45,33	0,625	0,45		
			2,00	1,60	1,80	2,88	48,00	0,556	0,43		
# 11	11,521	4,06	1,40	1,00	1,20	3,30	55,00	0,833	0,73	0,420	**384**
			1,60	1,20	1,40	3,63	60,50	0,714	0,69		
			1,80	1,40	1,60	3,92	65,33	0,625	0,65		
			2,00	1,60	1,80	4,15	69,17	0,556	0,61		
# 12	11,521	4,05	1,40	1,00	1,20	2,50	41,67	0,833	0,55	0,282	**319,6**
			1,60	1,20	1,40	2,78	46,33	0,714	0,53		
			1,80	1,40	1,60	3,00	50,00	0,625	0,50		
			2,00	1,60	1,80	3,22	53,67	0,556	0,47		
# 13	11,461	4,07	1,40	1,00	1,20	3,14	52,33	0,833	0,70	0,382	**383,1**
			1,60	1,20	1,40	3,44	57,33	0,714	0,66		
			1,80	1,40	1,60	3,75	62,50	0,625	0,63		
			2,00	1,60	1,80	3,98	66,33	0,556	0,59		
# 14	11,521	4,05	1,40	1,00	1,20	2,21	36,83	0,833	0,49	0,192	**332,4**
			1,60	1,20	1,40	2,52	42,00	0,714	0,48		
			1,80	1,40	1,60	2,75	45,83	0,625	0,46		
			2,00	1,60	1,80	2,95	49,17	0,556	0,43		
# 15	11,521	4,08	1,40	1,00	1,20	2,55	42,50	0,833	0,57	0,266	**346,4**
			1,60	1,20	1,40	2,81	46,83	0,714	0,54		
			1,80	1,40	1,60	3,12	52,00	0,625	0,52		
			2,00	1,60	1,80	3,30	55,00	0,556	0,49		
# 16	11,521	4,08	1,40	1,00	1,20	2,55	42,50	0,833	0,57	0,266	**345,9**
			1,60	1,20	1,40	2,81	46,83	0,714	0,54		
			1,80	1,40	1,60	3,10	51,67	0,625	0,52		
			2,00	1,60	1,80	3,31	55,17	0,556	0,49		

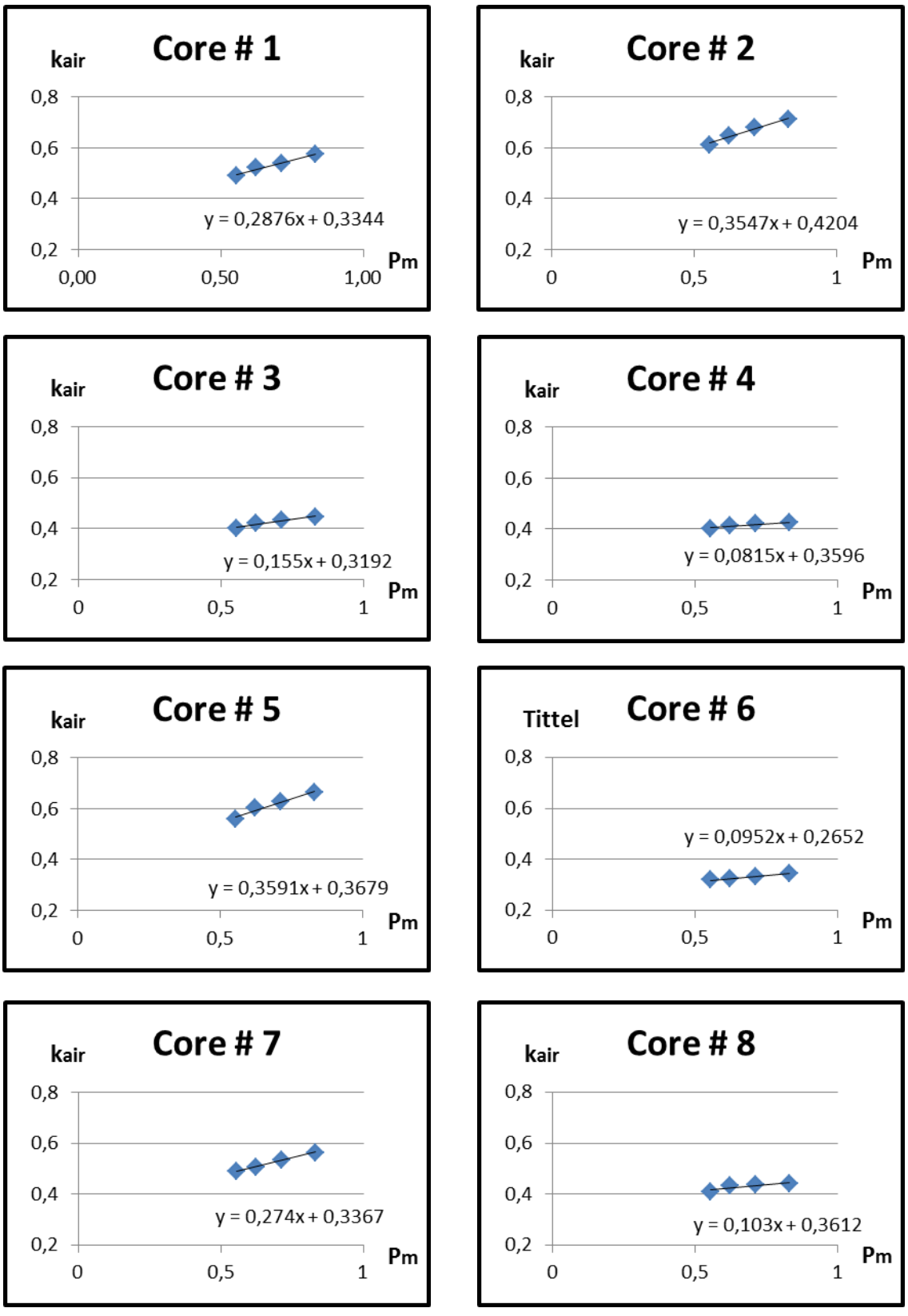

Figure A-1: Klinkenberg plots for cores #1 - #8

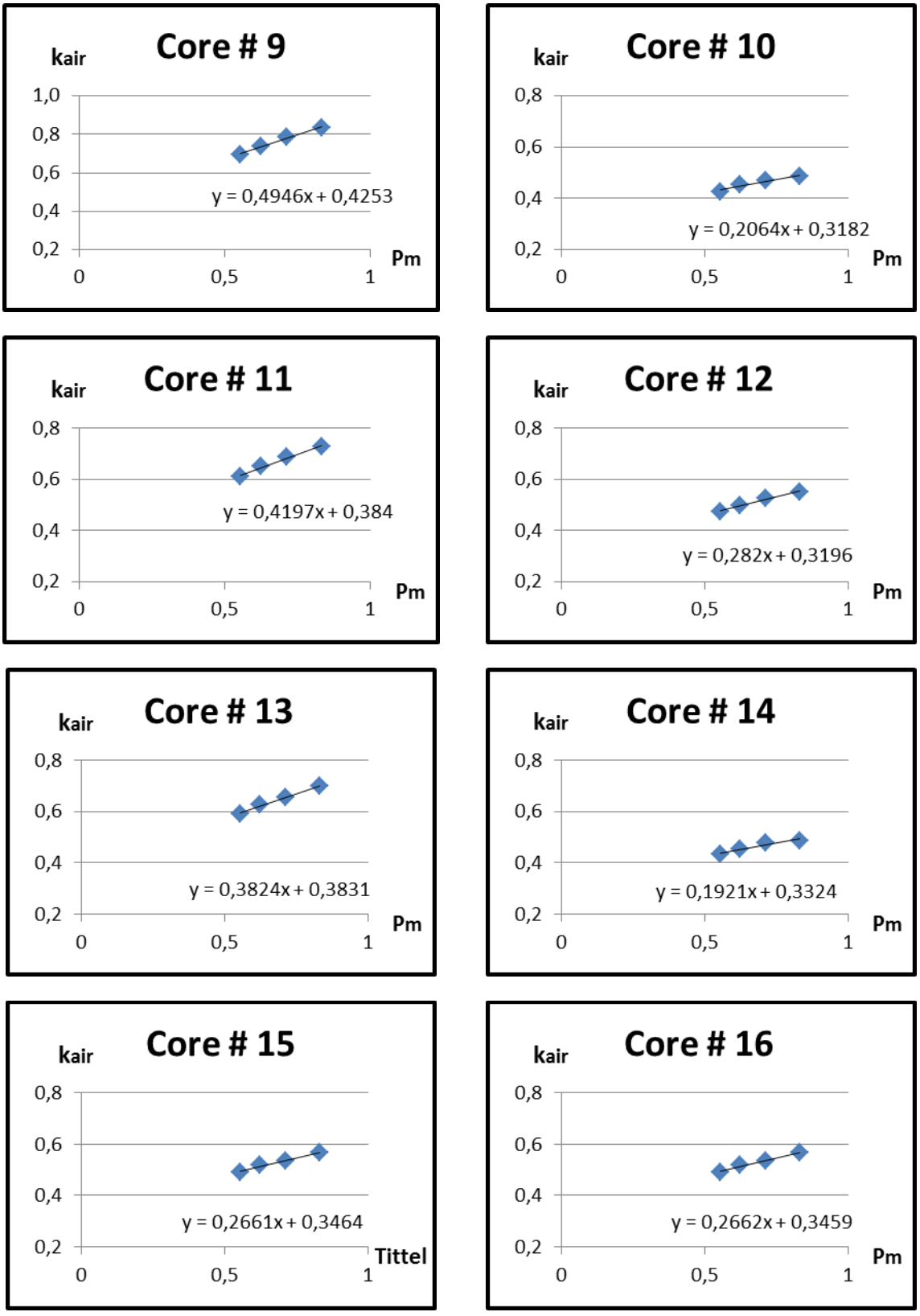

Figure A-2: Klinkenberg plots for cores #9 - #16

A-3 Initial wettability - Spontaneous imbibition rates

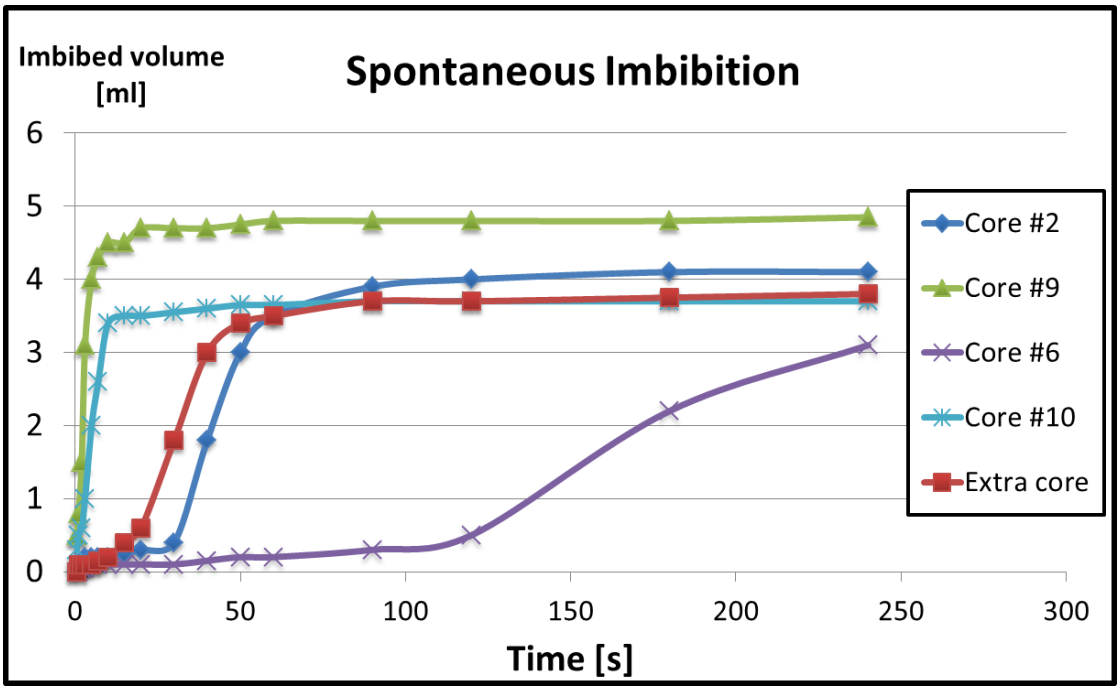

Figure A-3: Spontaneous imbibition rates for initial wettability establishment

A-4 New Porosity

Table A-4: Core dimensions and New Porosity measurements

Pair	Core nr	Diameter [cm]	Height [cm]	Bulk Volume [cm^3]	Dry weight [g]	V1 [cm^3]	V2 [cm^3]	Grain Volume [cm^3]	Pore Volume [cm^3]	Porosity
1	**# 1**	3,83	4,05	46,66	**102,32**	72,00	32,50	39,50	7,16	**15,34 %**
	# 7	3,82	4,07	46,65	**103,01**	72,00	32,20	39,80	6,85	**14,68 %**
2	**# 3**	3,83	4,08	47,01	**102,91**	72,00	32,75	39,25	7,76	**16,50 %**
	# 12	3,83	4,05	46,66	**102,83**	72,00	32,40	39,60	7,06	**15,13 %**
3	**# 4**	3,82	4,08	46,76	**103,27**	72,00	32,10	39,90	6,86	**14,67 %**
	# 8	3,83	4,07	46,89	**103,15**	72,00	32,20	39,80	7,09	**15,12 %**
4	**# 5**	3,83	4,07	46,89	**101,33**	72,00	32,90	39,10	7,79	**16,61 %**
	# 14	3,83	4,05	46,66	**103,66**	72,00	32,20	39,80	6,86	**14,70 %**
5	**# 11**	3,83	4,06	46,77	**101,47**	72,00	32,90	39,10	7,67	**16,41 %**
	# 13	3,82	4,07	46,65	**101,97**	72,00	32,80	39,20	7,45	**15,96 %**
6	**# 15**	3,83	4,08	47,01	**103,22**	72,00	32,20	39,80	7,21	**15,33 %**
	# 16	3,83	4,08	47,01	**103,46**	72,00	32,20	39,80	7,21	**15,33 %**

A-5 New Air Permeability and Klinkenberg Plots

Table A-5: New air permeability measurements

Pair	Core nr	Area [cm^2]	Length [cm]	P1 [bar]	P2 [bar]	Pm [bar}	Qatm [L/min]	Qatm [cm^3/s]	1/Pm [1/bar]	kair [D]	Klinkenberg constant, b	Permeability [mD]
1	# 1	11,521	4,05	1,40	1,00	1,20	2,86	47,67	0,833	0,63	0,336	**354,6**
				1,60	1,20	1,40	3,17	52,83	0,714	0,60		
				1,80	1,40	1,60	3,43	57,17	0,625	0,57		
				2,00	1,60	1,80	3,65	60,83	0,556	0,54		
	# 7	11,461	4,07	1,40	1,00	1,20	2,48	41,33	0,833	0,55	0,270	**334,4**
				1,60	1,20	1,40	2,80	46,67	0,714	0,54		
				1,80	1,40	1,60	3,05	50,83	0,625	0,51		
				2,00	1,60	1,80	3,20	53,33	0,556	0,48		
2	# 3	11,521	4,08	1,40	1,00	1,20	2,23	37,17	0,833	0,50	0,202	**335,3**
				1,60	1,20	1,40	2,58	43,00	0,714	0,49		
				1,80	1,40	1,60	2,80	46,67	0,625	0,47		
				2,00	1,60	1,80	2,96	49,33	0,556	0,44		
	# 12	11,521	4,05	1,40	1,00	1,20	1,99	33,17	0,833	0,44	0,132	**333,8**
				1,60	1,20	1,40	2,30	38,33	0,714	0,44		
				1,80	1,40	1,60	2,52	42,00	0,625	0,42		
				2,00	1,60	1,80	2,74	45,67	0,556	0,40		
3	# 4	11,461	4,08	1,40	1,00	1,20	1,72	28,67	0,833	0,38	0,129	**275,4**
				1,60	1,20	1,40	1,91	31,83	0,714	0,37		
				1,80	1,40	1,60	2,12	35,33	0,625	0,36		
				2,00	1,60	1,80	2,34	39,00	0,556	0,35		
	# 8	11,521	4,07	1,40	1,00	1,20	0,86	14,33	0,833	0,19	0,061	**141,1**
				1,60	1,20	1,40	0,98	16,33	0,714	0,19		
				1,80	1,40	1,60	1,09	18,17	0,625	0,18		
				2,00	1,60	1,80	1,17	19,50	0,556	0,17		
4	# 5	11,521	4,07	1,40	1,00	1,20	3,10	51,67	0,833	0,69	0,386	**373,0**
				1,60	1,20	1,40	3,47	57,83	0,714	0,66		
				1,80	1,40	1,60	3,72	62,00	0,625	0,62		
				2,00	1,60	1,80	3,92	65,33	0,556	0,58		
	# 14	11,521	4,05	1,40	1,00	1,20	2,19	36,50	0,833	0,48	0,190	**328,1**
				1,60	1,20	1,40	2,48	41,33	0,714	0,47		
				1,80	1,40	1,60	2,72	45,33	0,625	0,45		
				2,00	1,60	1,80	2,92	48,67	0,556	0,43		
5	# 11	11,521	4,06	1,40	1,00	1,20	2,67	44,50	0,833	0,59	0,290	**348,9**
				1,60	1,20	1,40	2,93	48,83	0,714	0,56		
				1,80	1,40	1,60	3,21	53,50	0,625	0,53		
				2,00	1,60	1,80	3,45	57,50	0,556	0,51		
	# 13	11,461	4,07	1,40	1,00	1,20	2,98	49,67	0,833	0,66	0,346	**378,4**
				1,60	1,20	1,40	3,28	54,67	0,714	0,63		
				1,80	1,40	1,60	3,60	60,00	0,625	0,60		
				2,00	1,60	1,80	3,80	63,33	0,556	0,56		
6	# 15	11,521	4,08	1,40	1,00	1,20	1,54	25,67	0,833	0,34	0,136	**230,0**
				1,60	1,20	1,40	1,72	28,67	0,714	0,33		
				1,80	1,40	1,60	1,92	32,00	0,625	0,32		
				2,00	1,60	1,80	2,04	34,00	0,556	0,30		
	# 16	11,521	4,08	1,40	1,00	1,20	1,00	16,67	0,833	0,22	0,064	**171,0**
				1,60	1,20	1,40	1,15	19,17	0,714	0,22		
				1,80	1,40	1,60	1,27	21,17	0,625	0,21		
				2,00	1,60	1,80	1,38	23,00	0,556	0,20		

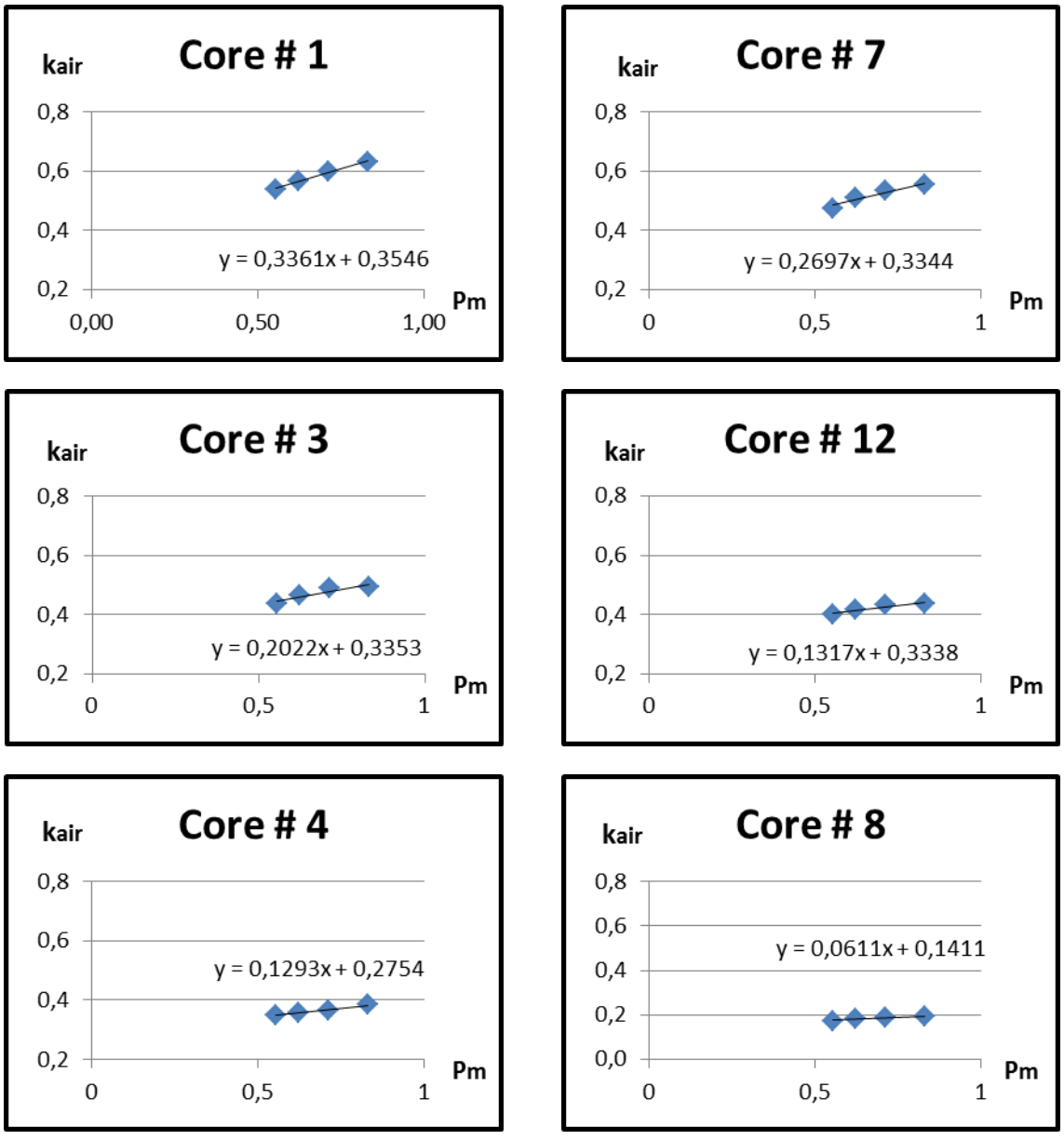

Figure A-4: New Klinkenberg plots for core pairs 1 - 3

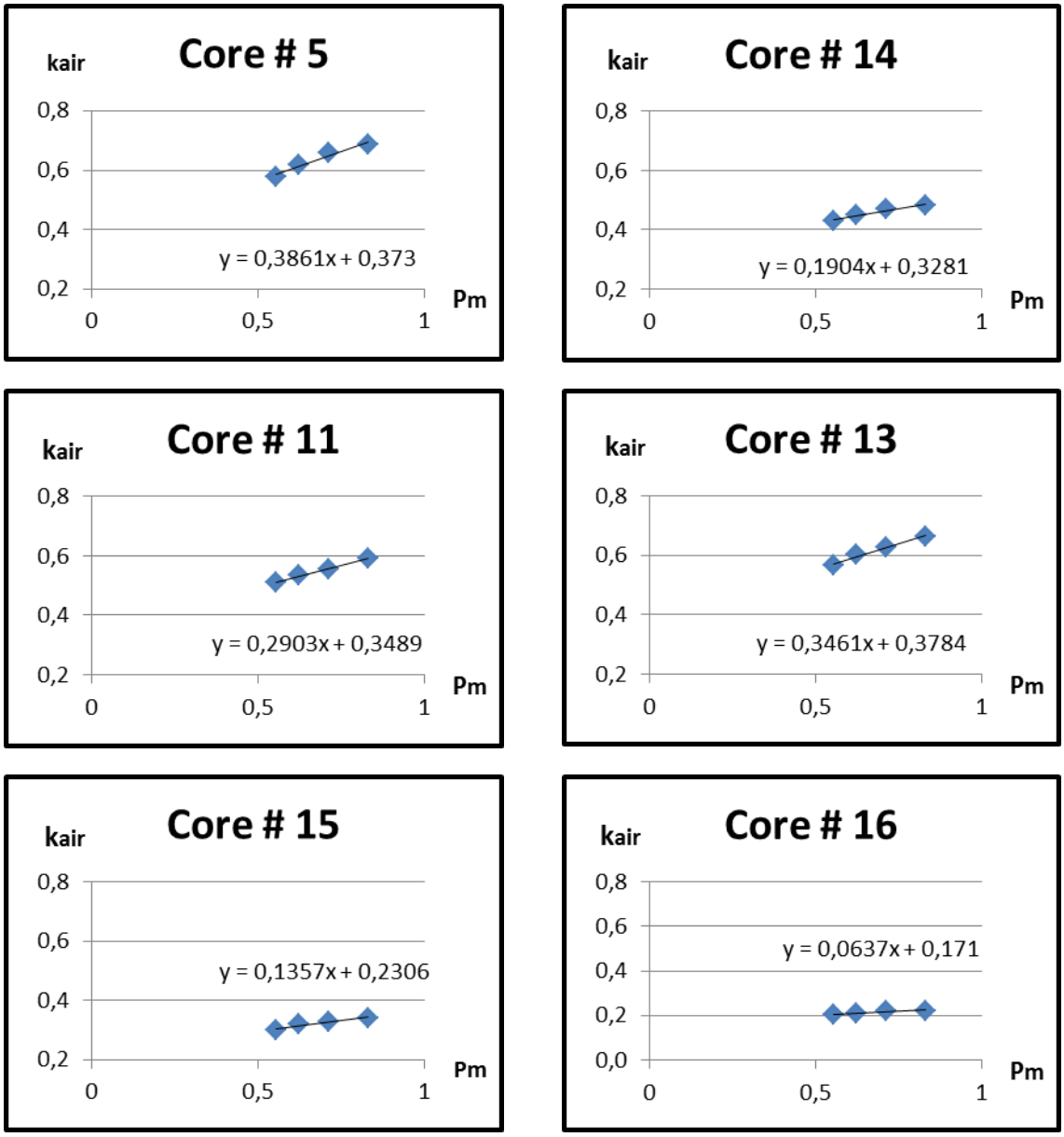

Figure A-5: New Klinkenberg plots for core pairs 4 - 6

A-6 New Wettability - Spontaneous imbibition rates

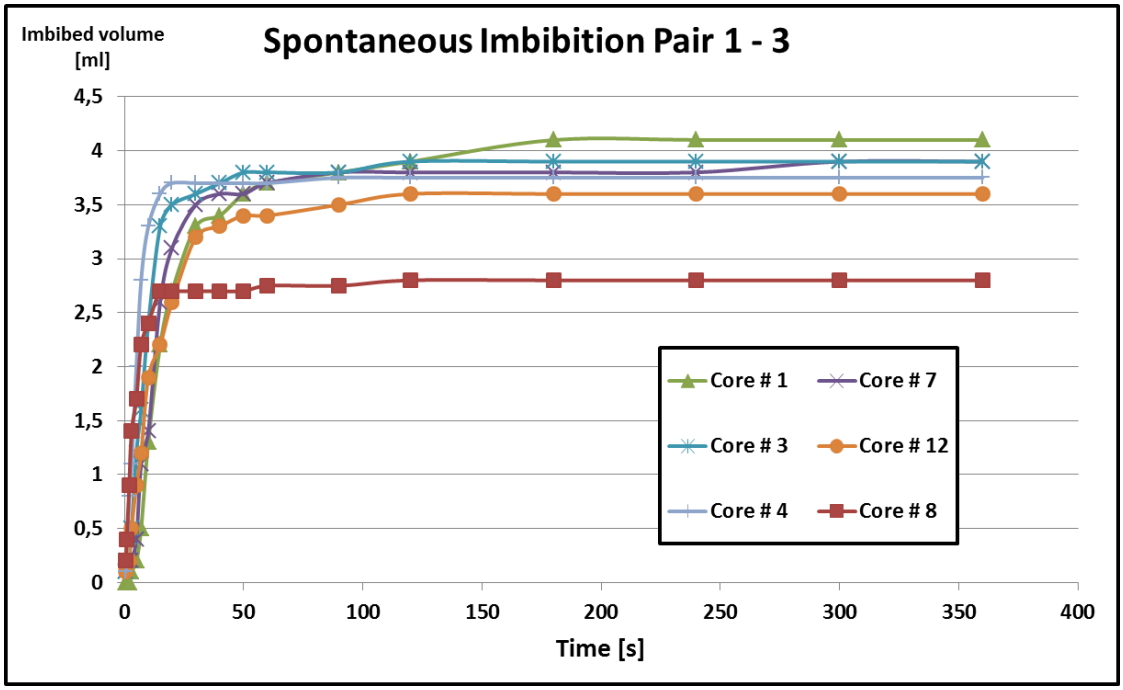

Figure A-6: Spontaneous imbibition rates core pairs 1 - 3

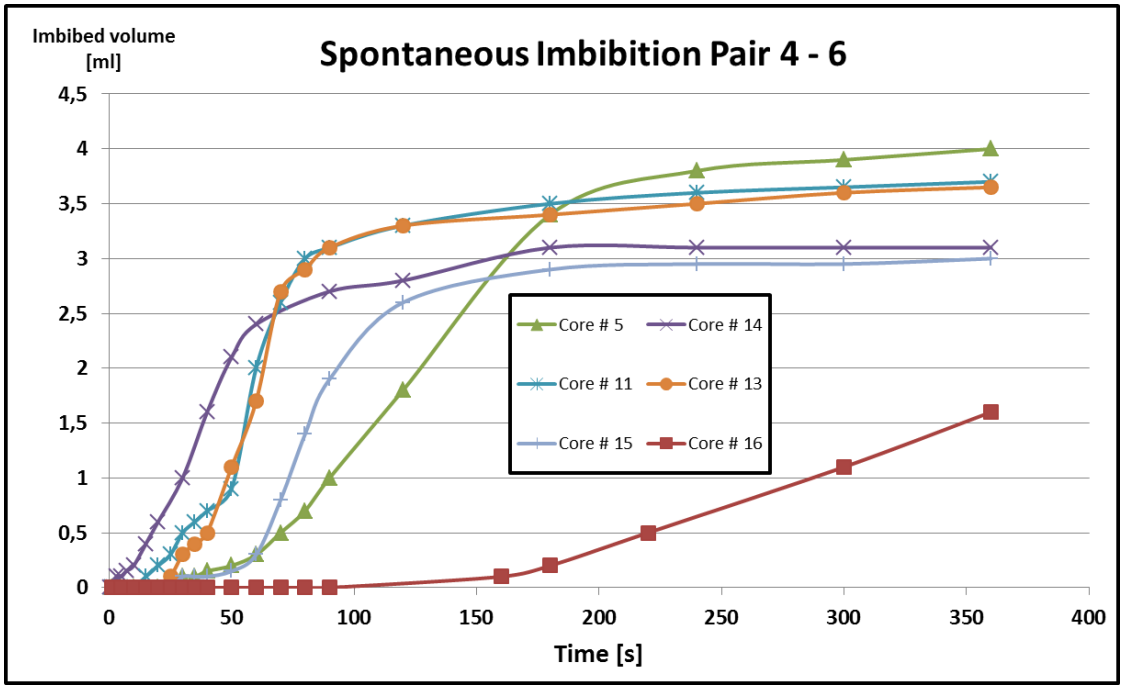

Figure A-7: Spontaneous imbibition rates core pairs 1 - 3

A-7 Fluid Density

Table A-6: Fluid densities

Fluid	Filled weight [g]	Pycnometer volume: [cm^3]	Density [g/cm^3]
Brine 3 wt. %	50,997	50,006	**1,020**
n-Decane	36,440	50,006	**0,729**
Hydrophilic 0,01 wt. %	50,981	50,006	**1,019**
Hydrophilic 0,1 wt. %	50,991	50,006	**1,020**
Hydrophilic 0,5 wt. %	51,122	50,006	**1,022**
Hydrophobic 0,01 wt. %	36,184	50,006	**0,724**
Hydrophobic 0,1 wt. %	36,164	50,006	**0,723**
Hydrophobic 0,5 wt. %	36,304	50,006	**0,726**

A-8 Fluid Viscosity

Table A-7: Fluid viscosities

Fluid	t1 [s]	t2 [s]	v [sST]	μ [cp]
Capillary viscometer nr 25:	K1 = 0,00198		K2 = 0,001635	
Brine 3 wt. %	499,00	603,00	0,987	**1,007**
Hydrophilic 0,01 wt. %	485,61	591,20	0,964	**0,983**
Hydrophilic 0,1 wt. %	542,40	707,07	1,115	**1,137**
Hydrophilic 0,5 wt. %	644,33	958,2	1,421	**1,453**
Capillary viscometer nr 50 (1):	K1 = 0,003667		K2 = 0,00271	
n-Decane	337,33	455,39	1,235	**0,900**
Hydrophobic 0,1 wt. %	336,42	456,76	1,236	**0,894**
Capillary viscometer nr 50 (2):	K1 = 0,003455		K2 = 0,002572	
Hydrophobic 0,01 wt. %	357,46	480,98	1,236	**0,894**
Hydrophobic 0,5 wt. %	361,00	481,82	1,243	**0,903**

A-9 Contact Angles

A-9.1 Brine in Oil

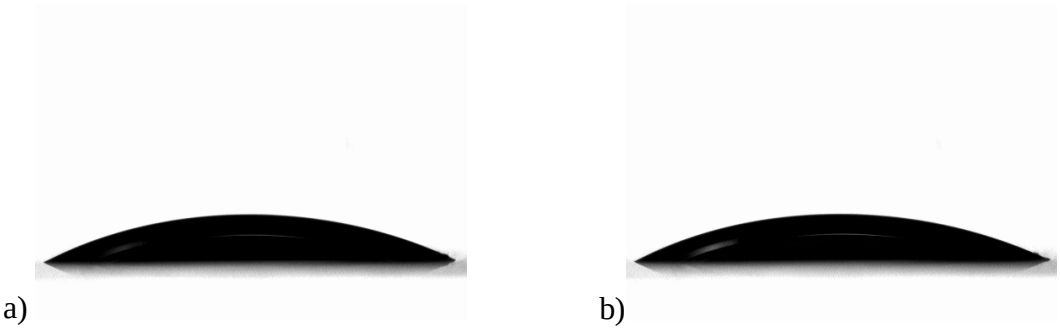

a) b)

Figure A-8: Brine in oil at a) start and b) end of experiment

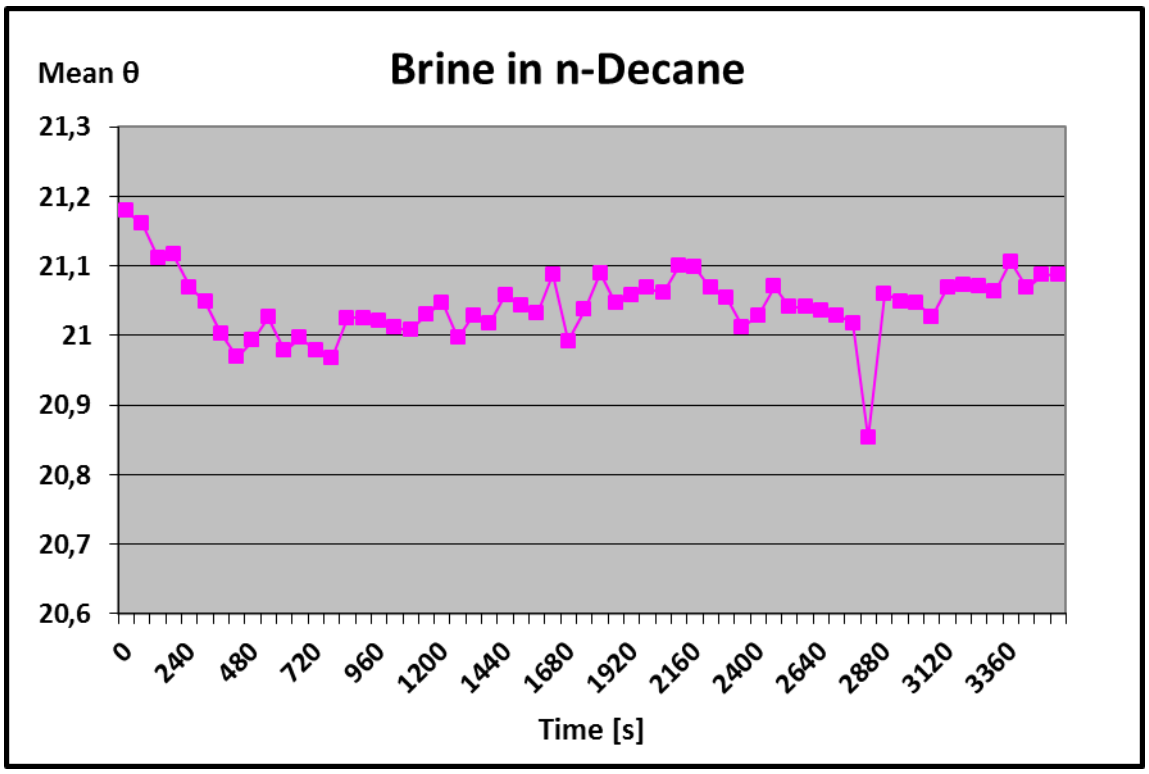

Figure A-9: Mean contact angle vs. time for brine in oil

A-9.2 Hydrophilic SNPs 0,01 wt. % in Oil

a) 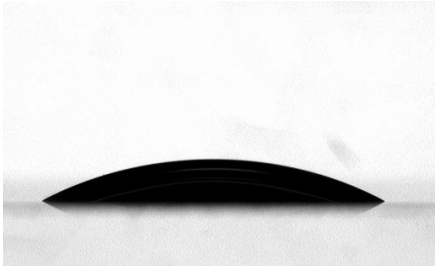 b) 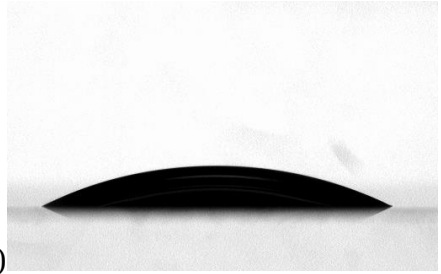

Figure A-10: Hydrophilic SNPs 0,01 wt. % in oil at a) start and b) end of experiment

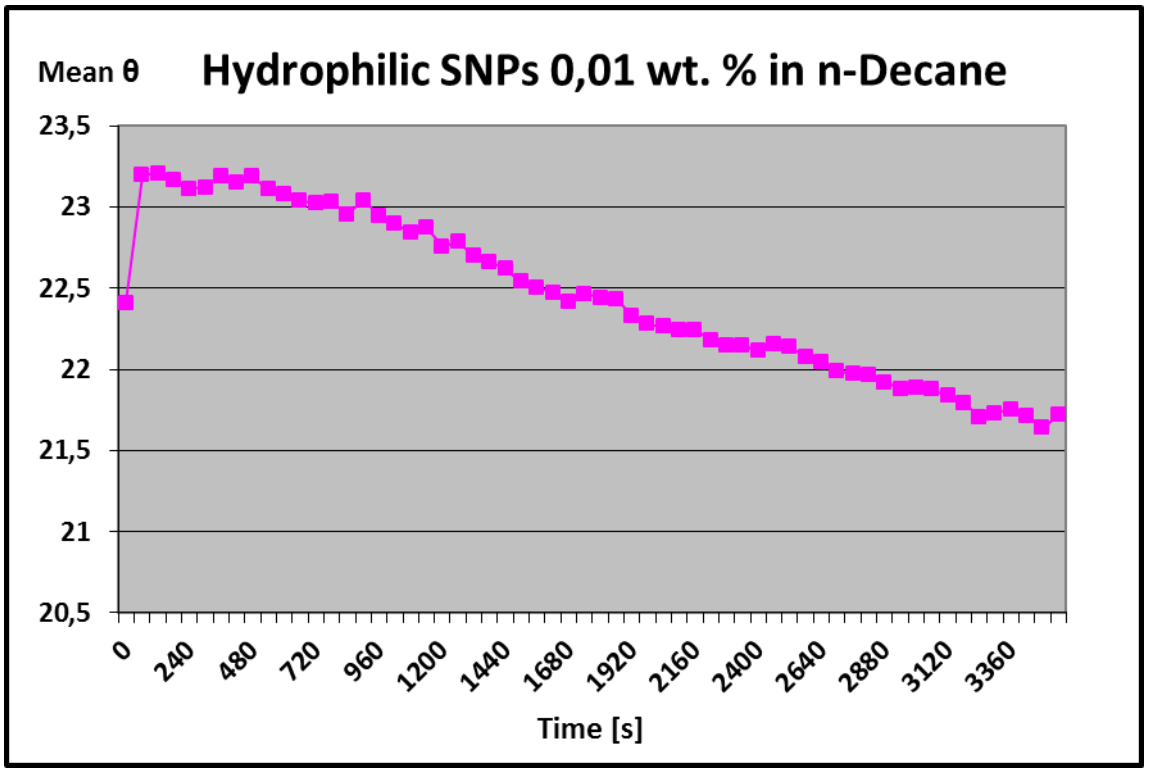

Figure A-11: Mean contact angle vs. time for hydrophilic SNPs 0,01 wt. % in oil

A-9.3 Hydrophilic SNPs 0,1 wt.% in Oil

a) 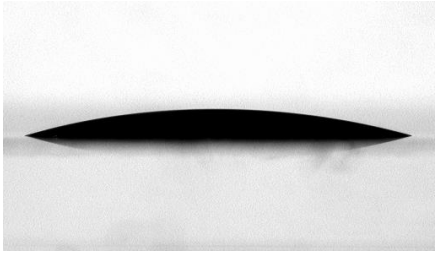 b) 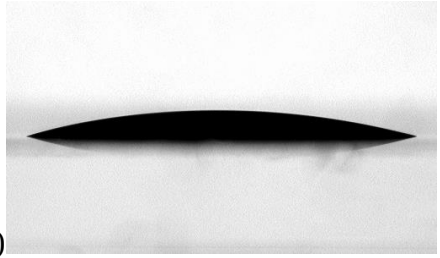

Figure A-12: Hydrophilic SNPs 0,1 wt. % in oil at a) start and b) end of experiment

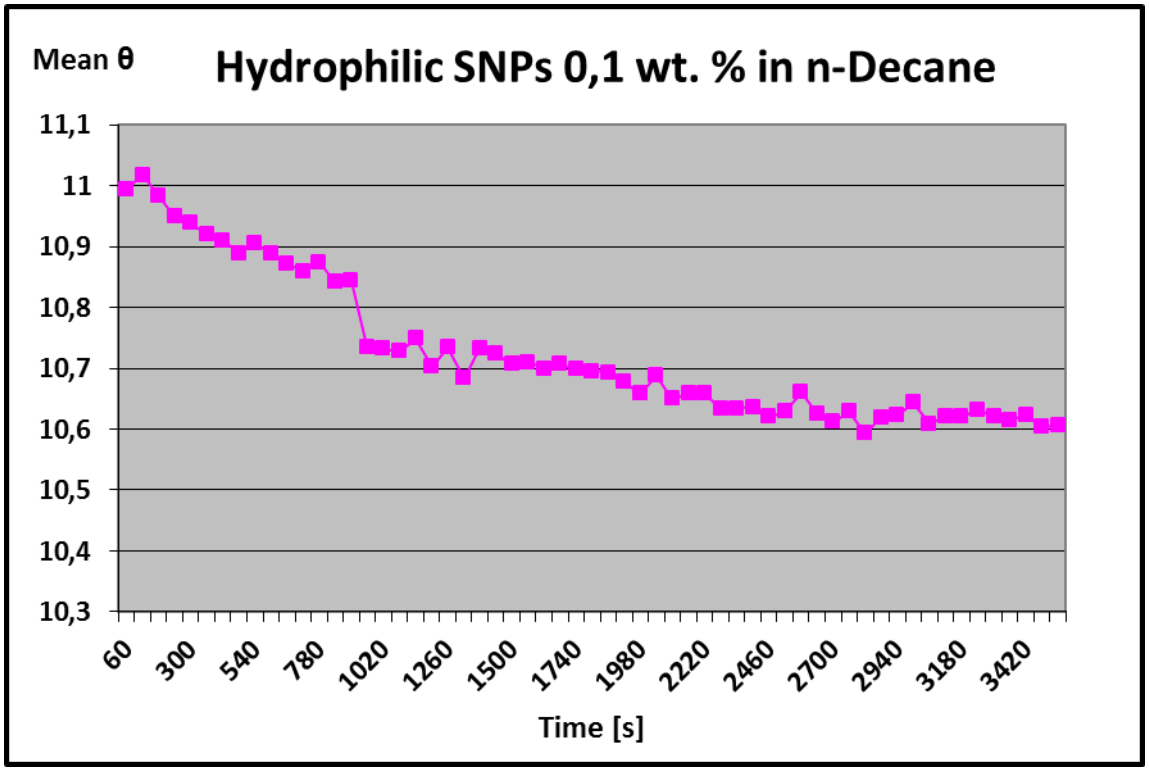

Figure A-13: Mean contact angle vs. time for hydrophilic SNPs 0,1 wt. % in oil

A-9.4 Hydrophilic SNPs 0,5 wt.% in Oil

a) 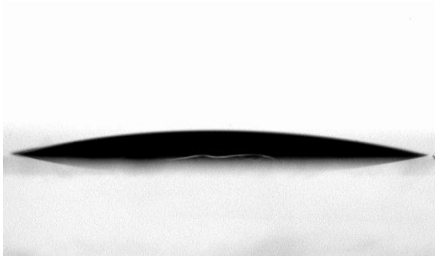 b) 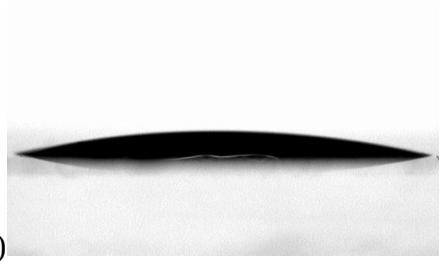

Figure A-14: Hydrophilic SNPs 0,5 wt. % in oil at a) start and b) end of experiment

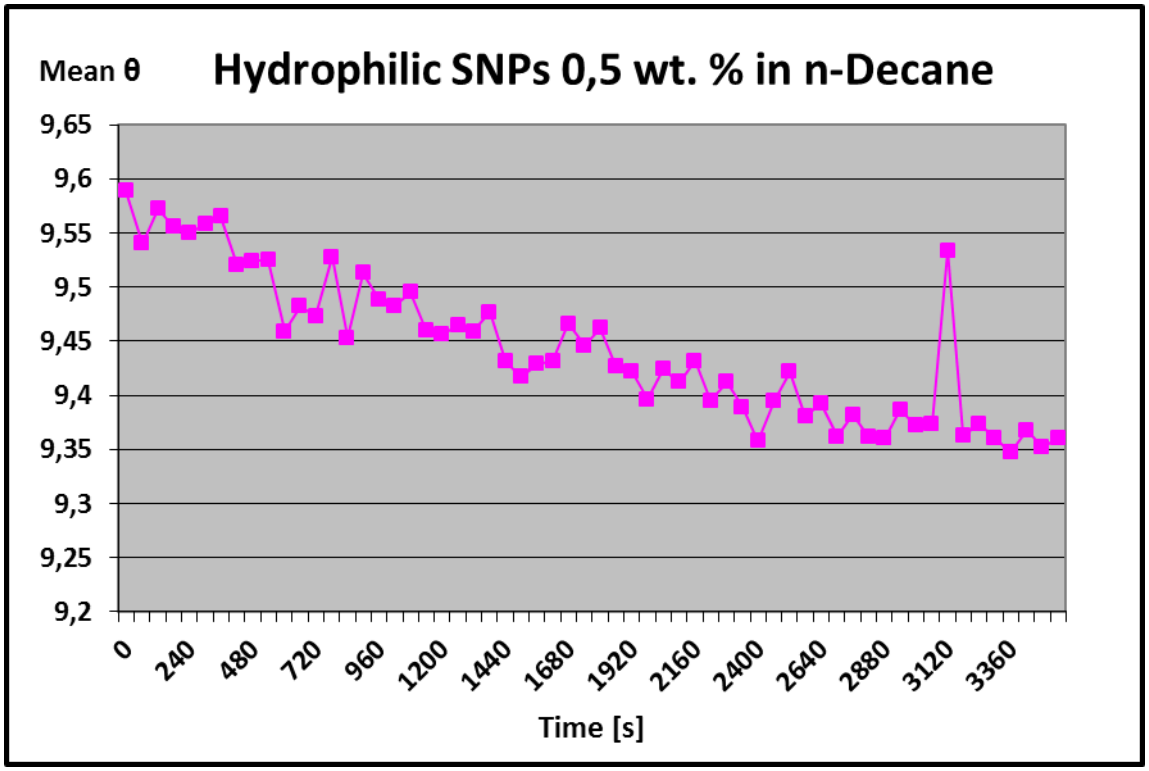

Figure A-15: Mean contact angle vs. time for hydrophilic SNPs 0,5 wt. % in oil

A-9.5 Oil in Brine

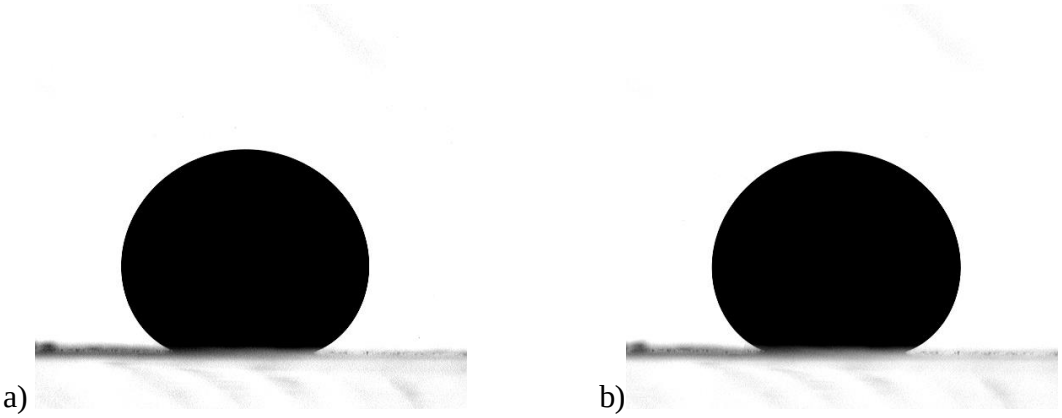

a) b)

Figure A-16: Oil in Brine at a) start and b) end of experiment

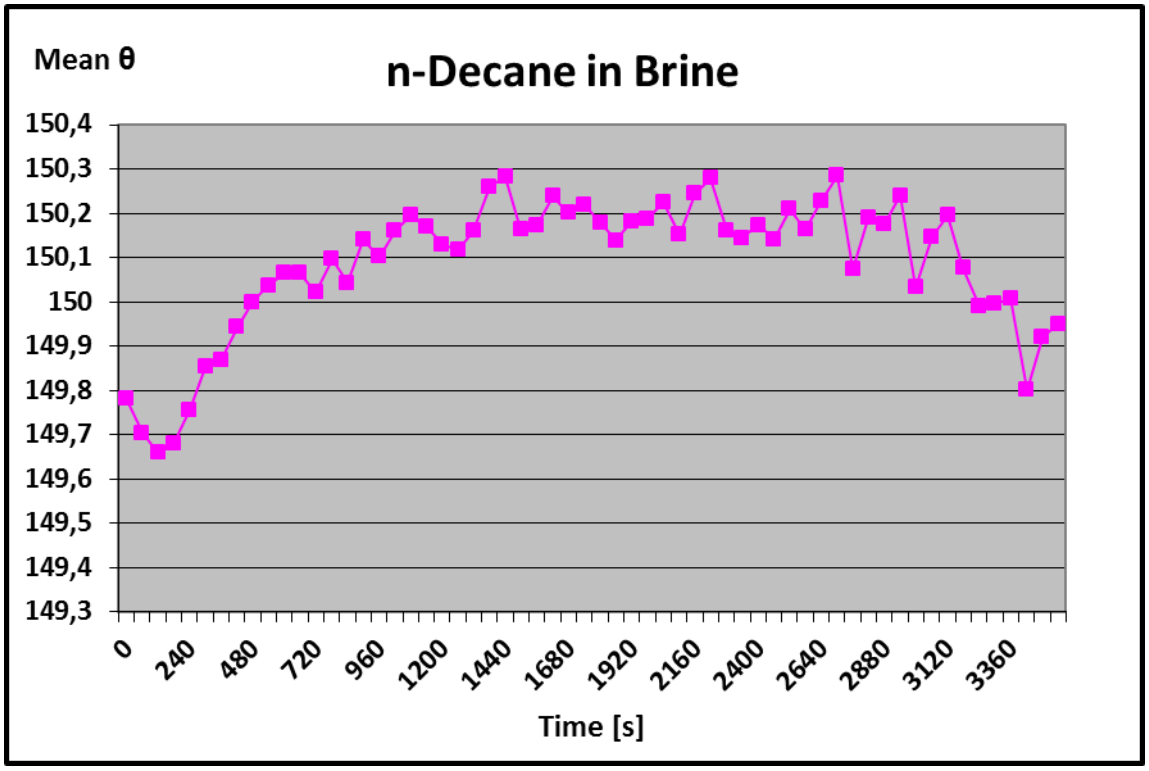

Figure A-17: Mean contact angle vs. time for oil in Brine

A-9.6 Oil in Hydrophilic SNPs 0,01 wt. %

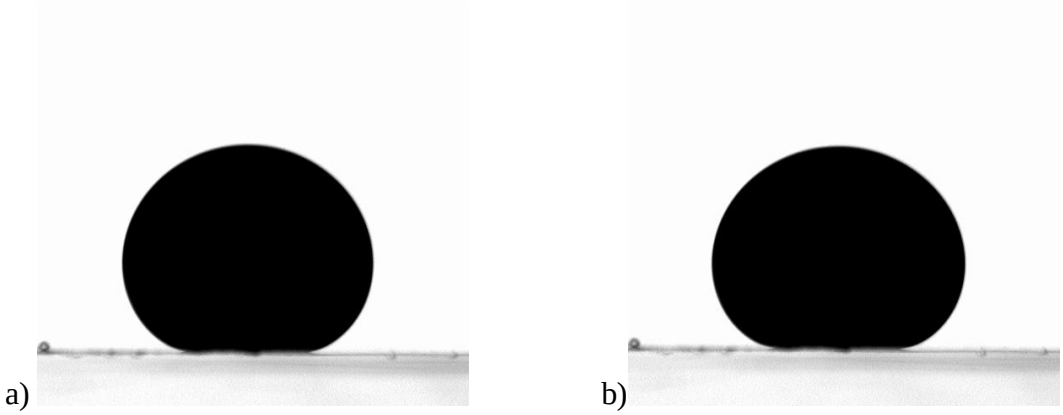

a) b)

Figure A-18: Oil in Hydrophilic SNPs 0,01 wt.% at a) start and b) end of experiment

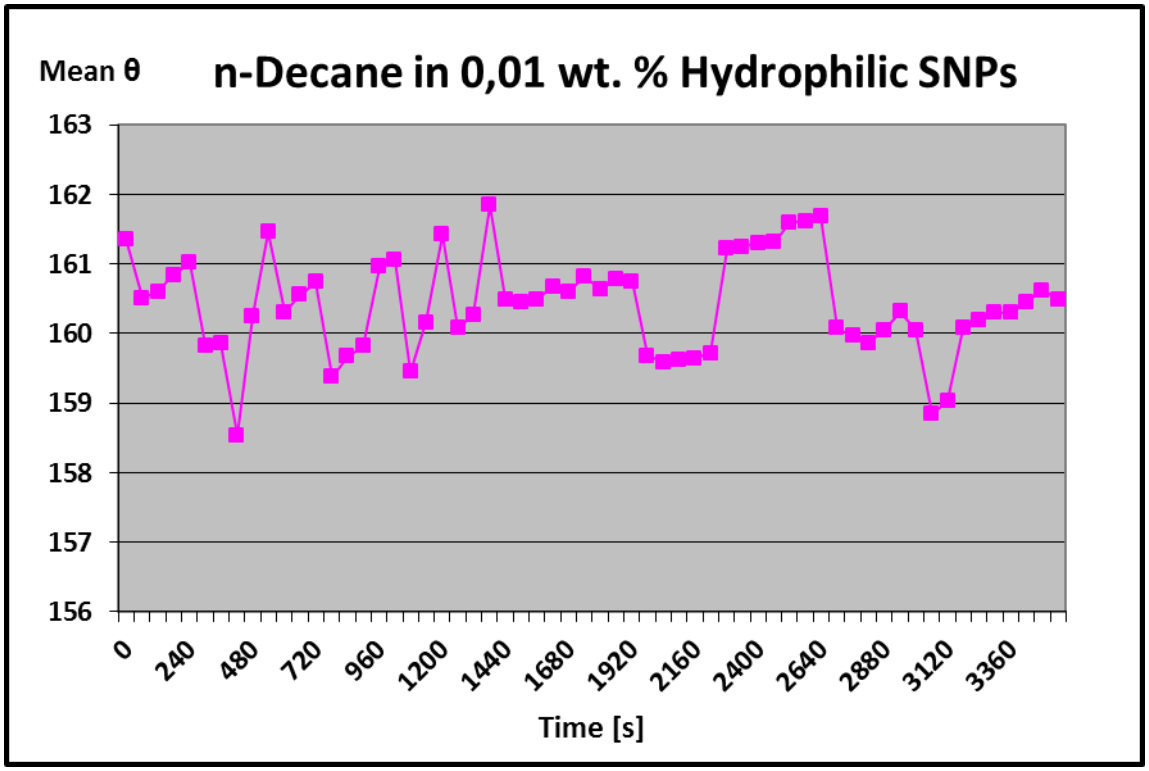

Figure A-19: Mean contact angle vs. time for oil in hydrophilic SNPs 0,01 wt. %

A-9.7 Oil in Hydrophilic SNPs 0,1 wt. %

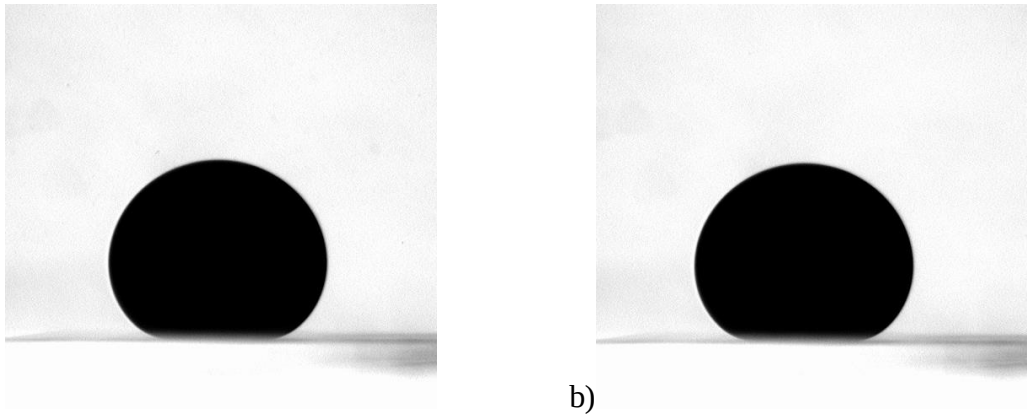

a) b)

Figure A-20: Oil in Hydrophilic SNPs 0,1 wt. % at a) start and b) end of experiment

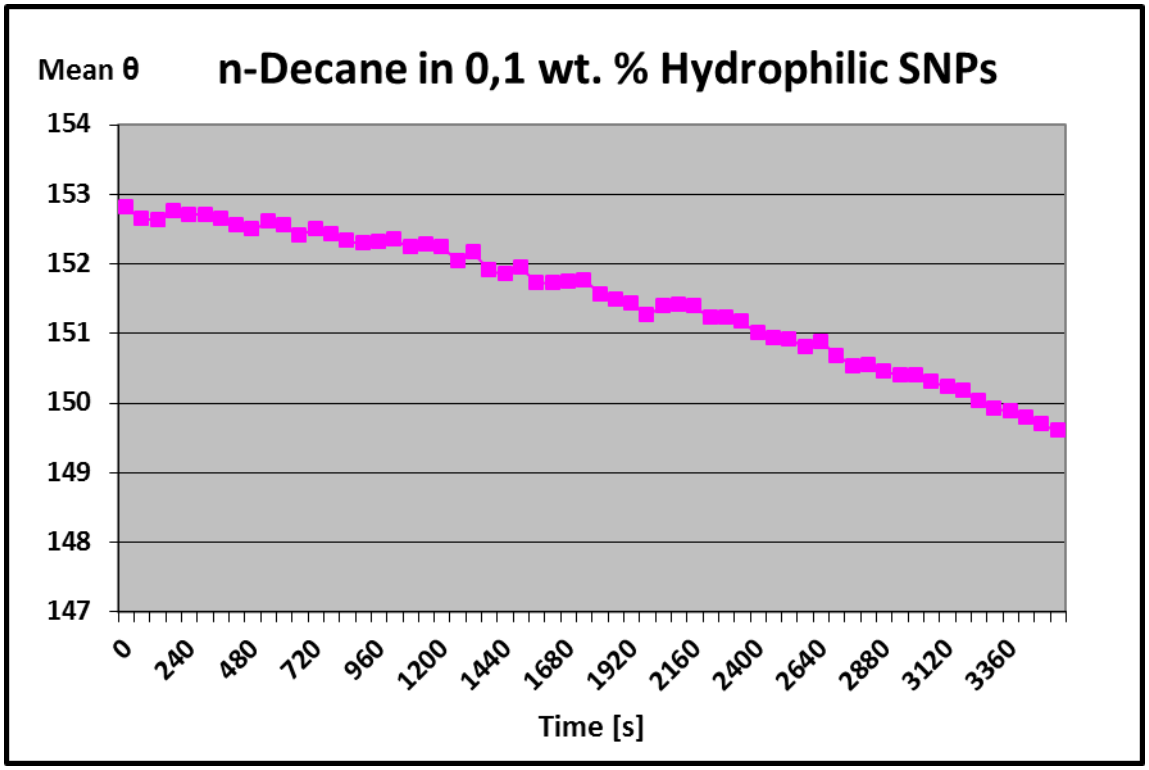

Figure A-21: Mean contact angle vs. time for oil in hydrophilic SNPs 0,1 wt. %

A-9.8 Oil in Hydrophilic SNPs 0,5 wt. %

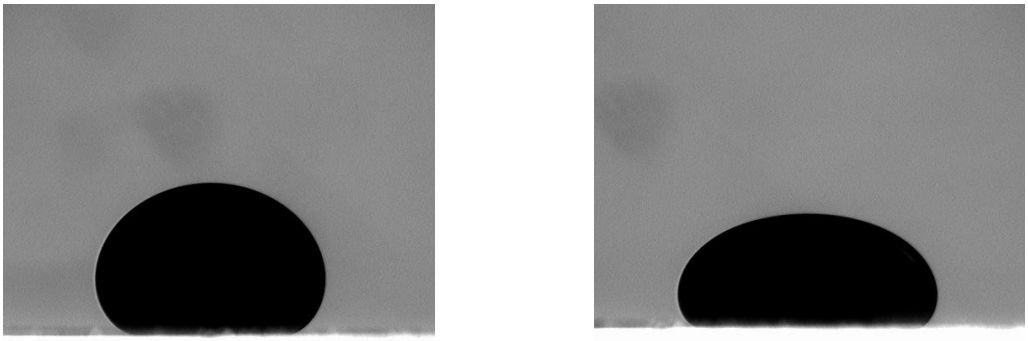

a) b)

Figure A-22: Oil in Hydrophilic SNPs 0,5 wt. % at a) start and b) end of experiment

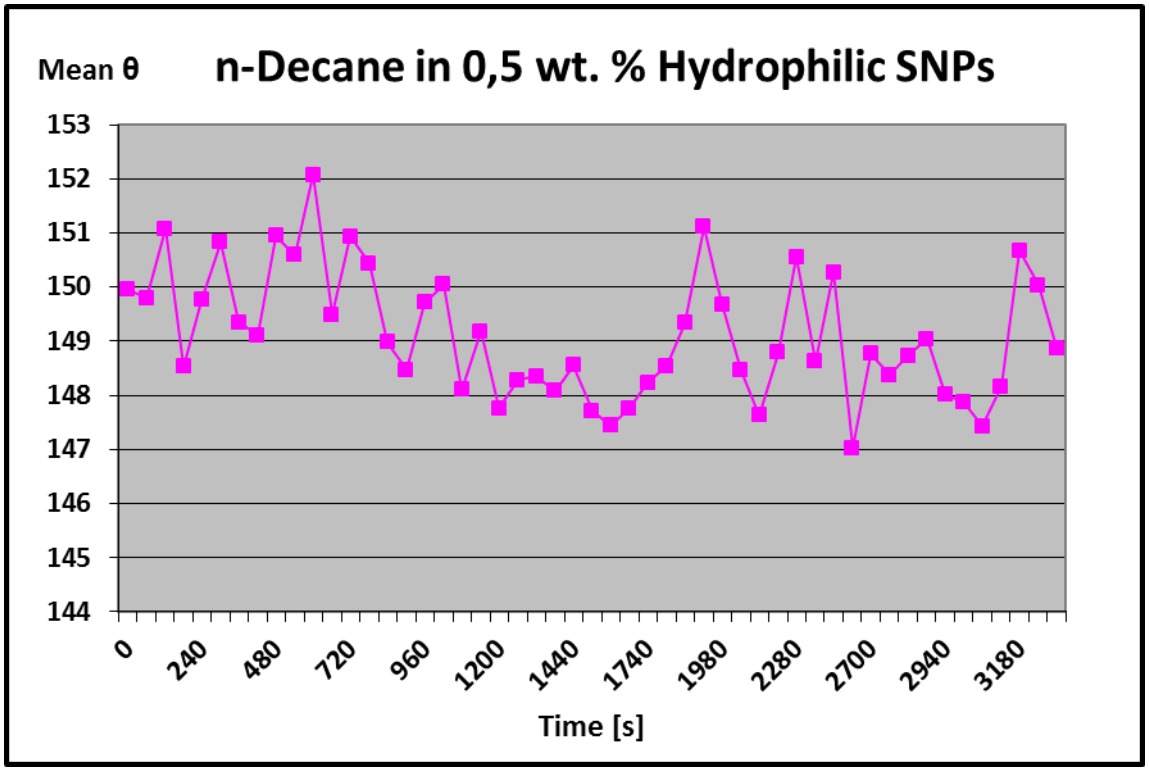

Figure A-23: Mean contact angle vs. time for oil in hydrophilic SNPs 0,5 wt. %

A-9.9 Oil and 0,01 wt. % Hydrophobic SNPs in Brine

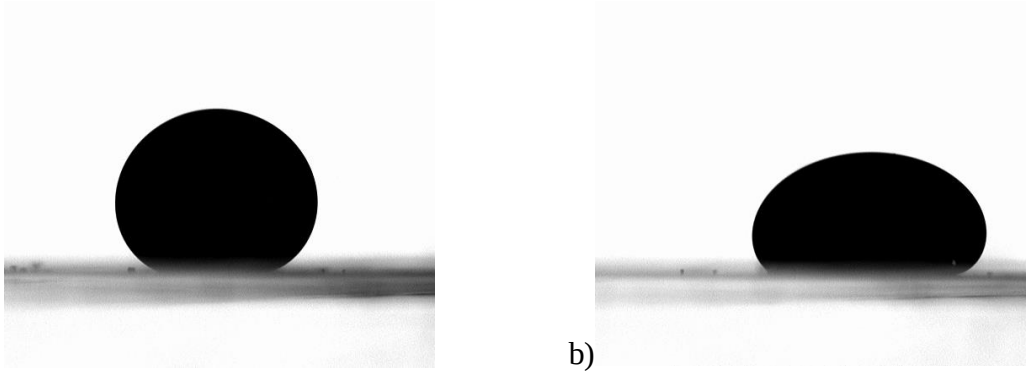

a) b)

Figure A-24: Hydrophobic SNPs 0,01 wt. % in Brine at a) start and b) end of experiment

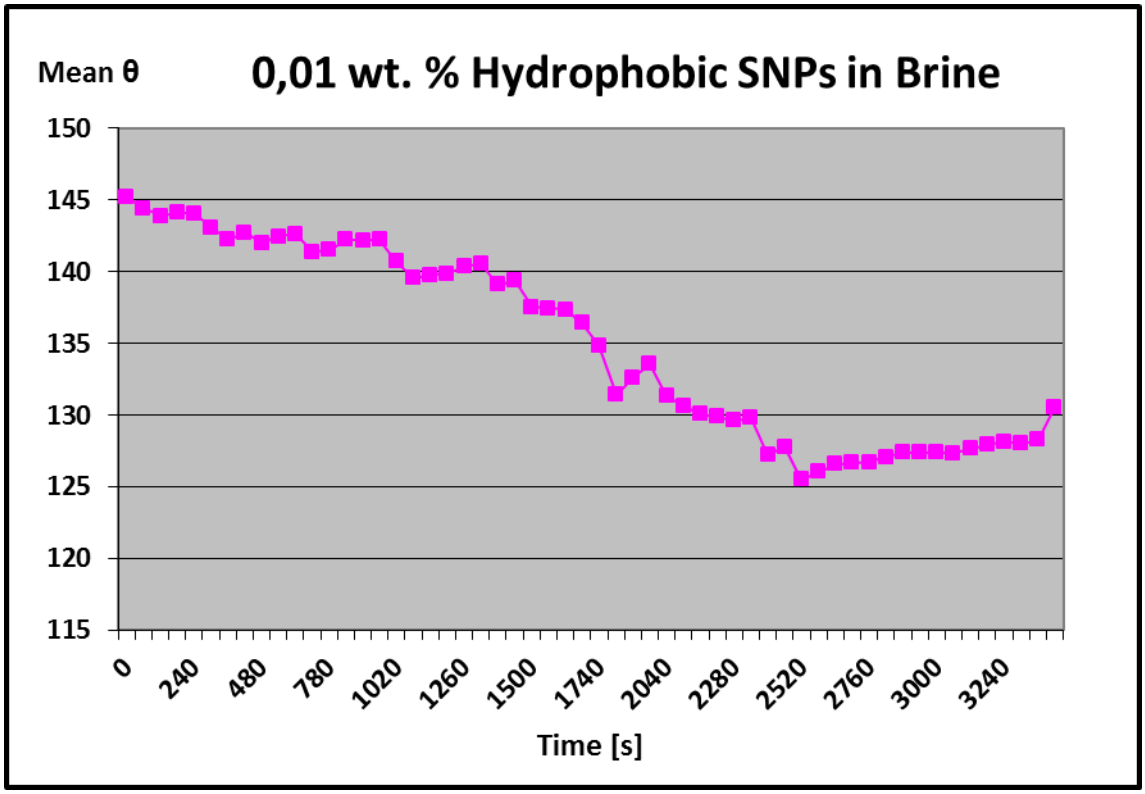

Figure A-25: Mean contact angle vs. time for hydrophobic SNPs 0,01 wt. % in Brine

A-9.10 Oil and 0,1 wt. % Hydrophobic SNPs in Brine

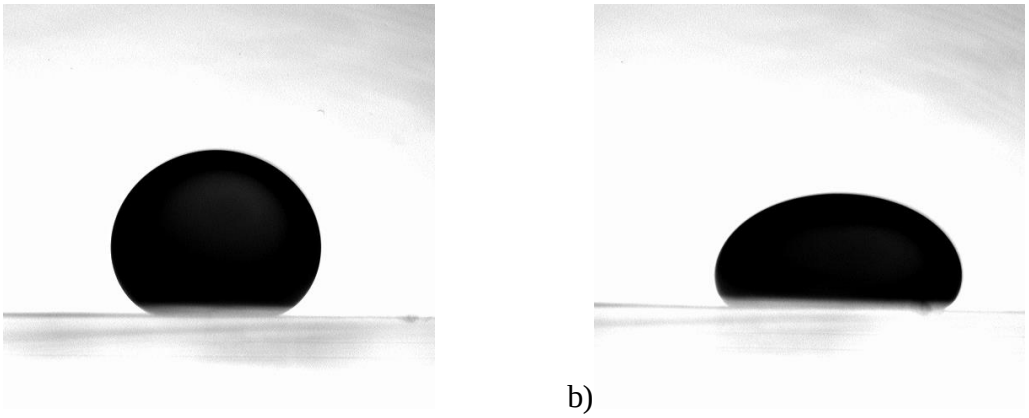

a) b)

Figure A-26: Hydrophobic SNPs 0,1 wt. % in Brine at a) start and b) end of experiment

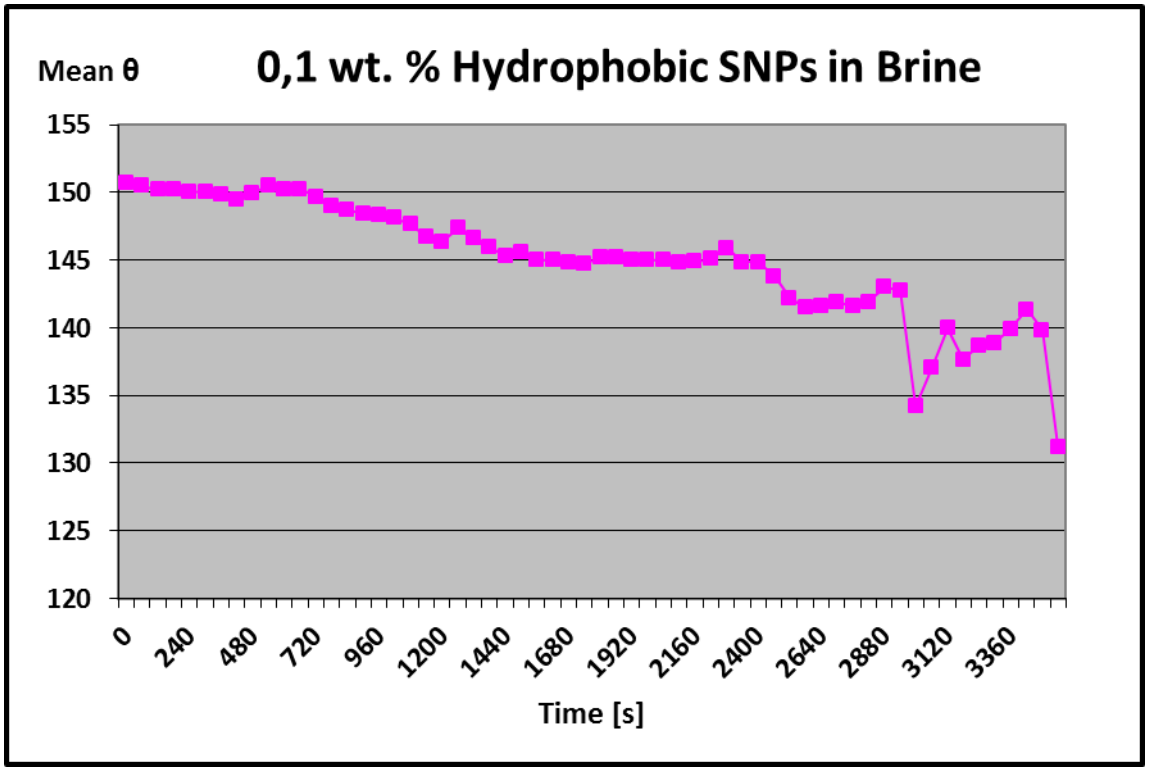

Figure A-27: Mean contact angle vs. time for hydrophobic SNPs 0,1 wt. % in Brine

A-9.11 Oil and 0,5 wt. % Hydrophobic SNPs in Brine

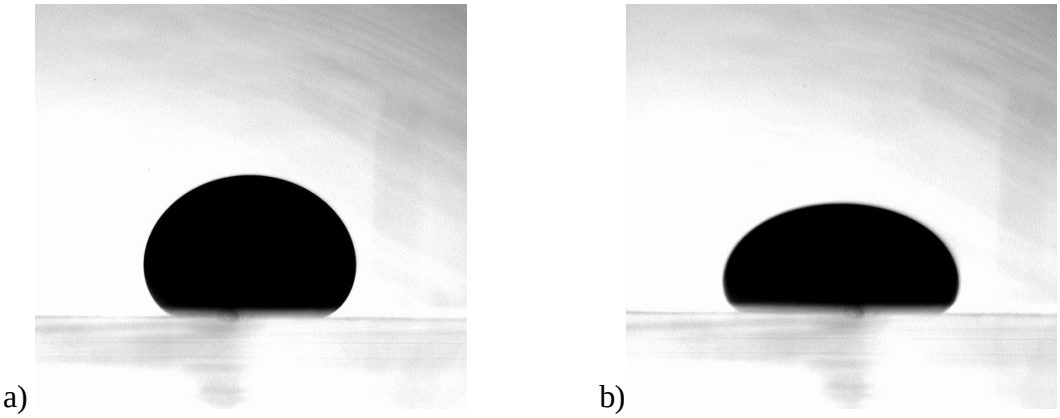

a) b)

Figure A-28: Hydrophobic SNPs 0,5 wt. % in Brine at a) start and b) end of experiment

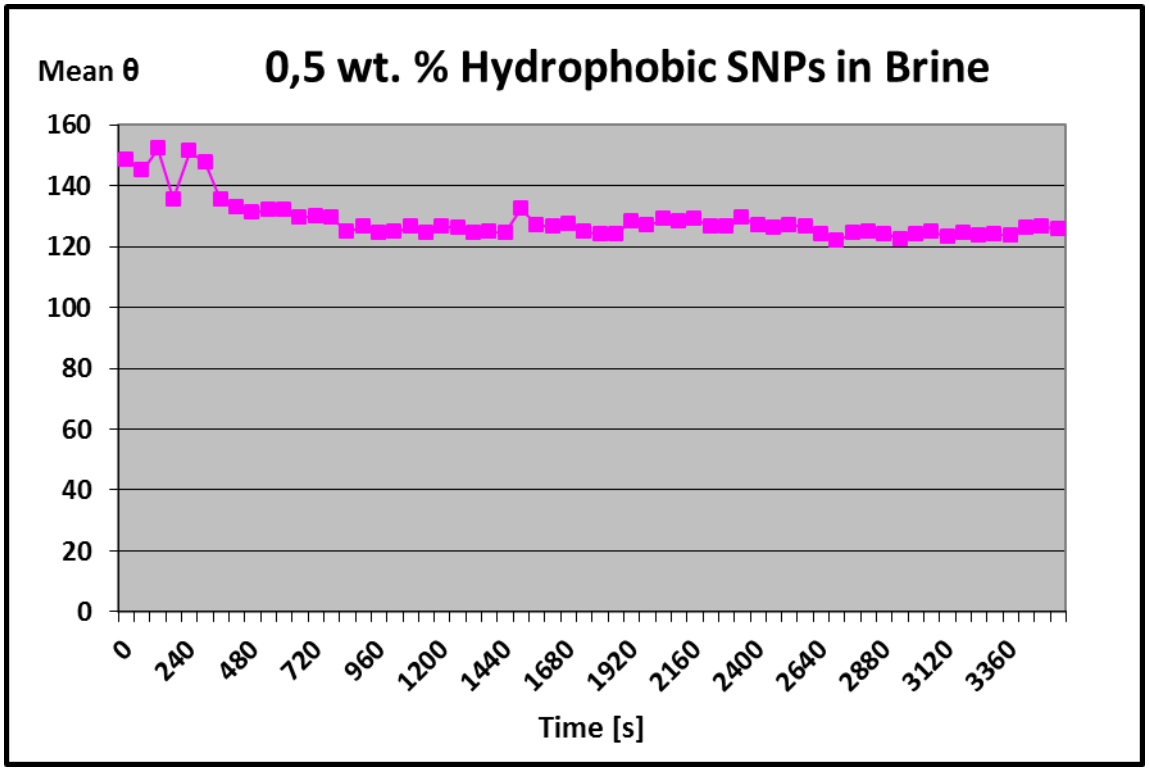

Figure A-29: Mean contact angle vs. time for hydrophobic SNPs 0,5 wt. % in Brine